

ON THE GENERATION OF INERTIAL-GRAVITY
WAVES IN THE OCEAN

by

JAMES B. SULLIVAN

B.C.E., Manhattan College
(1963)

M.S., New York University
(1966)

SUBMITTED IN PARTIAL FULFILLMENT
OF THE REQUIREMENTS FOR THE
DEGREE OF DOCTOR OF PHILOSOPHY

at the

MASSACHUSETTS INSTITUTE OF TECHNOLOGY

June, 1970

Signature of Author
Department of Meteorology, May 28, 1970

Certified by
Thesis/Supervisor

Accepted by
Chairman, Departmental Committee on
Graduate Students

WITHDRAWN
FROM
JUN 11 1970
MIT LIBRARIES



Room 14-0551
77 Massachusetts Avenue
Cambridge, MA 02139
Ph: 617.253.5668 Fax: 617.253.1690
Email: docs@mit.edu
<http://libraries.mit.edu/docs>

DISCLAIMER OF QUALITY

Due to the condition of the original material, there are unavoidable flaws in this reproduction. We have made every effort possible to provide you with the best copy available. If you are dissatisfied with this product and find it unusable, please contact Document Services as soon as possible.

Thank you.

Due to the poor quality of the original document, there is some spotting or background shading in this document.

ON THE GENERATION OF INERTIAL-GRAVITY

WAVES IN THE OCEAN

by

James B. Sullivan

Submitted to the Department of Meteorology on May 28, 1970
in partial fulfillment of the requirements for the degree of
Doctor of Philosophy

ABSTRACT

A model is presented for the generation of inertial-gravity waves in the ocean by wind stress acting on the surface. The ocean is considered to rotate uniformly and has a constant eddy coefficient of viscosity as well as uniform stratification. Thermal diffusion is neglected. The singularities in the Ekman-Stokes layers associated with this system are removed by frictional considerations. The vertical structure of the near inertial motions is found to be confined to a surface layer with thickness proportional to $E^{1/4}$ ($E = \text{Ekman number} = \frac{\nu}{\Omega H^2}$). The motion due to an idealized travelling front is solved for at all depths by numerical integration and at the surface by analytical methods. The theoretical amplitudes and frequencies so obtained are in reasonable agreement with typical observations in the upper layers of the ocean. The persistence time for a slowly moving front is found to be about one week; faster moving fronts leave a longer trail behind them. A comparison is made with a simpler layer model due to Pollard and Millard (1970).

CONTENTS

1. Introduction and summary of thesis	
1.1 Observations and existing theories	1.
1.2 Summary of thesis	5.
2. Formulation	
2.1 The equations of motion	6.
2.2 The boundary conditions, the nature of the forcing	8.
2.3 Simplifying assumptions	9.
3. The vertical structure of the motion	
3.1 The characteristic equation	11.
3.2 Properties of the inviscid roots	19.
3.3 The role of friction	24.
4. The response to an idealized travelling wind distribution	
4.1 Specification of an idealized stress field for a travelling front	30.
4.2 Method of solution for the problem	36.
4.3 Discussion of solutions	37.
5. The response to an idealized travelling wind distribution; the case of an infinitely deep ocean	57.
5.1 The response to a travelling sinusoidal stress pattern	58.
5.2 The response to the idealized travelling front	63.
6. Comparison with a simpler model and conclusions	
6.1 Comparison of solutions with the Pollard- Fofonoff model	74.

6.2 Discussion and conclusions	88.
Appendix 1 Discussion of the numerical procedure	93.
Appendix 2 Calculation of the branch cut integrals of Chapter 5	
A-2.1 Evaluation of an integral used on the branch cuts	97.
A-2.2 Evaluation of the branch cut integrals	98.
References	101.

1. Introduction and summary of thesis

1.1 Observations and existing theories

The occurrence of inertial oscillations at almost all locations and depths of the world ocean is a well documented and accepted fact; they appear in current records as a spectral peak slightly above the inertial frequency (given at latitude θ by $2 \sin \theta$ cycles per day). A sample spectrum is shown in figure 1.1. Webster (1968) gives an excellent survey of the substantiating observational data. The motion is characterized by the fluid particles traversing an almost circular path with a period slightly shorter than the local inertial period. The amplitudes are typically of the order of 10 cm sec^{-1} . These oscillations belong to the class of waves called inertial-gravity waves which can exist in fluids, such as the ocean, which are subjected to both rotational and gravitational restoring forces.

The source of these ubiquitous oscillations has not yet been satisfactorily explained. There are two types of mechanisms which can act to produce the observed spectral peak. The first, a wave guide mechanism, allows a global generation of waves and is based on a physical restriction that the waves' frequency be greater than the local inertial frequency but less than the Brunt-Väisälä frequency (given by $\sqrt{\frac{-g}{\rho} \frac{\partial \rho}{\partial z}}$ where g is gravity, ρ is density, and z is a vertical coordinate). Since the inertial frequency increases with latitude, waves produced at a lower latitude can only travel poleward until they

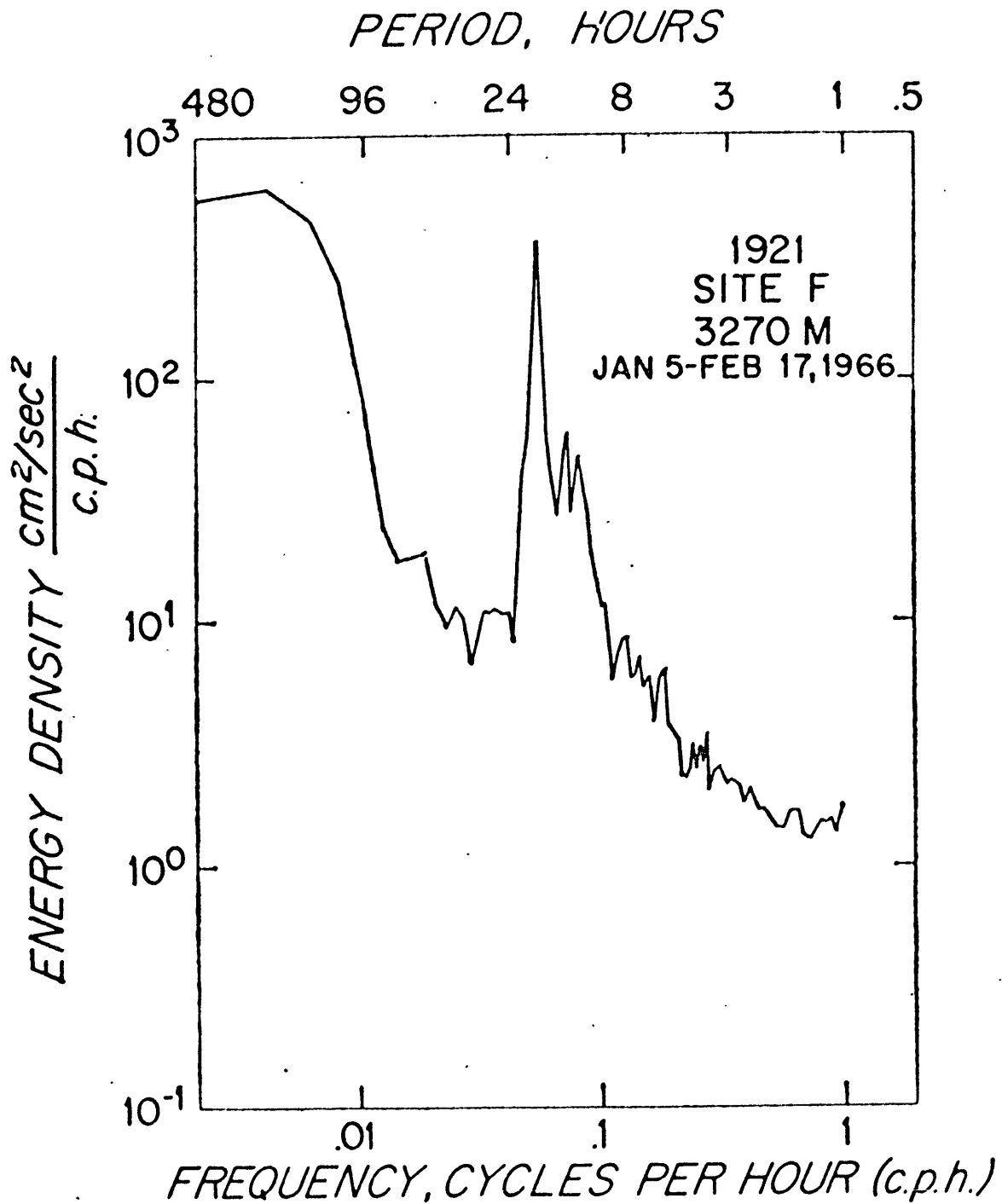


Figure 1.1 Kinetic energy density spectrum for measurements collected at site F ($38^{\circ}30'N, 70^{\circ}W$). The local inertial period is 19.3 hours. The dominant peak in the spectrum has a period near 18.5 hours. (from Webster 1968)

reach the latitude at which their frequency is equal to the local inertial frequency. The global generation theory (e.g. see Munk and Phillips, 1968), then, states that at a given latitude the inertial motion will be a superposition of all those waves produced further equatorward whose frequency is equal to the inertial frequency at that given latitude. The kinematics of the waves in the vicinity of this "turning latitude" is such that they have their maximum amplitude there. The second mechanism involves local generation of the waves and is based on the fact that the oceanic "transfer function" between an input variable (e.g. a time dependent, atmospheric wind stress) and the oceanic motion field has a peak slightly above the inertial frequency. Both theories have weaknesses (see Munk and Phillips) if they are used individually to explain inertial oscillations in the ocean. The global generation theory does not explain the observed intermittency of the motion (persistence times of the order of one week) while the local generation theory does not explain the short coherence distances in the records (of the order of 10 m vertically and several tens of kilometers horizontally).

The purpose of this paper is to present a model for the local generation of inertial-gravity waves by travelling atmospheric fronts. The evidence for wind generation of inertial-gravity waves is quite strong (Day and Webster, 1965; Saalen, 1963; Hunkins, 1967; Pollard and Millard, 1970), and has led to various models involving different air-sea interaction mechanisms. Pollard (1970) assumed that the mixed layer, several tens of meters thick at the ocean surface, absorbs

the momentum, generated by the wind stress at the surface, by turbulent mixing in a time period short compared with the inertial period. The applied stress is thereby allowed to be considered as a body force acting over the entire depth of the mixed layer rather than as a surface force. Viscous diffusion of momentum is subsequently ignored. As an alternate mechanism, Hasselmann (1970) considered the driving force as arising from the weakly nonlinear Stokes drift associated with wind-driven surface gravity waves. Both models assume the ocean to be essentially inviscid.

The mechanism treated in this paper assumes the oceanic turbulence to be modelled by a constant eddy coefficient of viscosity. This is the classical model for transferring momentum downward from a steady wind stress applied at the ocean surface and it is here extended to the case of a time dependent stress. At frequencies removed from inertial, the structure of the motion in this model has been well explained (e.g., see Tomczak 1967) but near the inertial frequency the behavior of the velocity fields is not at all understood. More specifically, the existing theory (see Tomczak) gives a boundary layer eruption and a singularity in the inviscid vertical wave number at the inertial frequency which must be resolved by a more complete treatment that is uniformly valid for all frequencies. The ocean's behavior near this point is important because it is precisely here that large energy concentrations are found.

1.2 Summary of thesis

In Chapter 2 the oceanic model is formulated. The equations of motion of the system are derived and non-dimensionalized; their limitations are discussed.

Chapter 3 contains what may be called a normal mode analysis of the model. The behavior of the boundary layer structures is discussed for all values of the frequency of excitation, including the inertial frequency. The oscillatory modes and their modification by friction are also analysed for all values of the forcing frequency.

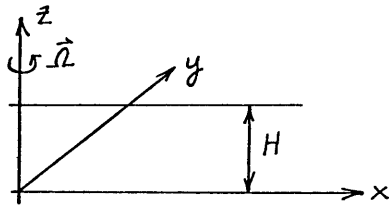
Chapter 4 contains solutions obtained by numerical integration for an ocean forced at the surface by stresses associated with a north-south front travelling in the eastward direction. The motion as a function of depth is found to die out rapidly, in accordance with the deductions in Chapter 3 concerning the effects of friction. The amplitude and dispersive character of the solutions are discussed.

In Chapter 5, an infinitely deep ocean is treated analytically. The motivation for this is to gain further insight into the solutions obtained in Chapter 4. More specifically, analytic solutions are obtained as well as expressions for the frequency of the inertial wake and its horizontal decay rate.

Chapter 6 contains a comparison of the model of Chapter 2 with the surface layer model used by Pollard and Millard (1970) to explain wind generation of inertial waves. There is also a discussion of the conclusions drawn from the model presented as well as some of its weaknesses.

2. Formulation of the model

Consider a stratified ocean rotating uniformly about a vertical axis as shown below



$$\begin{aligned} -\infty < x < \infty \\ -\infty < y < \infty \\ 0 \leq z \leq H \end{aligned}$$

and where the following correspondences hold

$$(x, y, z) \leftrightarrow (\hat{i}, \hat{j}, \hat{k}) \leftrightarrow (u, v, w)$$

2.1 The equations of motion

The equations governing the motion in the system are taken as

$$\frac{d\vec{u}}{dt} + 2\vec{\Omega} \times \vec{u} = -\frac{1}{\rho} \nabla p - g \hat{k} + \nu \nabla^2 \vec{u}$$

$$\frac{d\rho}{dt} = \kappa \nabla^2 \rho$$

$$\nabla \cdot \vec{u} = 0$$

where ν and κ are the kinematic viscosity and thermal diffusivity respectively.

The stratification will be modelled by a linear gradient of density, $\partial \bar{\rho} / \partial z$, perturbed by variations, ρ' , due to the motion of the fluid. Thus,

$$\rho = \bar{\rho} + \rho'$$

7.

Define $\rho_0 \equiv \frac{1}{H} \int_0^H \bar{\rho} dz$

and ρ_1 so that $\bar{\rho} = \rho_0 + \rho_1$

Making the Boussinesq approximation and linearizing then gives

$$\frac{\partial \vec{u}}{\partial t} + 2\vec{\Omega} \times \vec{u} = -\frac{1}{\rho_0} \nabla p' - g \frac{\rho'}{\rho_0} \hat{k} + \nu \nabla^2 \vec{u}$$

$$\frac{\partial \rho'}{\partial t} + w \frac{\partial \bar{\rho}}{\partial z} = \kappa \nabla^2 \rho'$$

$$\nabla \cdot \vec{u} = 0$$

where the static pressure, $\bar{p} = g \int_z^H \bar{\rho} dz$, has been subtracted
and $p' = p - \bar{p}$

The equations are now non-dimensionalized by the following transformations:

$$\vec{u} = \Omega H \vec{u}'$$

$$\vec{x} = H \vec{x}'$$

$$t = \Omega^{-1} t'$$

$$\Omega = \frac{f}{2}$$

$$p' = \left(H \frac{\partial \bar{p}}{\partial z} \right) p''$$

$$p' = \rho_0 \Omega^2 H^2 p''$$

In chapter 5 the case of an infinitely deep ocean will be

considered and H then loses its meaning. It is not inconsistent, however, to continue to use it as a simple non-dimensionalizing parameter.

The following parameters can be defined:

$$N = \sqrt{\frac{-g}{\rho_0} \frac{\partial \bar{\rho}}{\partial z}},$$

taken to be $2 \times 10^{-3} \text{ sec}^{-1}$, characteristic of the oceanic main thermocline

$$S = N^2 / \Omega^2,$$

taken as 1872.4, corresponding to latitude $39^\circ 20.5' \text{N}$ (WHOI station D) and N above

$$E = \frac{\nu}{\Omega H^2}$$

corresponding to an Ekman layer 40 m thick with $H = 4 \text{ km}$

$$\sigma = \frac{\nu}{\kappa}$$

the Prandtl number.

With these values the velocity scaling is $\Omega H = 18.45 \text{ cm/sec}$.

The equations may then be written, after dropping the primes:

$$\frac{\partial \vec{u}}{\partial t} + 2\hat{k} \times \vec{u} = -\nabla p + S \rho \hat{k} + E \nabla^2 \vec{u}$$

$$\frac{\partial p}{\partial t} + w = \frac{E}{\sigma} \nabla^2 p \quad (2.1)$$

$$\nabla \cdot \vec{u} = 0$$

2.2 The boundary conditions - the nature of the forcing

The generation mechanism considered will be mechanical and is expressed non-dimensionally by the boundary conditions:

$$z=0: \vec{u} = 0$$

9.

$$z=1: w=0, \frac{\partial \vec{u}}{\partial z} = \vec{\tau}$$

(2.2)

where the stress is non-dimensionalized by $\rho_0 \Omega^2 H^2 E = 0.0340 \text{ dynes cm}^{-2}$.

To simplify the problem, $\vec{\tau}$ is taken as a one dimensional (in x) stress pattern moving with constant speed U across the ocean surface. Consequently, it is assumed that $\frac{\partial}{\partial y} = 0$. The pattern is described in detail in chapter 4.

2.3 Simplifying assumptions

Probably the most severe restriction on the model is the neglect of the earth's curvature, i.e., the beta effect. It is well known (e.g., see Phillips 1966) that internal gravity waves of frequency ω_0 at low latitudes can travel northward until they reach their so-called inertial latitude given by $\omega_0 = f$, at which point they are almost purely inertial in character and beyond which they cannot propagate. This wave guide behavior might account for the appearance of inertial oscillations far from any region of forcing. The model presented here, as a result of its having no north-south variation, does not allow this flow of energy.

For mathematical tractability, the basic stratification is taken to vary linearly with depth. In the ocean, this is obviously not the case. The effect of this assumption, however, does not

alter qualitatively the conclusions drawn.

Another major assumption regards the role of oceanic turbulence in the generation and decay of inertial-gravity waves. The turbulence is modeled as being an eddy viscosity with magnitude $7.4 \times 10^2 \text{cm}^2 \text{sec}^{-1}$. This corresponds to an Ekman layer 40 m thick at site D and is assumed to be constant with depth.

Since mechanical forcing is of interest here, the model allows no thermal diffusion, i.e., $\sigma \rightarrow \infty$. This is not too crucial in the light of the other assumptions and purposes for studying the model.

3. The vertical structure of the motion

The vertical structure of the motion may be determined by studying the behavior of the vertical wave numbers for all the possible modes of motion of the system. In the model formulated in Chapter 2, one expects both frictional boundary layers and, far away from the boundaries, relatively inviscid motion.

3.1 The characteristic equation

Solutions of the basic equations (2.1) with $\sigma \rightarrow \omega$ are sought of the form

$$e^{i(kx + mz - \omega t)}$$

where ω is taken as a Doppler frequency $\omega = Uk$. U is a constant velocity and will be considered as positive. ω , then, is positive or negative depending on k . Later on, more general forcing functions will be Fourier synthesized ($-\infty < k < \infty$) with the above functions. This form may be substituted directly into the five equations of motion or the combined equation:

$$\frac{\partial}{\partial t} \left(\frac{\partial}{\partial t} - E \nabla^2 \right)^2 \nabla^2 \psi + S \left(\frac{\partial}{\partial t} - E \nabla^2 \right) \nabla_1^2 \psi + 4 \frac{\partial}{\partial t} \frac{\partial^2 \psi}{\partial z^2} = 0$$

where ψ is any dependent variable and $\nabla_1^2 = \frac{\partial^2}{\partial x^2}$. This results in a sixth order polynomial in m :

$$E^2 m^6 + \alpha_1 E m^4 + [-(\omega^2 - 4) + \alpha_2 E] m^2 + [k^2 (S - \omega^2) + E \alpha_3] = 0 \quad (3.1)$$

(1) (2) (3) (4) (5) (6)

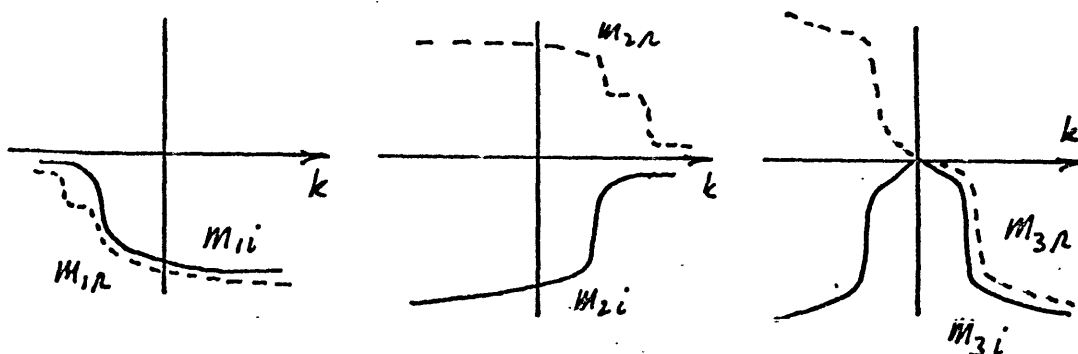
where

$$\alpha_1 = -2i\omega + 3k^2 E$$

$$\alpha_2 = -i \frac{k^2}{\omega} (4\omega^2 - 5) + 3E k^4$$

$$\alpha_3 = -2i\omega k^4 + i \frac{5k^4}{\omega} + k^6 E^2$$

A numerical solution of (3.1) for m as a function of k was carried out for three values of U (13.411, 54.083, 100.0) and the results appear in figures 3.1 to 3.6. Since the equation is a cubic in m^2 , only the positive solutions for positive k are plotted. It can be shown that if $(m, +k)$ is a solution of (3.1), then $(m^*, -k)$ where $*$ denotes the conjugate is also a solution and, thus, one quadrant suffices to show the behavior of m . To identify the roots more precisely, the sketch below shows the real and imaginary parts of the three wave numbers with negative imaginary parts. The root labeled m_3 has a change of sign in its imaginary part at the origin and, hence, is drawn here as being discontinuous in its first derivative at the origin.



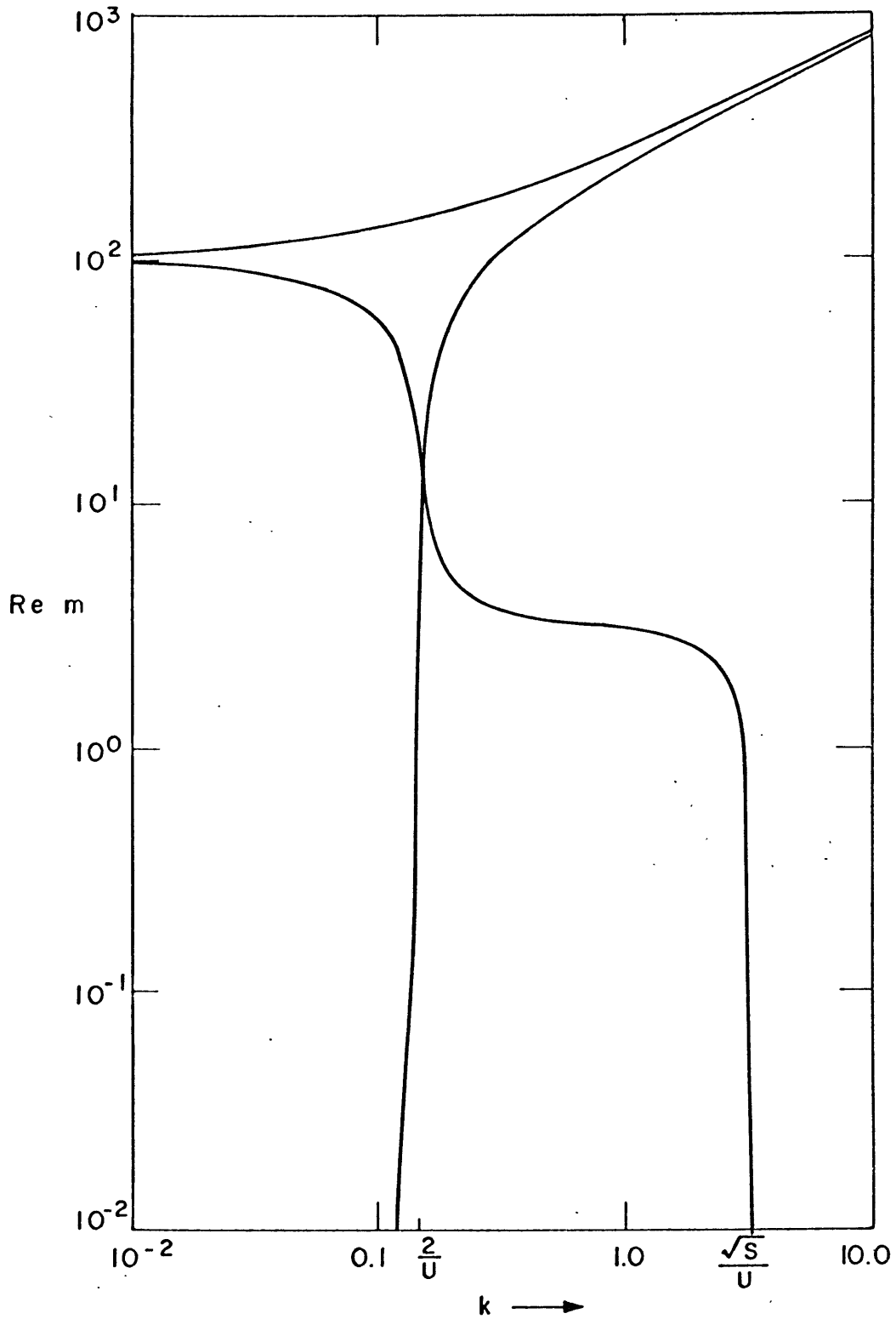


Figure 3.1 $Re\ m$ vs, k as the solution of (3.1) for $U = 13.411$ ($2.5\ \text{msec}^{-1}$),
 $E = 10^{-4}$, $S = 1872.4$.

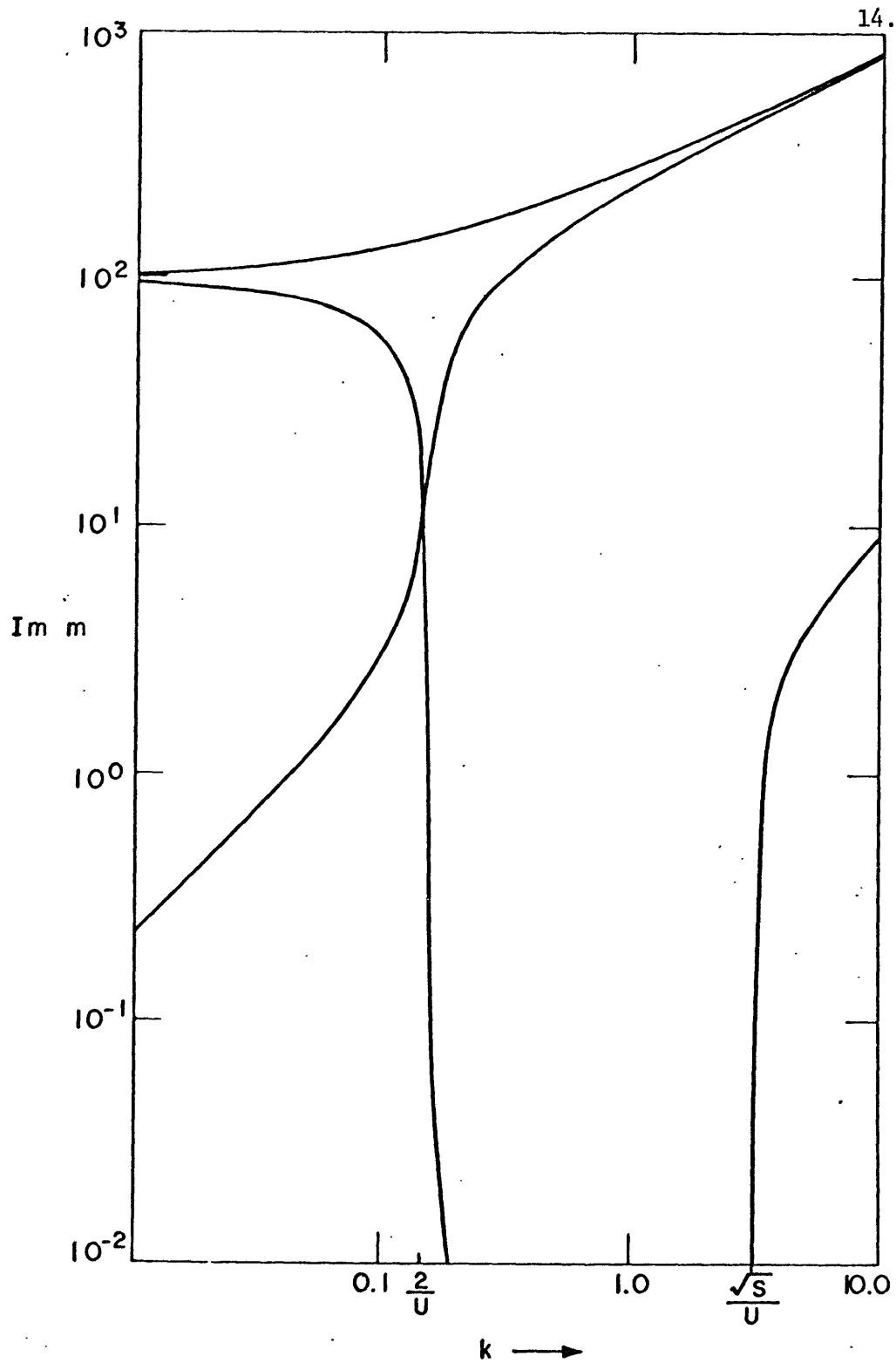


Figure 3.2 $\text{Im } m$ vs. k as the solution of (3.1) for $U = 13.411$
 (2.5 m sec^{-1}), $E = 10^{-4}$, $S = 1872.4$.

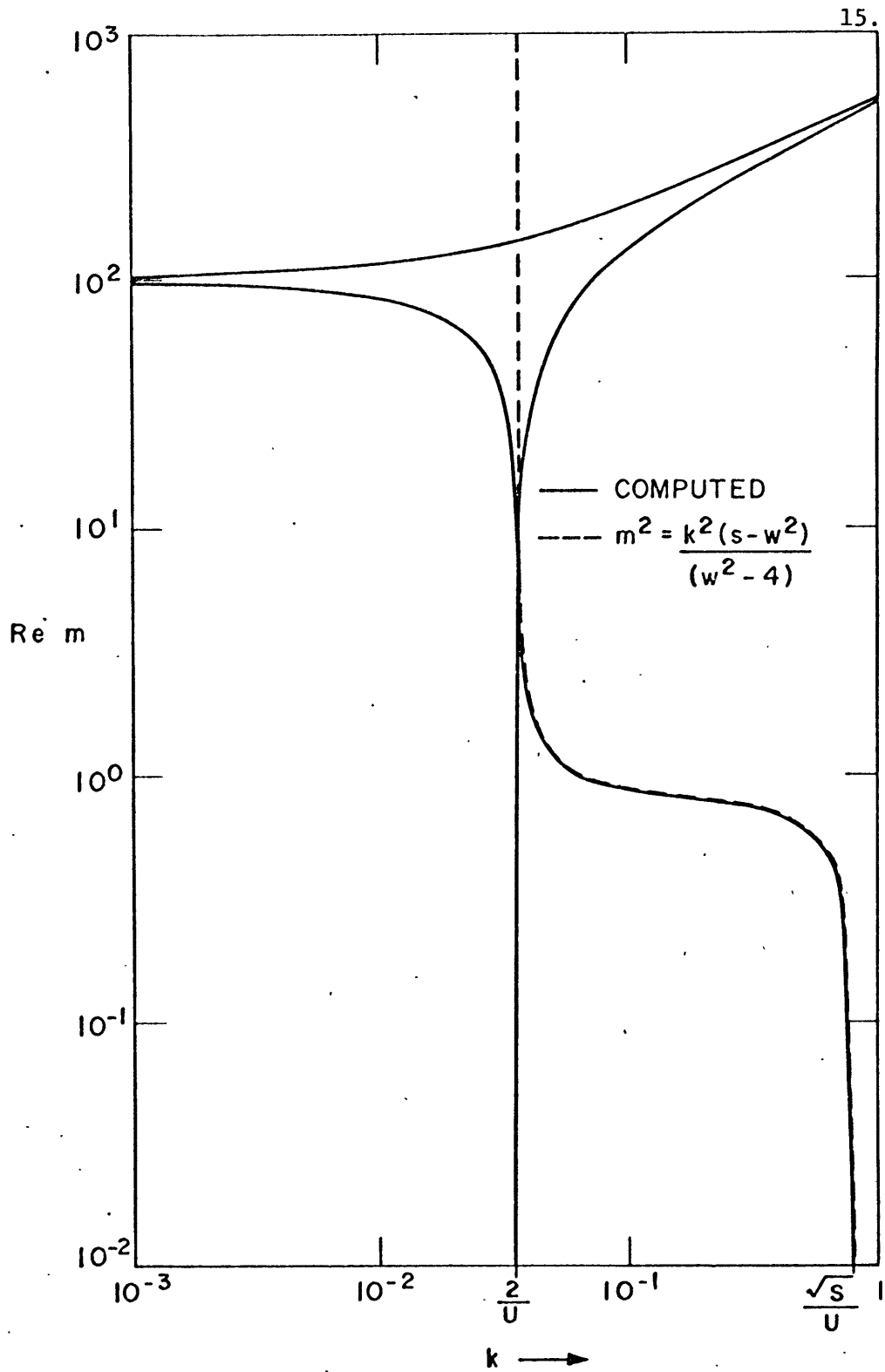


Figure 3.3 Same as 3.1 but for $U = 54.083$ (10 m sec^{-1}).

The dashed line represents the inviscid wave number.

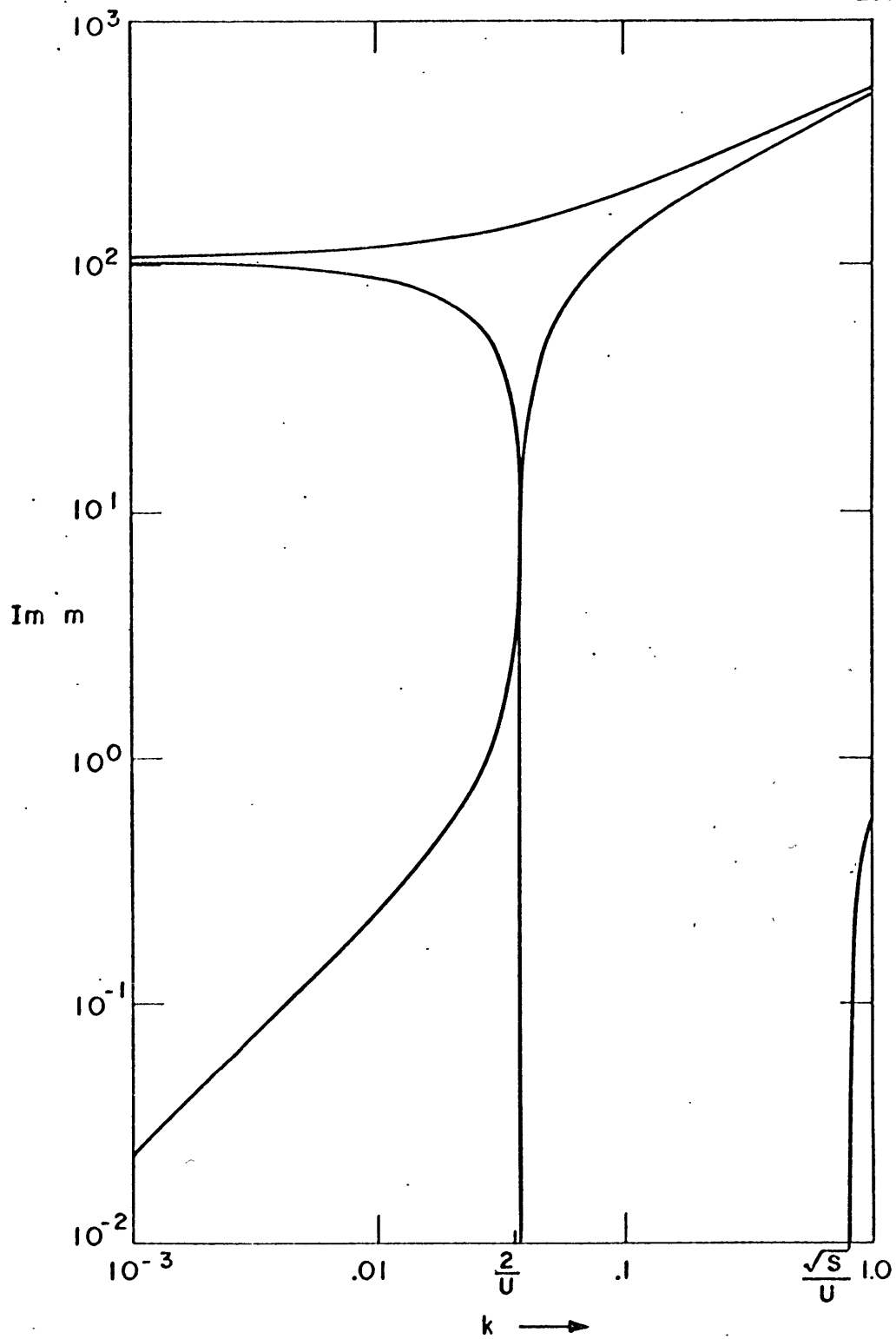


Figure 3.4 The same as 3.2 but for $U = 54.083$ (10 m sec^{-1}).

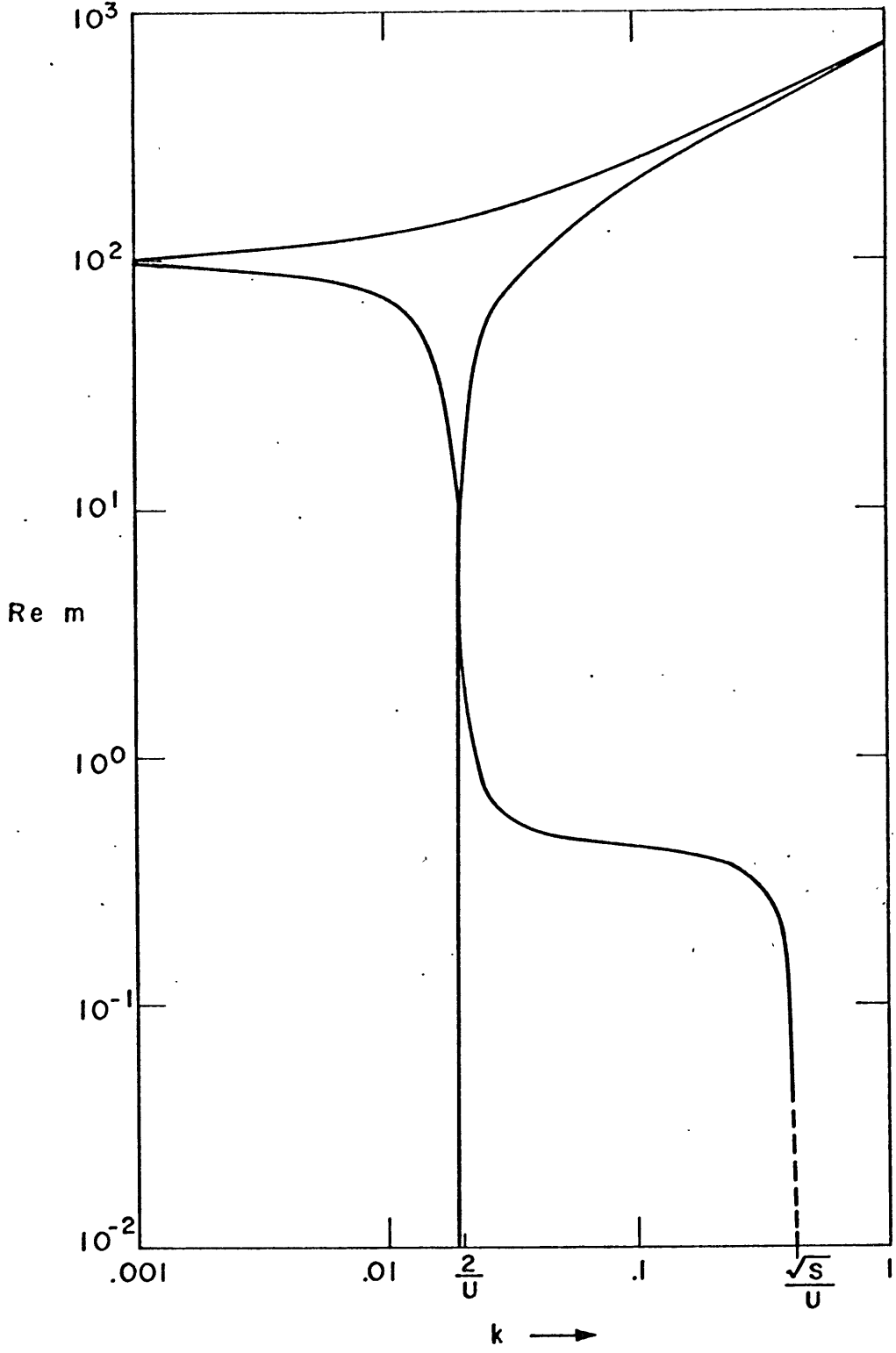


Figure 3.5 The same as 3.1 but for $U = 100.0$ ($18.45\ m\ sec^{-1}$).

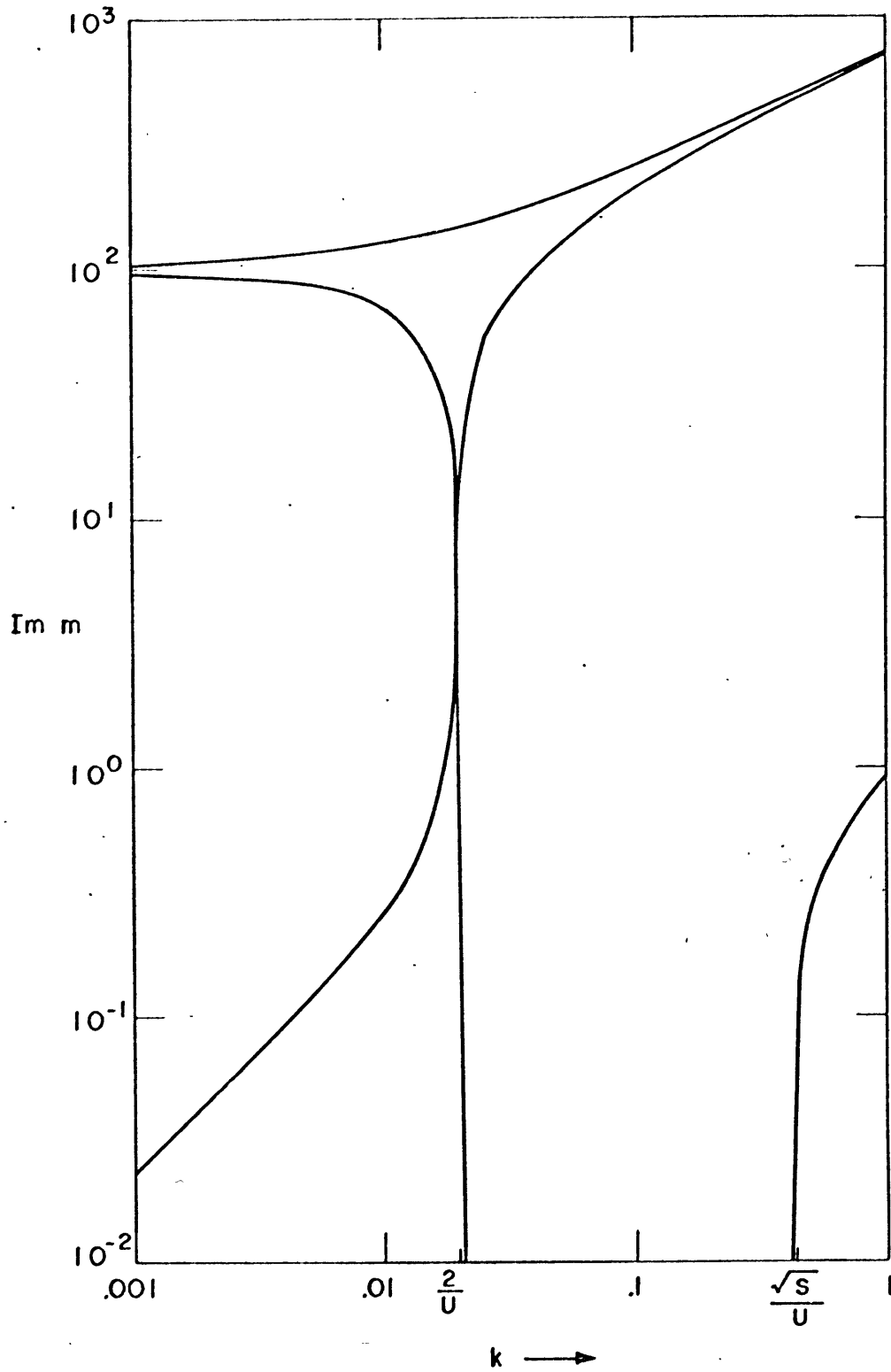


Figure 3.6 The same as 3.2 but for $U = 100.0$ (18.45 m sec^{-1}).

Figure 3.3 also shows a plot of the inviscid wave number

$$m^2 = \frac{k^2(S - \omega^2)}{(\omega^2 - 4)}$$

If the ocean has a finite depth, all six vertical wave numbers are needed to synthesize a solution. If the ocean is infinitely deep ($-\infty < z \leq 0$), only those wave numbers with negative imaginary parts are permitted for a bounded solution as $z \rightarrow -\infty$.

The discussion of the roots of (3.1) which follows holds in a strict sense only in the limit as E approaches zero since U and S take on values which are not $O(1)$. Since here $E = 10^{-4} \neq 0$, the validity of the arguments presented rests on the numerical solutions. For the parameter values used, these solutions do in fact substantiate the arguments.

3.2 Properties of the inviscid roots

Consider the roots of (3.1) in the limiting case of zero friction, i.e., $E = 0$. The sixth order equation in m reduces to a quadratic one:

$$m^2 = \frac{k^2(S - \omega^2)}{(\omega^2 - 4)} \quad (3.2)$$

These wave numbers represent travelling inertial-gravity waves which will be discussed now. The singular points at $\omega^2 = 4$ require a non-inviscid resolution and will be considered afterwards.

The inviscid phase velocity is given by the solution of

$$\begin{aligned} \vec{x} \cdot \vec{x} - \omega t &= 0 & \vec{x} &= k \hat{i} + m \hat{k} \\ \vec{x} \cdot \frac{\vec{x}}{t} &\equiv \vec{x} \cdot \vec{c}_p = \omega & & \\ \vec{c}_p &= \frac{\omega}{|\vec{x}|^2} \vec{x} & & \end{aligned} \quad (3.3)$$

Waves produced by a travelling disturbance moving on the ocean surface with speed U must have their trace speeds equal to U . By trace speed is meant the speed with which the intersection point of the ocean surface and a constant phase line moves. Thus, $\vec{x} \cdot \vec{x} - \omega t = (\text{const.})$ and $z=1$ yield $kx - \omega t = 0$ and, hence, ω/k for the trace speed. This allows only waves for which $c_{px} > 0$.

The group velocity of the inviscid waves is of special importance and is given by

$$\begin{aligned} \vec{c}_g &= \nabla_k \omega \\ &= \frac{1}{m\omega(s-4)} \left[\pm \sqrt{(\omega^2-4)(s-\omega^2)^3}, - (s-\omega^2)/(\omega^2-4) \right] \end{aligned} \quad (3.4)$$

This is shown in figures 3.7 and 3.8. Note that $|\vec{c}_g| \rightarrow 0$ as $\omega \rightarrow 2$.

It can easily be shown from (3.4) that $\vec{c}_p \cdot \vec{c}_g = 0$. Furthermore, if

ω is considered positive and since positive m then corresponds

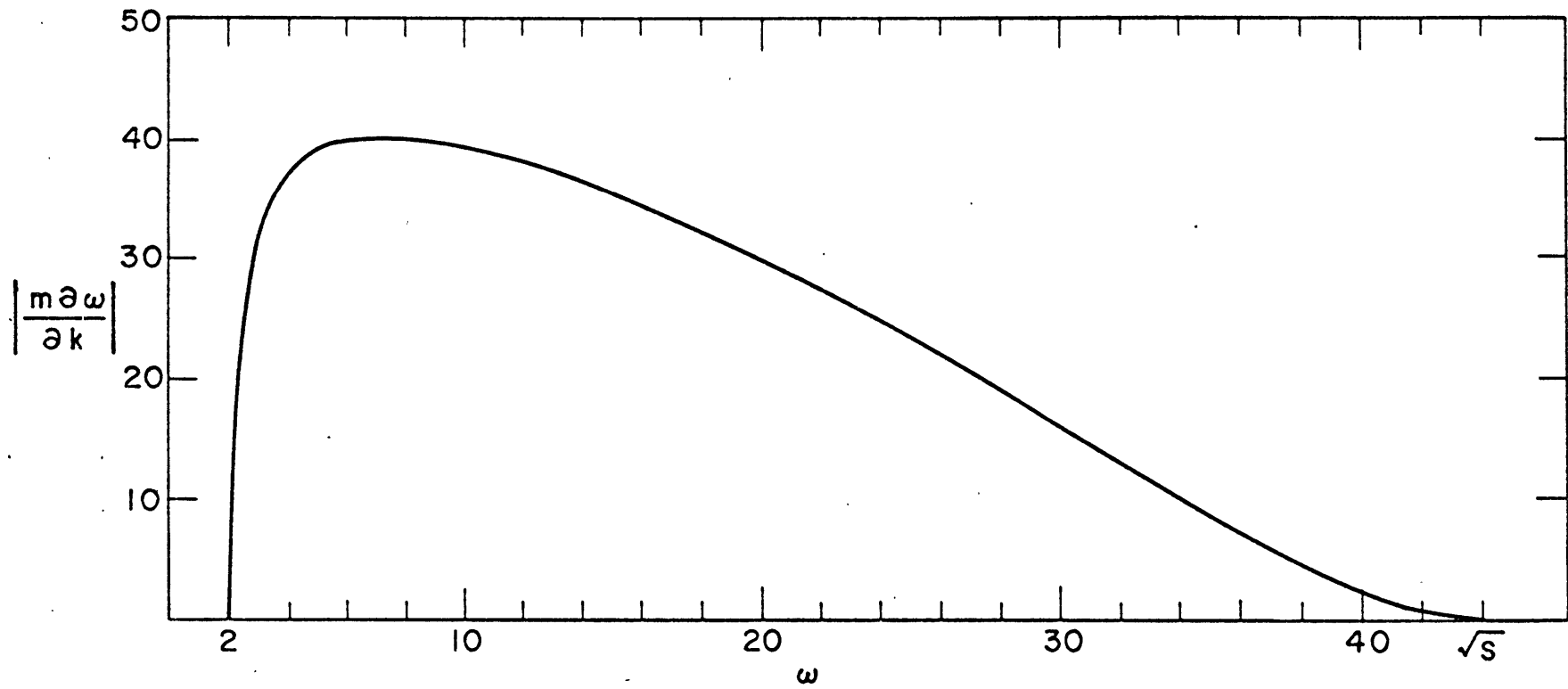


Figure 3.7 The horizontal group velocity (multiplied by the vertical wave number m) as a function of ω .

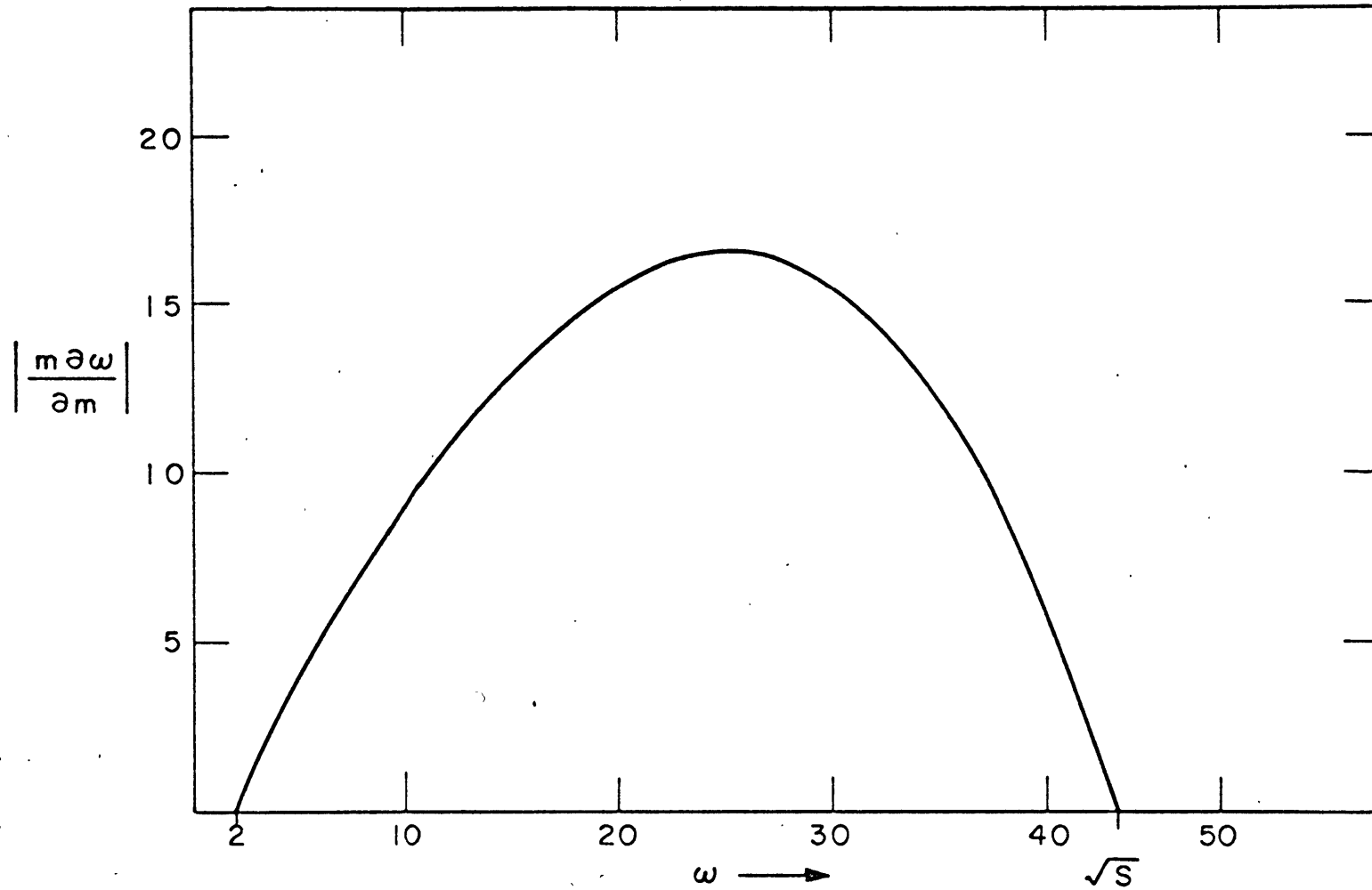
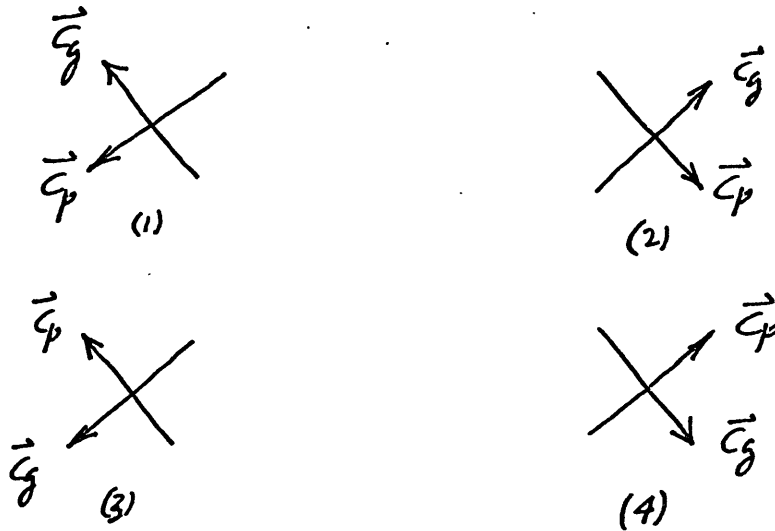


Figure 3.8 The vertical group velocity (multiplied by the vertical wave number m) as a function of ω .

to waves travelling in the positive z direction, the familiar result emerges that the vertical components of the group and phase velocities are in opposite directions. The following sets of arrows indicate the possible directions for \vec{c}_g and \vec{c}_p :



Combinations (2) and (4) are the only ones allowed here. Waves of type (4) can synthesize a disturbance at the surface or reflections from the surface while type (2) waves represent energy propagated from the bottom. If the ocean were infinite, only type (4) would be allowed.

The table below gives the frequencies $\omega = Uk$ for the first five normal modes of the system which satisfy the inviscid dispersion relation (3.2):

n \ U	13.411	54.083	100.0
1	12.0811	2.0680	2.0192
2	2.3296	2.0164	2.0047
3	2.1283	2.0074	2.0023
4	2.0692	2.0043	2.0016
5	2.0435	2.0032	2.0013

As the speed of the disturbance increases, the response will thus become more inertial. The relation (3.2) shows that $\omega = \pm 2$ are accumulation points for the normal modes of the system.

Finally, the familiar frequency limitation to $4 < \omega^2 < 5$ is seen, both in equation 3.2 and figures 3.1 to 3.6.

3.3 The role of friction

The characteristic equation is a cubic in m^2 and thus has three pairs of plus and minus roots. This suggests two boundary layer structures corresponding to the two viscous pairs of roots as well as the inviscid pair just discussed.

First consider the effect of friction on the inviscid roots, i.e., the propagating waves. Inspection of (3.1) suggests that, for these roots, m^2 be expanded in powers of E :

$$m^2 = \sum_{n=0} E^n (m^{(n)})^2 \quad (3.6)$$

This yields the following equations

$$O(E^0): \quad M^{(0)2} = \frac{k^2(5-\omega^2)}{(\omega^2-4)} \quad (3.7)$$

$$O(E): \quad M^{(1)2} = \frac{[-2i\omega M^{(0)4} - \frac{ik^2}{\omega}(4\omega^2-5)M^{(0)2} - 2i\omega k^4 + i\frac{5k^4}{\omega}]}{(\omega^2-4)}$$

This expansion breaks down when $E M^{(1)2} / M^{(0)2}$ is $O(1)$. As the inviscid wave number grows when $\omega^2 \rightarrow 4$, the largest term in $M^{(1)2}$ grows as

$$-\frac{2i\omega M^{(0)4}}{(\omega^2-4)}$$

Thus, when
$$\frac{-2i\omega M^{(0)4} E}{(\omega^2-4)} = O(1) \quad (3.8)$$

i.e., when $(\omega^2-4) = O(E^{1/2})$ the first two terms of the expansion are of the same order and a new expansion is necessary. The expansion also is invalid for large values of k , i.e., for $k = O(E^{-1/2})$.

Thus, waves with non-inertial frequencies and horizontal wave numbers of $O(1)$ or less travel vertically for an e-folding distance of $O(E^{-1/2})$. As their frequency approaches inertial, however, the waves decrease their vertical wavelength, thus allowing friction a stronger role. The inviscid balance between terms (3) and (5) in (3.1) and the inviscid expansion (3.6) fail when (3.8) holds. Term

(2) which represents friction due to vertical shear of the horizontal velocities becomes important. At this point $M^{(0)2} = O(E^{-1/2})$ and the previously inviscid root has grown to $O(E^{-1/4})$. The wave motion will thus be trapped frictionally in a layer whose thickness is $O(E^{1/4})$. For $E=10^{-4}$ this thickness amounts to one tenth of the ocean's depth.

Now consider the boundary layer structures. These are the roots corresponding to the upper two curves in the numerical solutions. If the wind stress were steady ($\omega=0$), an Ekman layer of thickness of $O(E^{1/2})$ would be established and this suggests that roots of $O(E^{-1/2})$ be looked for. To do this write

$$M^2 = E^{-1} \sum_{n=0} E^n \zeta^{(n)2} \quad (3.9)$$

which yields the following sequence:

$$O(E^0): \zeta^{(0)6} - 2i\omega \zeta^{(0)4} - (\omega^2 - 4) \zeta^{(0)2} = 0$$

$$O(E): 3\zeta^{(0)4} \zeta^{(1)2} - 4i\omega \zeta^{(0)2} \zeta^{(1)2} + 3k^2 \zeta^{(0)4} - (\omega^2 - 4) \zeta^{(1)2} - i \frac{k^2}{\omega} (4\omega^2 - 5) \zeta^{(0)2} + k^2 (5 - \omega^2) = 0$$

and hence, $\zeta^{(0)2} = i(\omega \pm 2)$

(3.10)

$$\zeta^{(1)2} = \frac{-3k^2 \zeta^{(0)4} - ik^2(4\omega^2 - 5)\zeta^{(0)2} + k^2(S - \omega^2)}{2\zeta^{(0)4} - 2i\omega \zeta^{(0)2}}$$

$\zeta^{(0)2} = i(\omega \pm 2)$ means that $M^{(0)2} = \frac{i(\omega \pm 2)}{E}$. For

$\omega = 0$, this reduces to the steady Ekman layer case. As ω becomes non-zero, the Ekman layer splits into two layers and these will be referred to as Ekman-Stokes layers. One is thicker than an Ekman layer (corresponding to the - sign for $\omega > 0$) and one is thinner (corresponding to the + sign for $\omega > 0$).

For $\omega > 0$, the thinner layer is well described by (3.10). The thicker layer, however, has a singularity near the inertial frequency.

As $\zeta^{(0)}$ approaches zero when $\omega \rightarrow \pm 2$, $\zeta^{(1)2}$ behaves like

$$\frac{k^2(S - \omega^2)}{-2i\omega \zeta^{(0)2}}$$

Thus, $E \zeta^{(1)2} / \zeta^{(0)2}$ approaches 0(1) when

$$\frac{Ek^2(S - \omega^2)}{-2i\omega \zeta^{(0)4}} = O(1) \quad (3.11)$$

i.e., when $\omega \pm 2 = O(E^{1/2})$. At this point $M = O(E^{-1/4})$.

The thicker Ekman-Stokes layer, then, grows to a thickness of $O(E^{1/4})$ as the frequency approaches inertial and the asymptotic

expansion (3.9) breaks down. What was a balance between terms (1), (2) and (3) in the characteristic equation (3.1) must now include other terms. For $m = O(E^{-1/4})$ it can be seen from (3.1) that a new balance among (2), (3) and (5) occurs.

As in the case of the inviscid root, the expansion (3.9) breaks down for $k = O(E^{-1/2})$.

To summarize the results of this chapter, figure 3.9 shows the dominant forces acting in the various frequency ranges discussed. The figure is plotted for $U = 13.411$ and is typical of all three speeds.

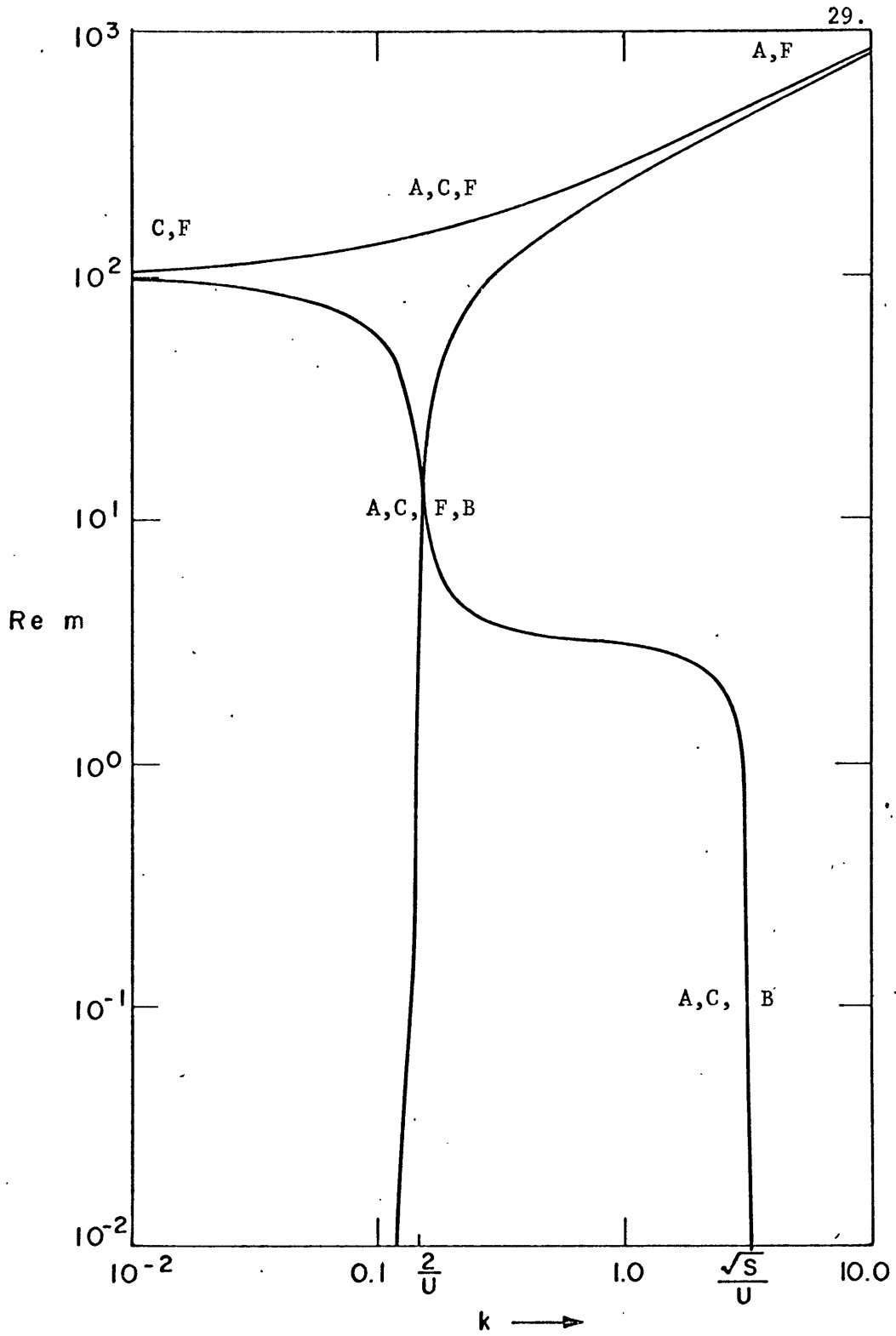


Figure 3.9 $Re\ m$ vs. k for $U = 13.411$. The letters refer to the various forces acting in each region and are A-acceleration, B-buoyancy force, C-Coriolis force, and F-frictional forces.

4. The response to an idealized travelling wind distribution

In this chapter is discussed the oceanic response to the idealized travelling wind distribution described below. The equations and boundary conditions are as posed in Chapter 2. Thermal conductivity is neglected.

4.2 Specification of an idealized stress field for a travelling front

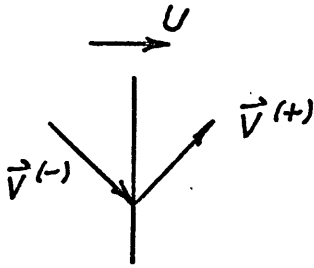
The frontal stress system to be modelled is one dimensional (no north-south variation), is travelling toward the east (positive x) and has an exponential decay of wind speed away from the frontal line. It takes the general form

$$\vec{\tau}(x-ut) = \vec{C}_1 e^{-\alpha(x-ut)} H(x-ut) + \vec{C}_2 e^{\alpha(x-ut)} H(-x+ut)$$

α^{-1} is the e-folding decay distance of the stress away from the front. It is set equal to 10^2 (or 400 km in dimensional units). $H(\xi)$ is the Heaviside function:

$$H(\xi) = \begin{cases} 0 & \xi < 0 \\ 1 & \xi > 0 \end{cases}$$

\vec{C}_1 and \vec{C}_2 are determined as follows. Far above the sea surface and in close proximity to the frontal line, the wind velocities are assumed to be:



$$\vec{V}^{(-)} = (V_x^{(-)}, V_y^{(-)}) = U(1, -1)$$

$$\vec{V}^{(+)} = (V_x^{(+)}, V_y^{(+)}) = U(1, 1)$$

where (+), (-) refer to "in front of" and "behind" the front respectively. The winds 10 meters above the sea surface are obtained from these "geostrophic" values by rotating them 22.5° to the left and decreasing their magnitude 60%. This simulates the effect of the atmospheric boundary layer. (See G.I. Taylor, 1915.) Thus, if these near surface winds are denoted by \vec{V}_s :

$$\begin{pmatrix} V_{sx}^{(\bar{+})} \\ V_{sy}^{(\bar{+})} \end{pmatrix} = 0.6 \begin{pmatrix} \cos 22.5^\circ & -\sin 22.5^\circ \\ \sin 22.5^\circ & \cos 22.5^\circ \end{pmatrix} \begin{pmatrix} V_x^{(\bar{+})} \\ V_y^{(\bar{+})} \end{pmatrix}$$

Then,

$$\vec{V}_s^{(-)} = U(0.784, -0.325)$$

$$\vec{V}_s^{(+)} = U(0.325, 0.784)$$

The assumption that the wind velocities are proportional to U , the speed of translation of the system, is to some extent an arbitrary simplification. A stationary front, for example, can have a discontinuity in the tangential velocity component.

To determine the stress on the ocean surface, it is assumed that its relation to the velocity is given in dimensionless form by:

$$\vec{T}' = \left(\frac{\rho_{air} C_D}{\rho_0 E} \right) |\vec{V}| \vec{V} \quad (4.4)$$

where \vec{T}' is the stress \vec{T} evaluated at $x-Ut=0$, $\rho_{air} = 1.225 \times 10^{-3} \text{ gm cm}^{-3}$ and C_D is a drag coefficient assumed to be $C_D = 0.002$ (Deacon et al 1956). \vec{C}_1 and \vec{C}_2 are now given by

$$\vec{C}_1 = \vec{T}^{(+)} = U^2 \times 10^{-2} (0.6703, 1.6296)$$

$$\vec{C}_2 = \vec{T}^{(-)} = U^2 \times 10^{-2} (1.6296, -0.6703)$$

It will be necessary to know the Fourier transform of the wind stress:

$$\begin{aligned} \vec{T}(k) &= \int_{-\infty}^{\infty} \vec{T}(\xi) e^{-ik\xi} d\xi \\ &= \int_{-\infty}^{\infty} [\vec{C}_1 e^{-\alpha\xi} H(\xi) + \vec{C}_2 e^{\alpha\xi} H(-\xi)] e^{-ik\xi} d\xi \\ &= \frac{\vec{C}_1}{\alpha+ik} + \frac{\vec{C}_2}{\alpha-ik} = \frac{-i(k+id)\vec{C}_1 + i(k-id)\vec{C}_2}{k^2+d^2} \quad (4.5) \end{aligned}$$

τ_x and τ_y as functions of $(x-Ut)$ are shown in figure 4.1, as is $|\tau_x|$ and $|\tau_y|$ as a function of k (real).

The response will be calculated for three values of the frontal speed U :

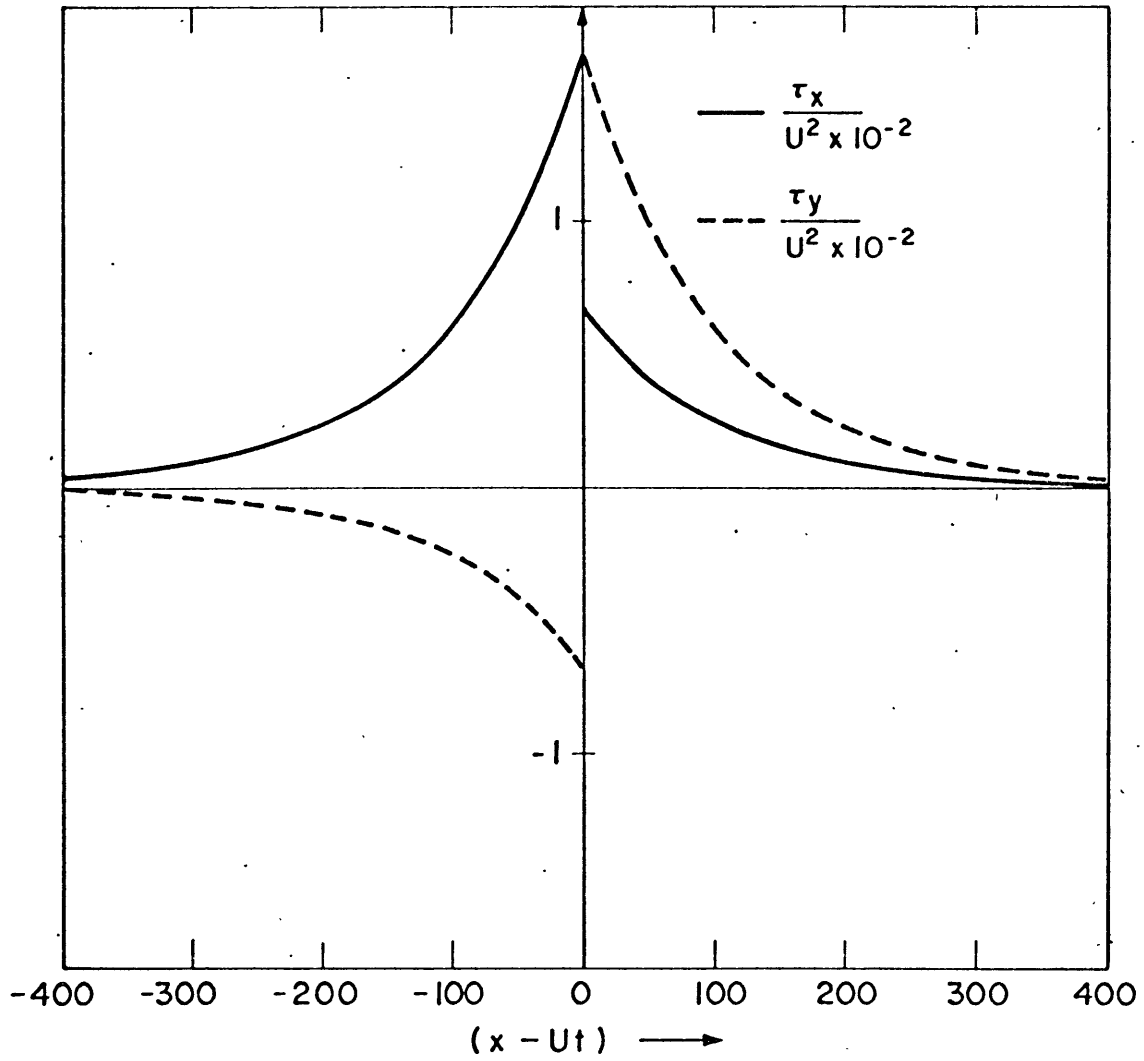


Figure 4.1a The wind stress $\vec{\tau}$ as a function of $x-Ut$. The e-folding distance is 100 (400 km.).

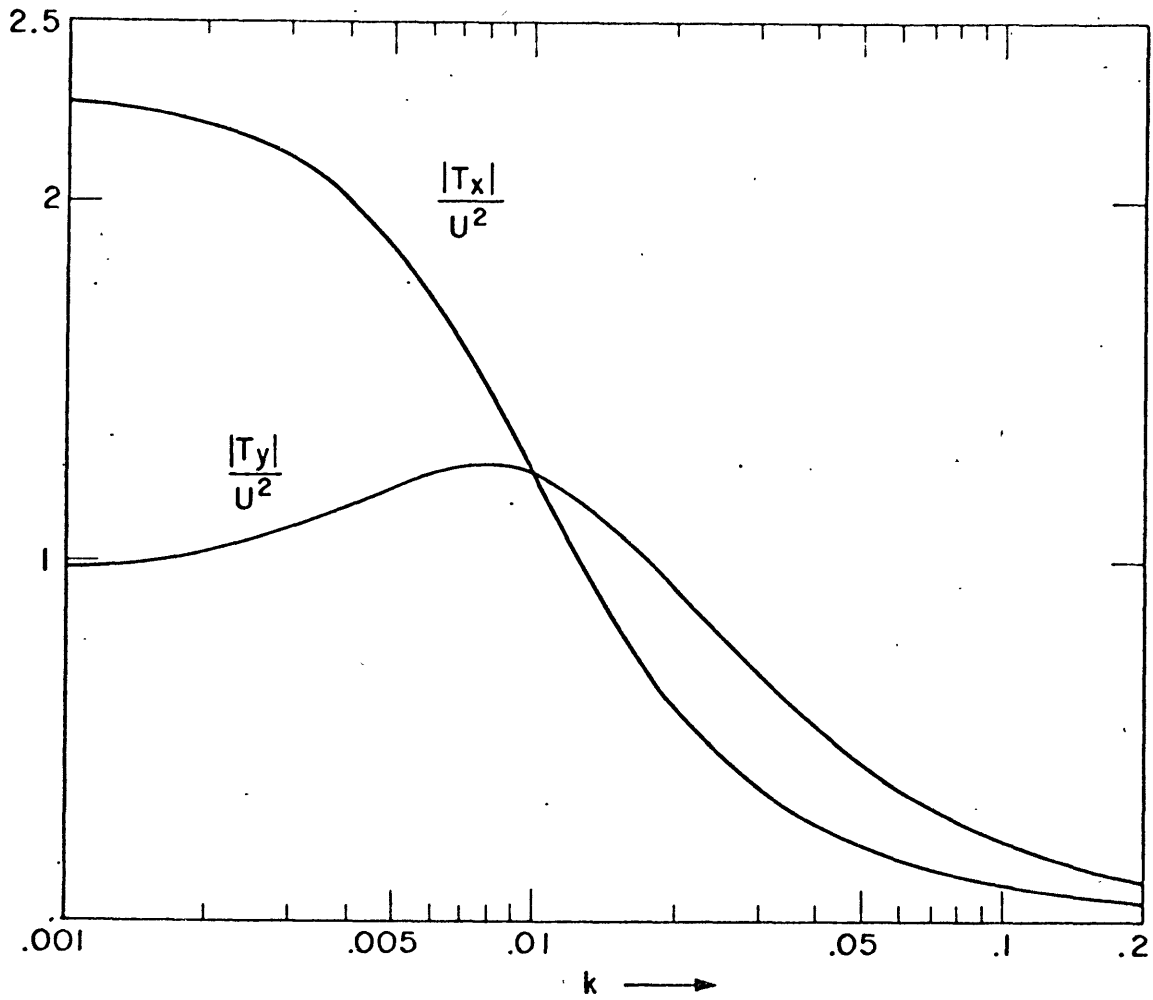


Figure 4.1b The transform, \vec{T} , of \vec{E} . The maximum of T_y is at $k = 0.00807$. The inertial wave numbers are (0.149, 0.0370, 0.020) corresponding to the three values of U : (13.411, 54.083, 100.0).

$$\begin{aligned}
 U_1 &= 13.411, & U_{\text{dimensional}} &= 2.48 \text{ m sec}^{-1} \\
 U_2 &= 54.083, & U_{\text{dimensional}} &= 10.0 \text{ m sec}^{-1} \\
 U_3 &= 100.0, & U_{\text{dimensional}} &= 18.45 \text{ m sec}^{-1}
 \end{aligned}$$

Different values of U were chosen to study the effect of frontal speed on the frequency of the response. $U_2 = 10 \text{ m sec}^{-1}$, dimensionally, is an average summer-winter storm speed.

The dimensional stresses, in dynes cm^{-2} , corresponding to these speeds are as follows:

U	U_{dim} (m sec^{-1})	\vec{c}_1 dimensional (dynes cm^{-2})	\vec{c}_2 dimensional (dynes cm^{-2})
13.411	2.48	(.04104, .09976)	(.09976, -.04104)
54.083	10.0	(0.667, 1.622)	(1.622, -0.667)
100.0	18.45	(2.282, 5.547)	(5.547, -2.292)

The velocity U has been used in two ways: to define the speed of progression of the stress system, and to define an amplitude for the stress. Within the linear framework of the model, this second use is arbitrary, and the numerical results shown in the figures can be reinterpreted by any reader who wishes to assign a different magnitude to the amplitude of the stress associated with one of the three translational speeds. One other point about this

stress system is that it models only that part of the atmospheric winds which are closely associated with the front. For example, a steady uniform geostrophic west wind could be superimposed if a more complete picture of the stress were sought. Except for some minor effects entering through the V^2 law in (4.4), this would only add a steady Ekman layer (with surface current directed SSE) to the solutions computed here.

4.2 Method of solution for the problem

The dependent variables will be synthesized from the set of exponential functions discussed in section 3.1. Thus, if φ is any dependent variable:

$$\varphi = \frac{1}{2\pi} \int_{-\infty}^{\infty} \Phi(k, z) e^{ik(x-ut)} dk$$

$$\Phi(k, z) = \sum_{j=1}^6 \Phi_j(k) e^{iM_j(k)z} \quad (4.6)$$

The M_j 's, as before, satisfy the characteristic equation (3.1). The w field is used here as the working dependent variable and the other fields can be obtained from it by the relations:

$$(u, v, p, \rho) \leftrightarrow (U_j, V_j, P_j, R_j) = \left(-\frac{M_j}{k}, \frac{2M_j}{k(-i\omega + Ek_j^2)}, \frac{-i\omega + Ek_j^2 + i\frac{S}{\omega}}{-iM_j}, \frac{-i}{\omega} \right) W_j$$

The boundary conditions (4.2) require that

$$z=0, \quad u=0 \rightarrow \sum_{j=1}^6 \frac{-\mu_j}{k} W_j = 0 \quad 37.$$

$$v=0 \rightarrow \sum_{j=1}^6 \frac{z \mu_j}{k(-i\omega + E x_j^2)} W_j = 0$$

$$w=0 \rightarrow \sum_{j=1}^6 W_j = 0$$

$$z=1, \quad \frac{\partial u}{\partial z} = T_x \rightarrow \sum_{j=1}^6 \frac{-i \mu_j^2}{k} e^{i \mu_j} W_j = T_x$$

$$\frac{\partial v}{\partial z} = T_y \rightarrow \sum_{j=1}^6 \frac{z i \mu_j^2}{k(-i\omega + E x_j^2)} W_j = T_y$$

$$w=0 \rightarrow \sum_{j=1}^6 W_j e^{i \mu_j} = 0$$

4.8

These equations completely determine the integrand of (4.6) and it remains only to invert the transform. This was done numerically and a discussion of the procedure involved appears in Appendix 1.

4.3 Discussion of solutions

The horizontal velocities u and v at various depths for $U = 13.411$ are shown in figures 4.2 to 4.6. On the surface, the passage of the front is preceded by a non-oscillatory buildup of velocity, showing no evidence of upstream waves. The fact that the u velocity is larger than the v velocity in this region, although the stress is oriented more in the y direction, indicates an incompletely established Ekman layer type structure. The ratio of u to v corresponds to the surface current being approximately 38° to

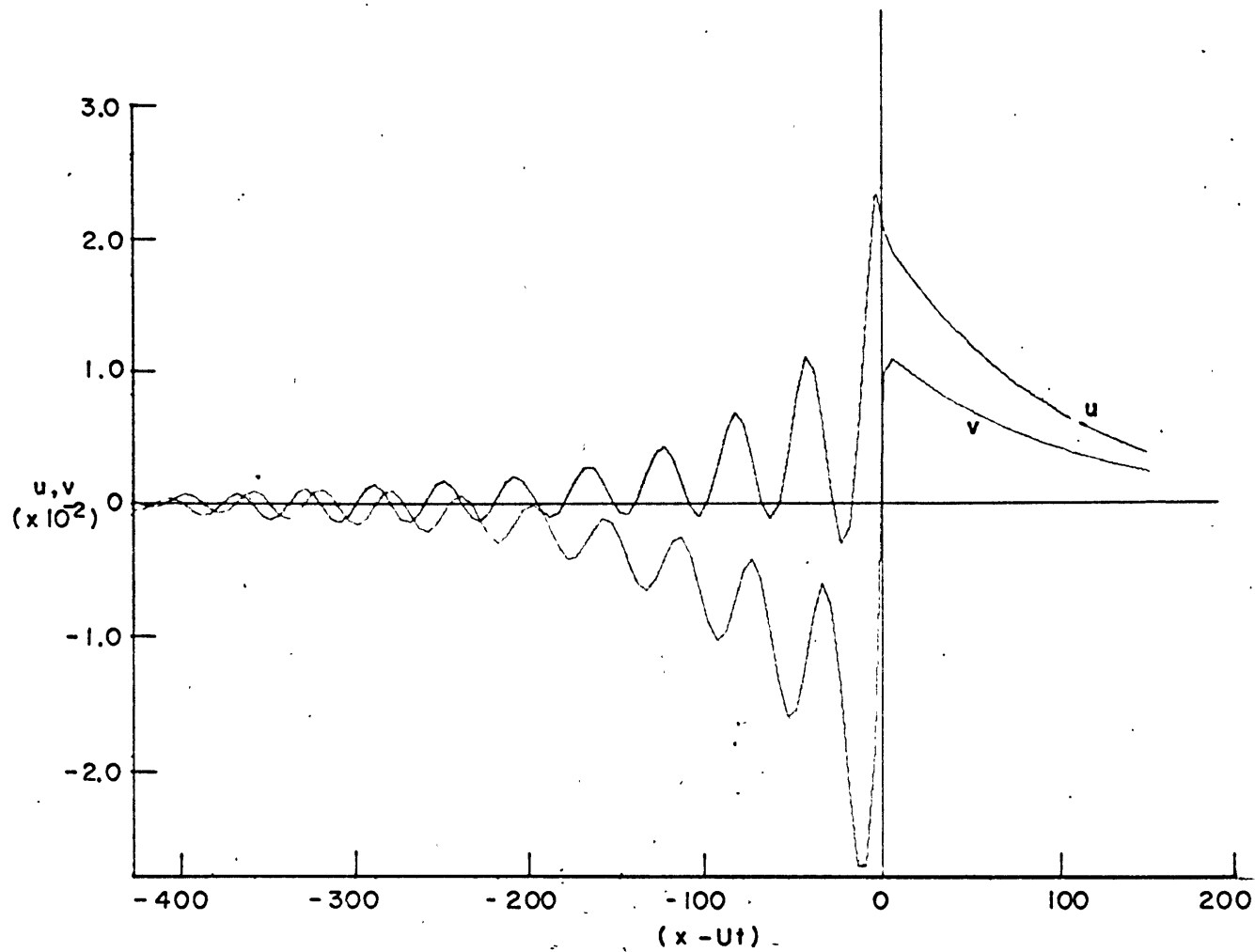


Figure 4.2 u and v for $U = 13.411$ (2.5 m sec^{-1}) and $Z = \text{surface}$. Unity on the ordinate is $18.45 \text{ cm sec}^{-1}$. Unity on the abscissa is 1 ocean depth (4 km.).

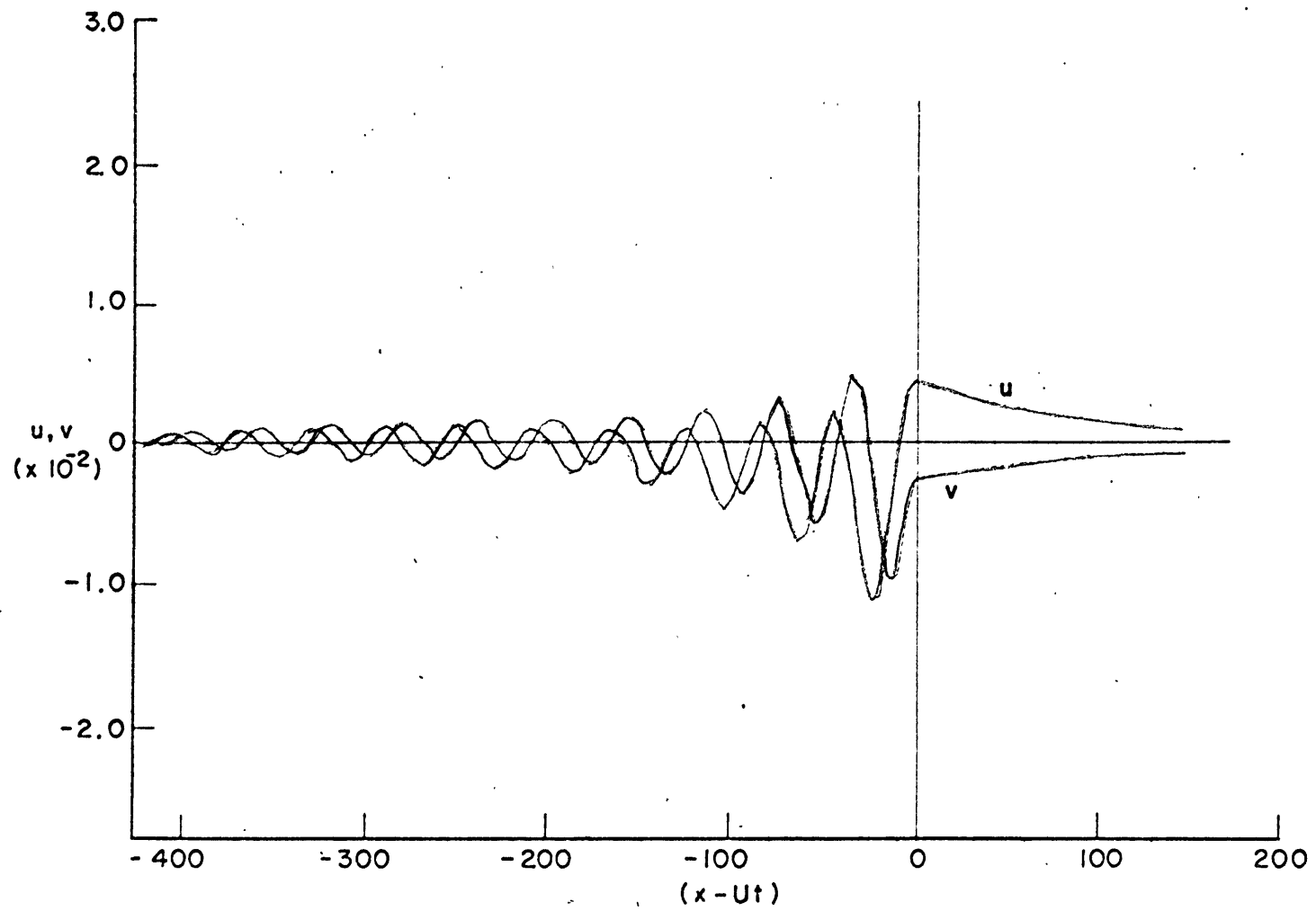


Figure 4.3 The same as 4.2 but $Z = 50$ m.

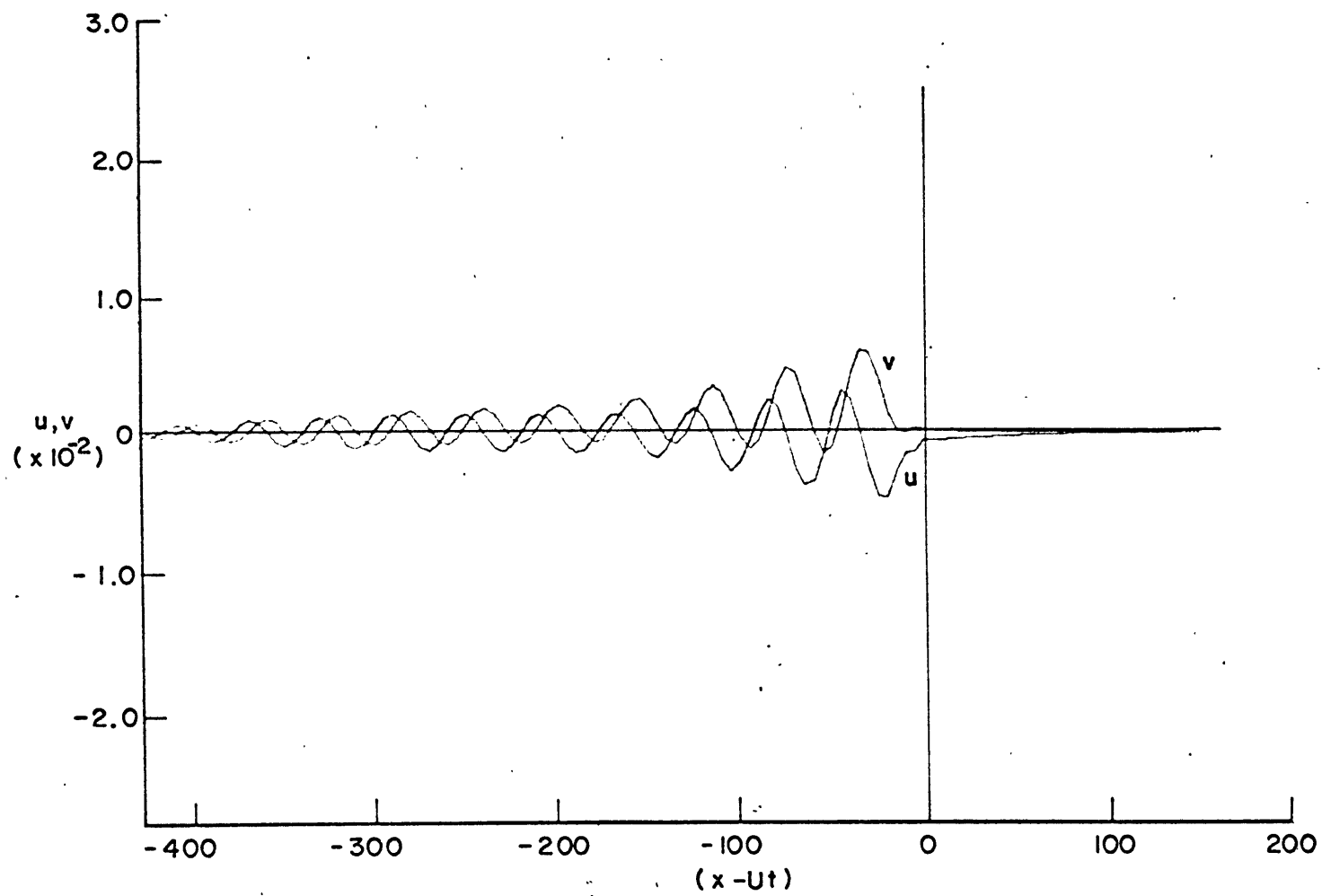


Figure 4.4 The same as 4.2 but $Z = 100$ m.

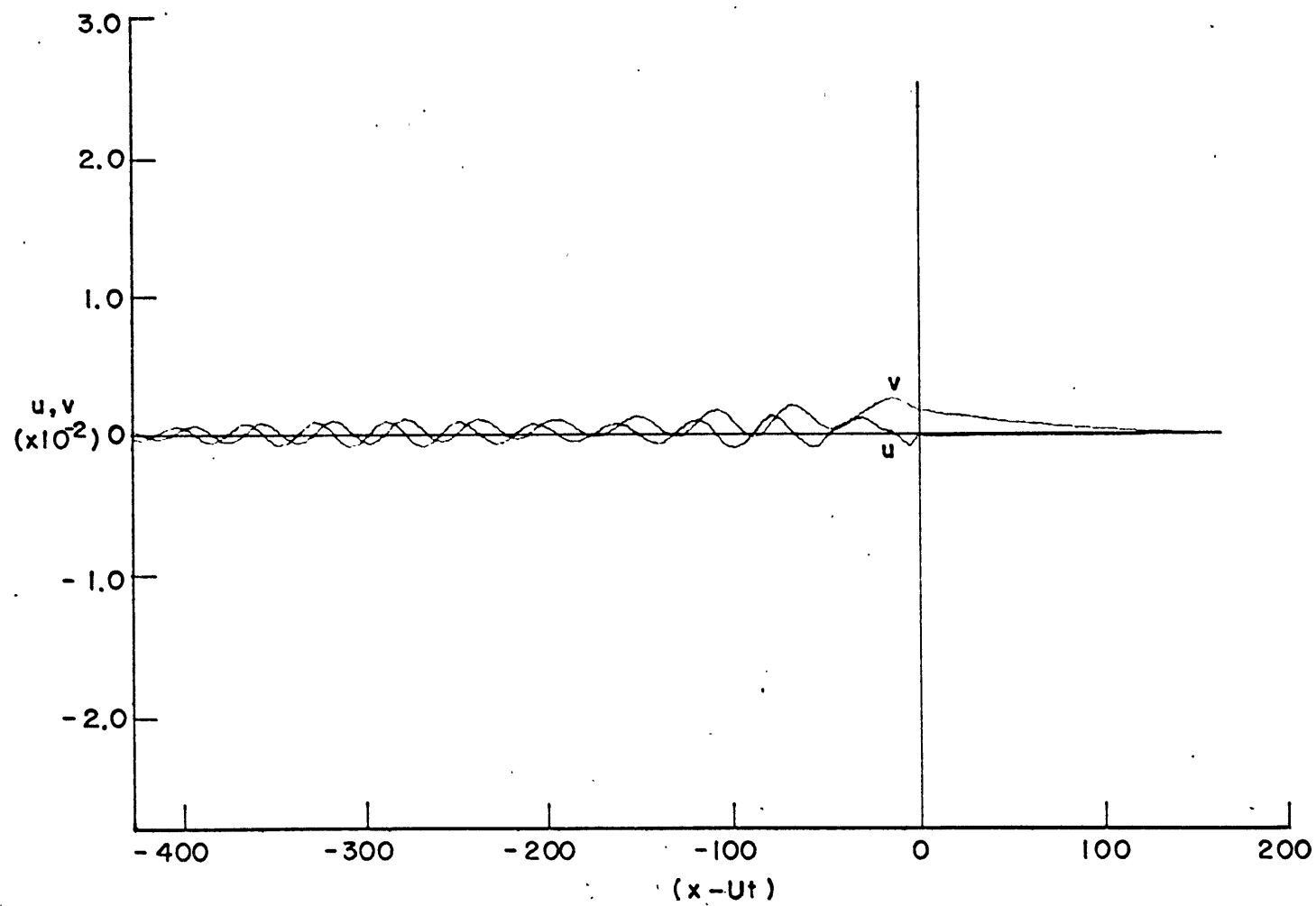


Figure 4.5 The same as 4.2 but $Z = 200$ m.

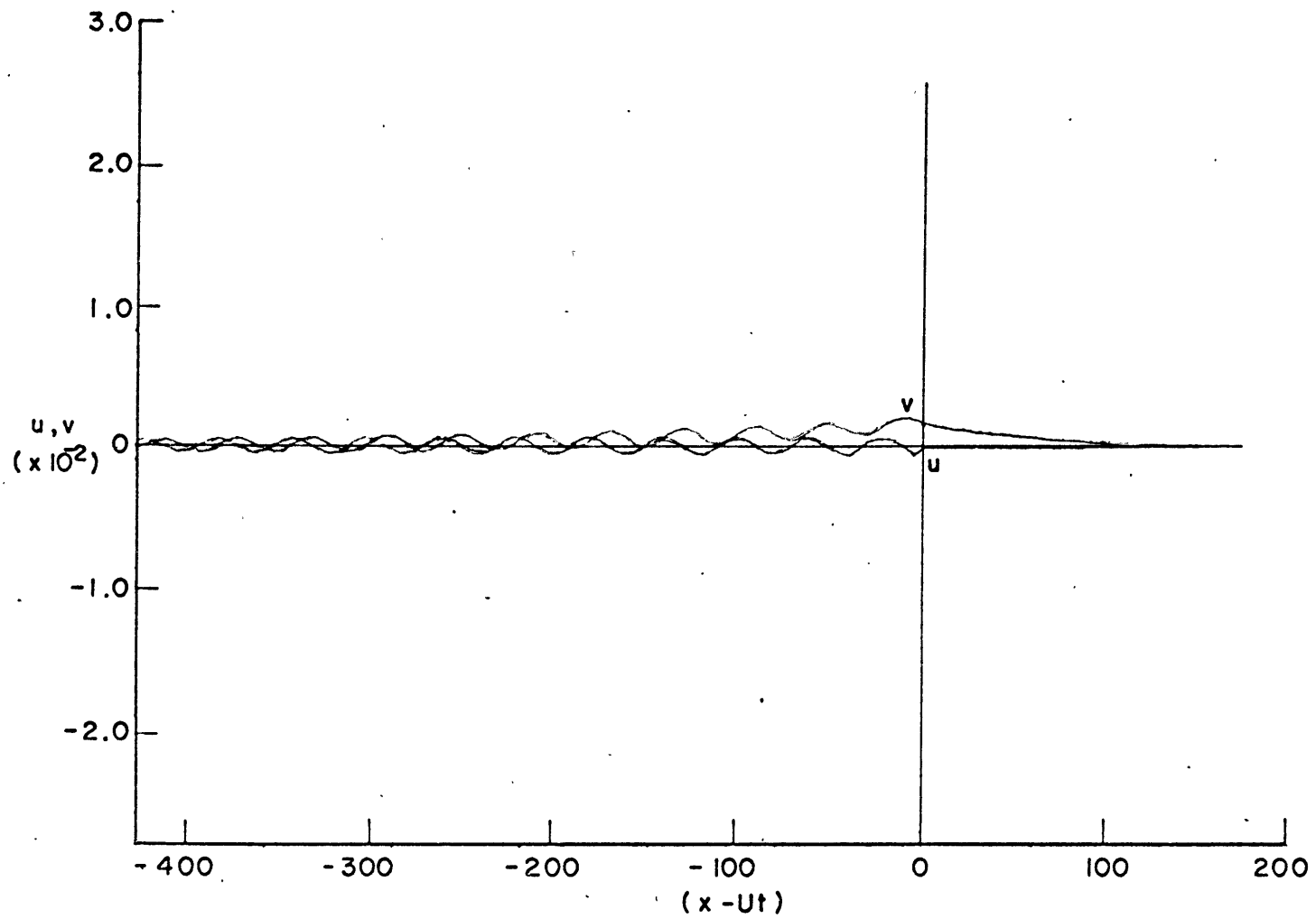


Figure 4.6 The same as 4.2 but $Z = 1000$ m.

the right of the wind stress (the stress is 22.5° to the right of the y axis before the front; see section 4.1). This compares to an angle of 45° in the steady state case. The horizontal variation of the pre-front velocity field is similar to that of the stress field.

Just as the front passes, the velocities reach their maximum values. The v velocity field has a strong jump corresponding to the jump in the y component of the applied stress. The u field similarly emulates the applied stress.

Behind the front the solution is a superposition of an exponentially decaying field and an oscillatory wake, also decaying in amplitude. The e-folding distance (100, or, dimensionally, 400 km) of the non-oscillatory part of the solution is independent of the speed of the front. In this case, $U = 13.411$, the superposition is most obvious. For this speed, the wavelength of the oscillatory solution is quite short (42.1, or, dimensionally, 168.4 km) and, hence, many wavelengths fit into the region of the non-oscillatory solution.

The frequency of the oscillations is approximately 3% higher than inertial. Of the three frontal speeds, this case shows the greatest deviation from the inertial frequency. This is to be expected from the discussion in section 3.2 of the frequencies of the inviscid normal modes.

The oscillatory response for all three cases is very close to inertial. This is because the scale of the forcing function (see figure 4.1) is attuned to forcing waves near the low end of the

allowable frequency range ($2 < \omega < \sqrt{S}$). The maximum in T_y can be shown to occur at

$$k = \pm \alpha \left[1 - 2 \left(\frac{C_{1y} + C_{2y}}{C_{1y} - C_{2y}} \right)^2 \right]^{1/2} = 0.00807$$

whereas the values of k given by $Uk=2$ are:

U	k
13.411	0.149
54.083	0.370
100.0	0.020

For this scale of disturbance, then, the response will be mostly inertial. To excite waves non-inertial in character, it would be necessary to have a smaller scale (greater α) disturbance. This would move the stress transform maximum to a higher value of k which, for fixed U , corresponds to a higher Doppler frequency.

The horizontal decay of the oscillatory wake at the surface is more rapid in this case than in the higher front speeds. By this is meant that the ratio of the amplitude of the N th crest after the front to the amplitude of the first crest is larger for the faster moving front. Figure 3.8 shows that the vertical group velocity increases from zero as the frequency increases from the inertial value. In this case, the waves are farthest from the inertial frequency and, hence, vertical dispersion of the energy put in at the surface by the wind stress will be greatest.

The depth dependence of the wave motion bears out the arguments of chapter 3. The wave motion is almost completely damped

at $z = 0.75$ (dimensionally 100 m). The e-folding distance of the $E^{1/4}$ layer discussed in chapter 3 is dimensionally 400 m and, hence, the motion should be approximately $\frac{1}{e^{2.5}} \approx \frac{1}{z}$ of the surface value of the oscillatory component. Comparison of figures 4.2 and 4.6 shows that this is approximately so in the computed solution.

The depth dependence of the non-oscillatory component of the solution shows a much more rapid decay. It has virtually disappeared at a depth of $z = 0.975$ (100 m) and this suggests that it is associated with the double Ekman-Stokes layer discussed in chapter 3. The depth behavior of this near front, non-oscillatory component of the response will be treated more fully in the case of $U = 54.083$.

The case $U = 54.083$ (10 m sec⁻¹) corresponds to a storm speed which is an average over summer and winter storms. The results for this case are presented in figures 4.7 - 4.10.

The pattern of velocities is similar to the slower moving case $U = 13.411$. The front is again preceded by a non-oscillatory solution and followed by the superposition of a decaying oscillatory wake and a decaying exponential.

The surface velocity preceding the front is again oriented to the right of the wind stress but several degrees less so than in the slowest moving case. The angle is now approximately 35° to the right of the stress. This smaller angle is due to the faster speed of the storm; the Ekman structure has less time to develop.

The structure of the solutions in the neighborhood of the

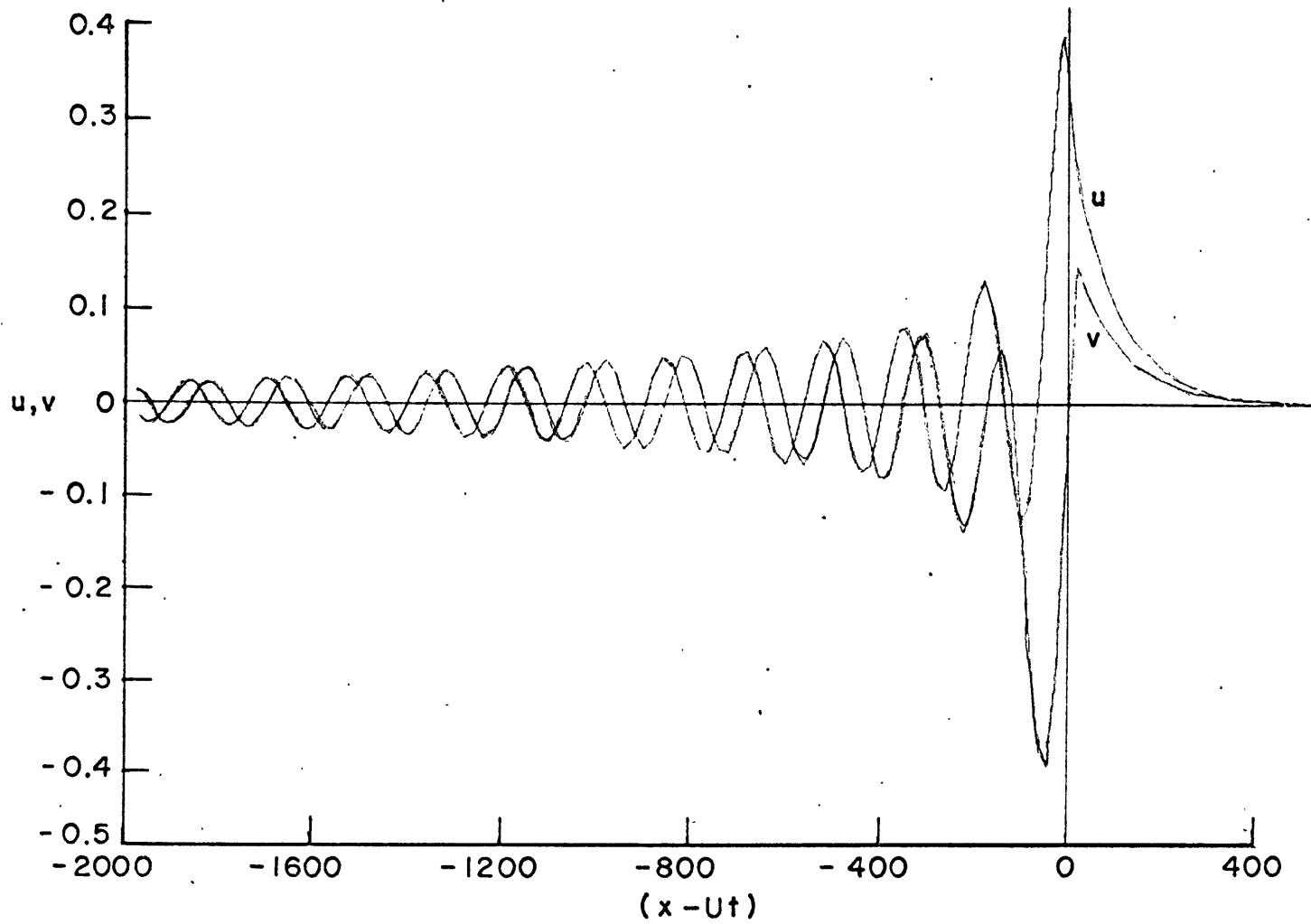


Figure 4.7 u and v for $U = 54.083$ (10 m sec.^{-1}) and $Z = \text{surface}$. Unity on both axes is the same as in figure 4.2.

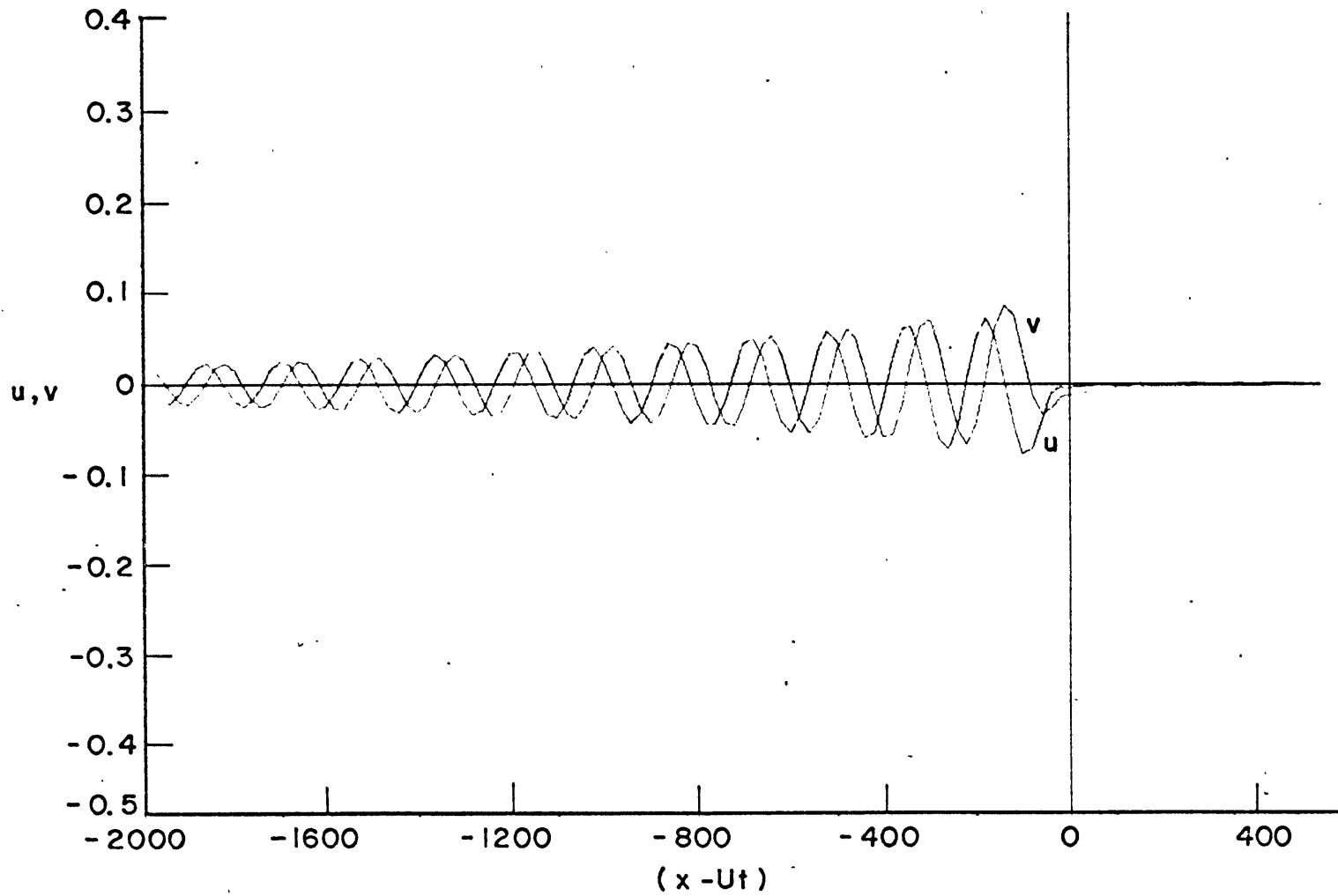


Figure 4.8 The same as 4.7 but $Z = 100$ m.

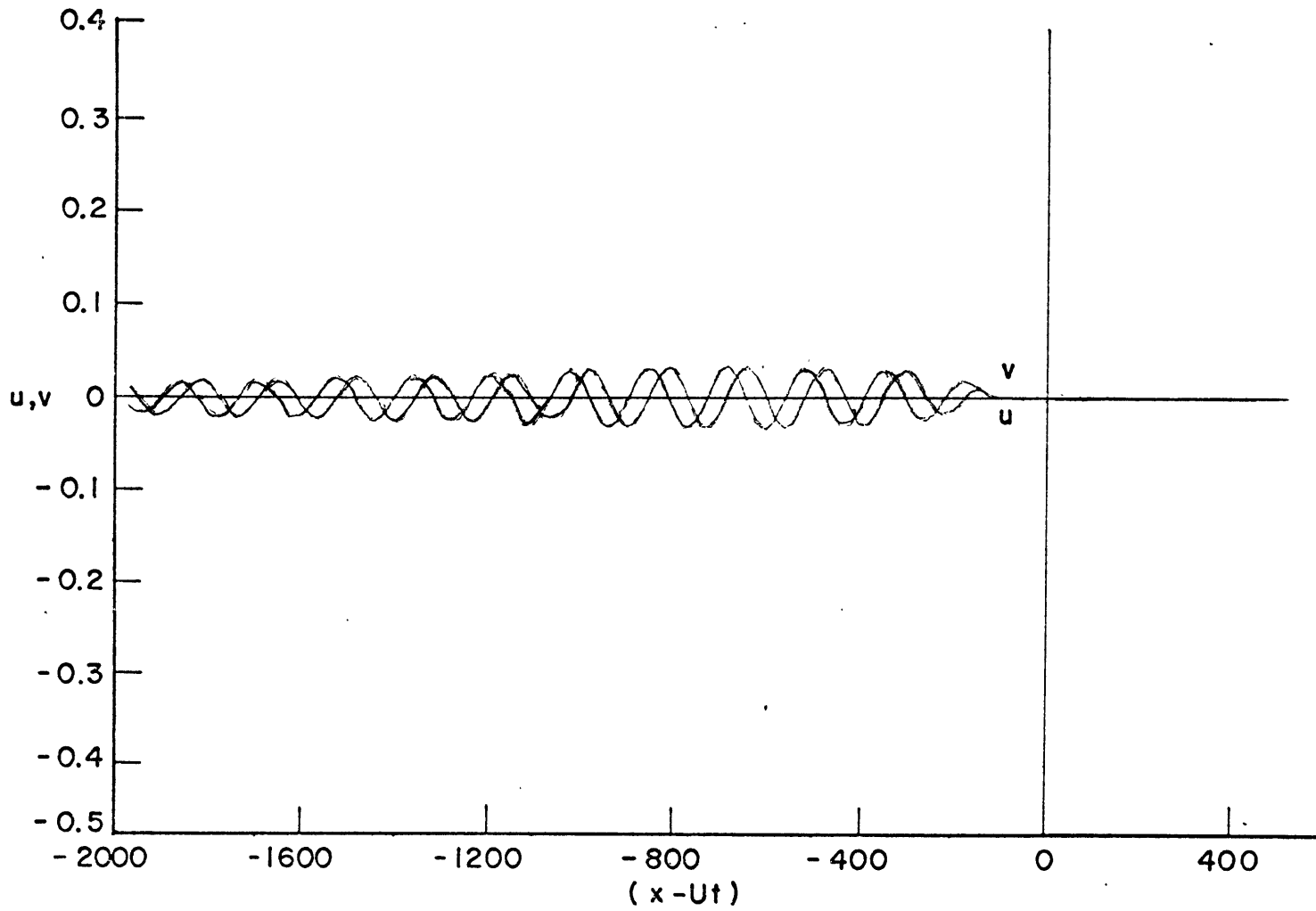


Figure 4.9 The same as 4.7 but $Z = 200$ m.

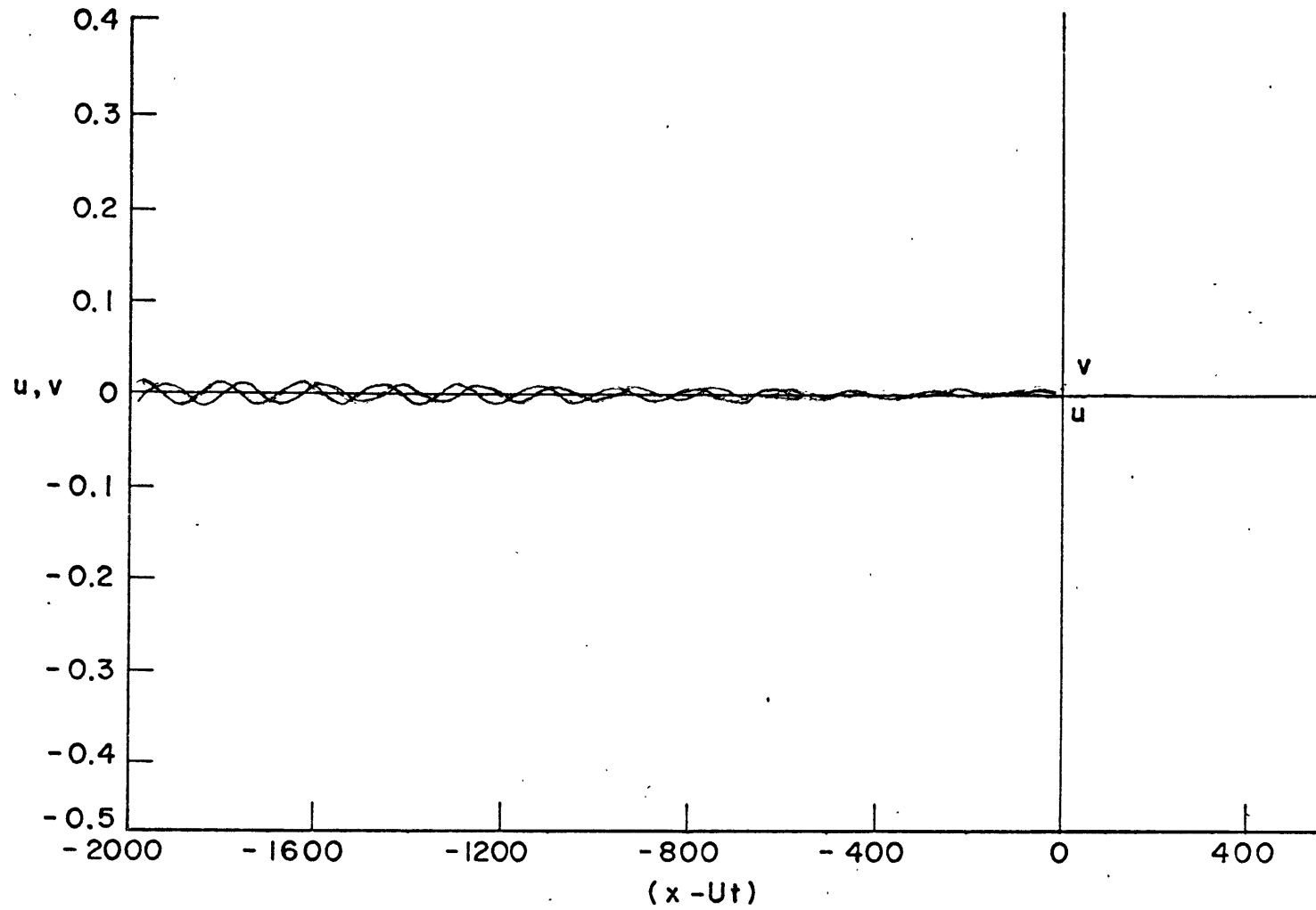


Figure 4.10 The same as 4.7 but $Z = 1000$ m.

front as a function of depth is shown in figure 4.11 for $U = 54.083$. These curves show that the non-oscillatory part of the solution is essentially confined to the double Ekman-Stokes layers discussed in chapter 3. The thickness of these layers is non-dimensionally

$$\delta = \left| \frac{E}{\sqrt{Uk \pm 2}} \right|$$

The length scales of the forcing function are $O(10^2)$ (see figure 4.1) and hence, $k = O(10^{-2})$. Then, $\delta = O(E^{1/2})$, or for the scaling used here, a dimensional e-folding thickness of 40 meters. Put another way, the Doppler frequency is close to zero and this results in the layers being close to the Ekman thickness. One would expect motion in these layers to be negligible after the five e-folding distances say, or 200 meters. This is indeed the case, as is seen in figure 4.11. The largest part of the total response, then, takes place in the near surface layers and in the immediate neighborhood of the front. The oscillatory wake, however, is not restricted to these thin layers.

Since in this case the horizontal wavelength in the wake is 170 (dimensionally 680 km) while the total storm length is around 400 (1600 km), the non-oscillatory component of the solution has disappeared after two or three waves have passed after the front. The wake regime, as a result, appears quite different from the slowest moving case

$$U = 13.411 .$$

The frequency of the waves is approximately 1% higher than inertial. The horizontal decay of the wave solutions for $U = 54.083$ is less rapid than in the $U = 13.411$ case due to its higher

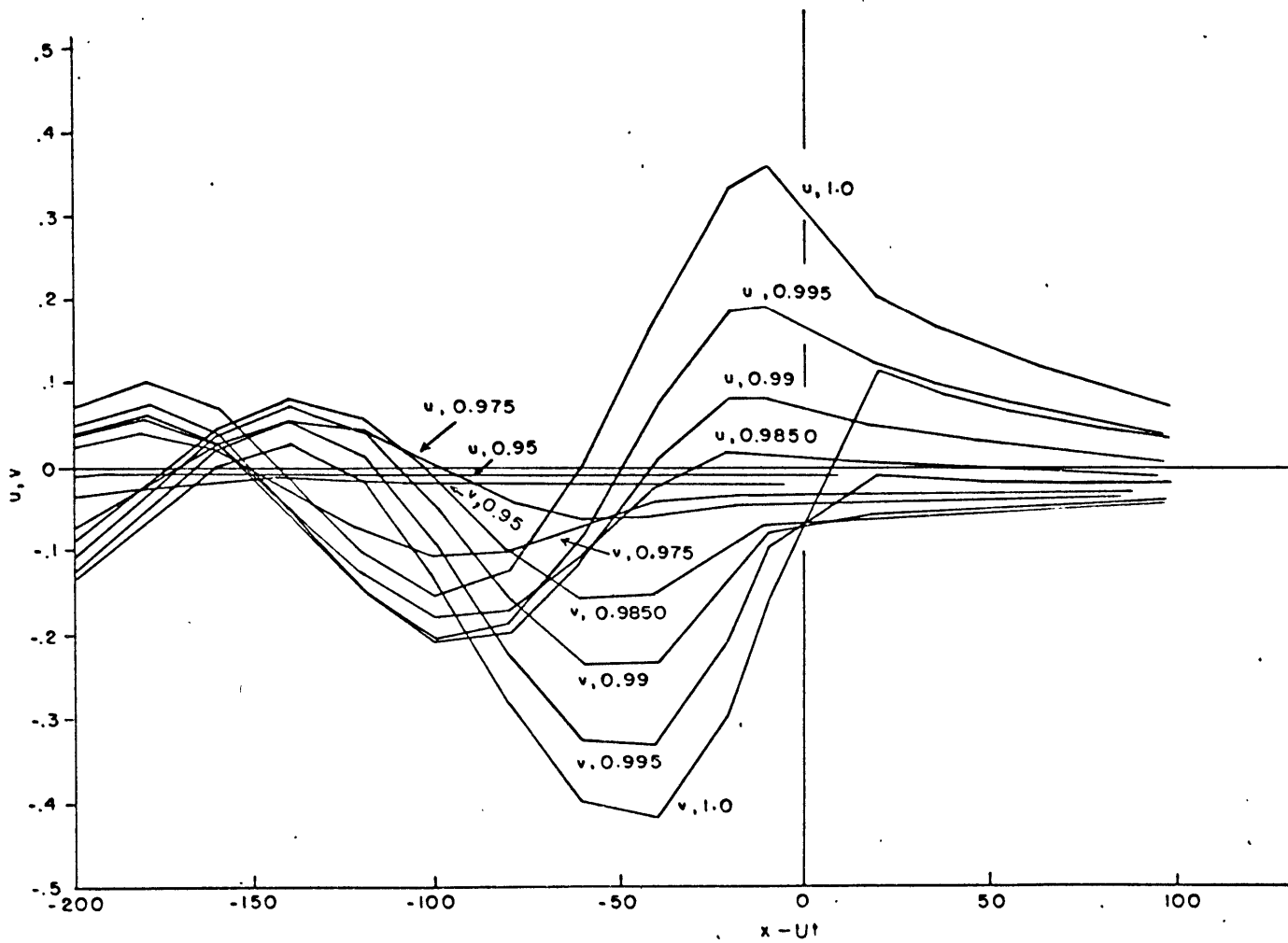


Figure 4.11 The structure of u and v as functions of $x-Ut$ for various values of Z near the front. $U = 54.083$. The axes here have the same scales as 4.7.

frequency and, hence, lower vertical group velocity. The vertical decay takes place over the upper 1000 m of the ocean as discussed in chapter 3.

The solutions for the fast frontal speed case $U = 100.0$ are shown in figures 4.12 - 4.15 and are similar to those for $U = 54.083$. The ratio of u to v in the solution preceding the front is the smallest for the three cases and corresponds to an angle of approximately 30° between the applied stress and the resultant surface velocity. This non-oscillatory solution again decays in the top 100 meters of the ocean and, because of the high speed, is a smaller part, spatially speaking, of the total solution than it is in the other two cases.

The frequency of the oscillatory wake is about 0.3% higher than inertial. The horizontal decay of the solution takes place more slowly than in the other cases due to the smaller dispersion resulting from the lower vertical group velocity.

The motion is substantially damped out at a depth of 1000 meters as in the previous cases.

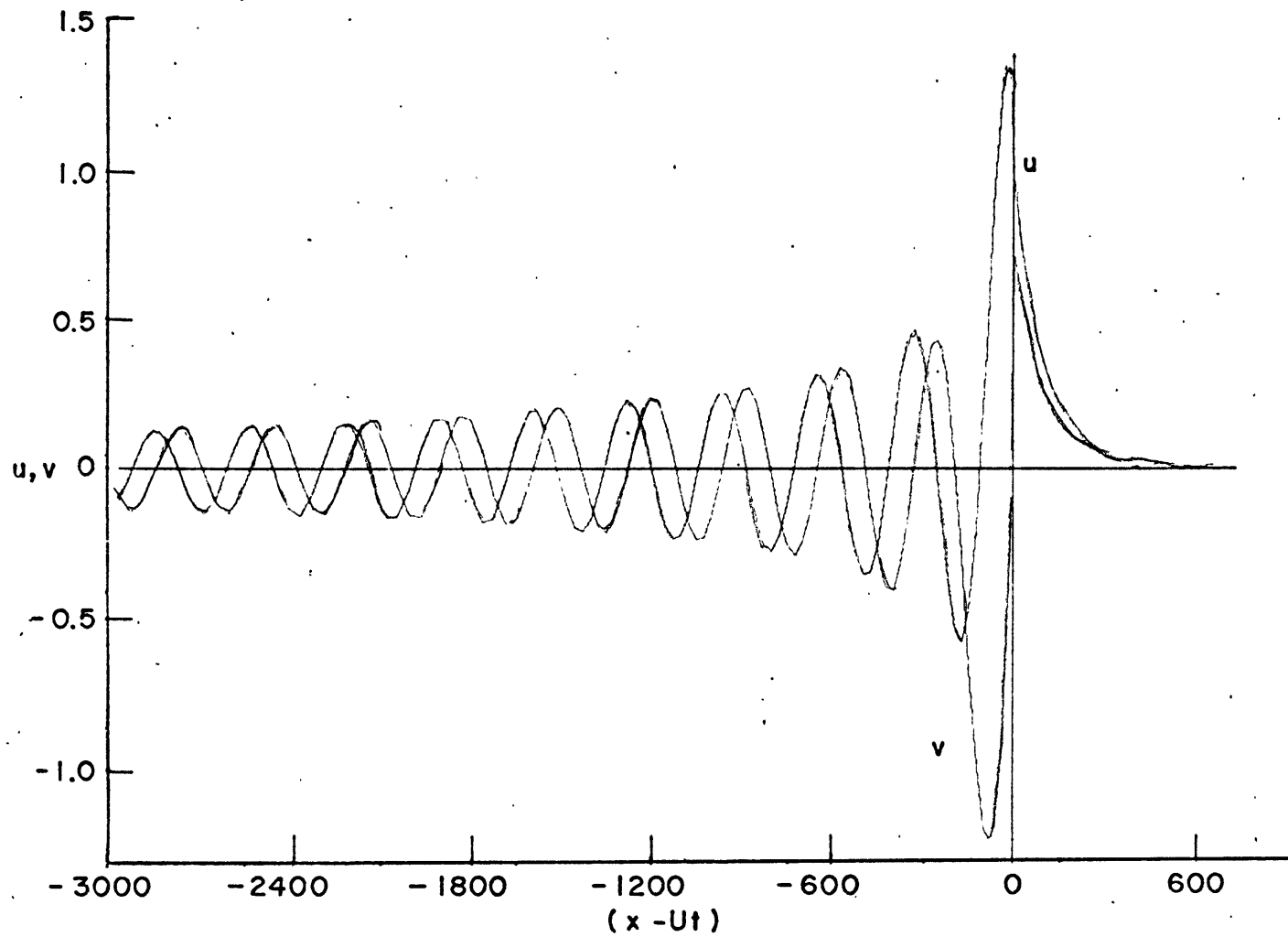


Figure 4.12 u and v for $U = 100.0$ ($18.45 \text{ m.sec.}^{-1}$) and $Z = \text{surface}$. Unity on both axes is the same as in figure 4.2.

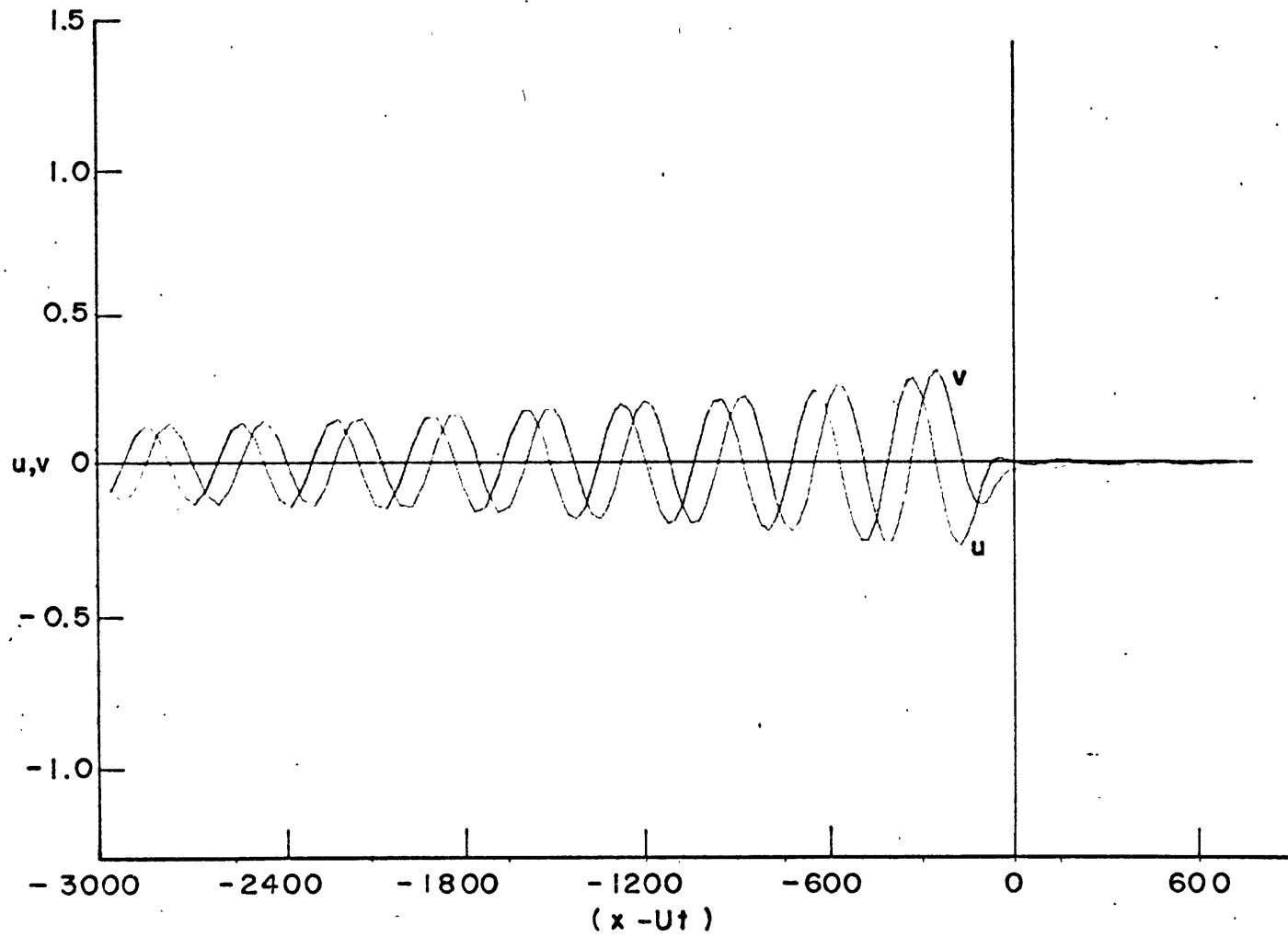


Figure 4.13 The same as 4.12 but $Z = 100$ m.

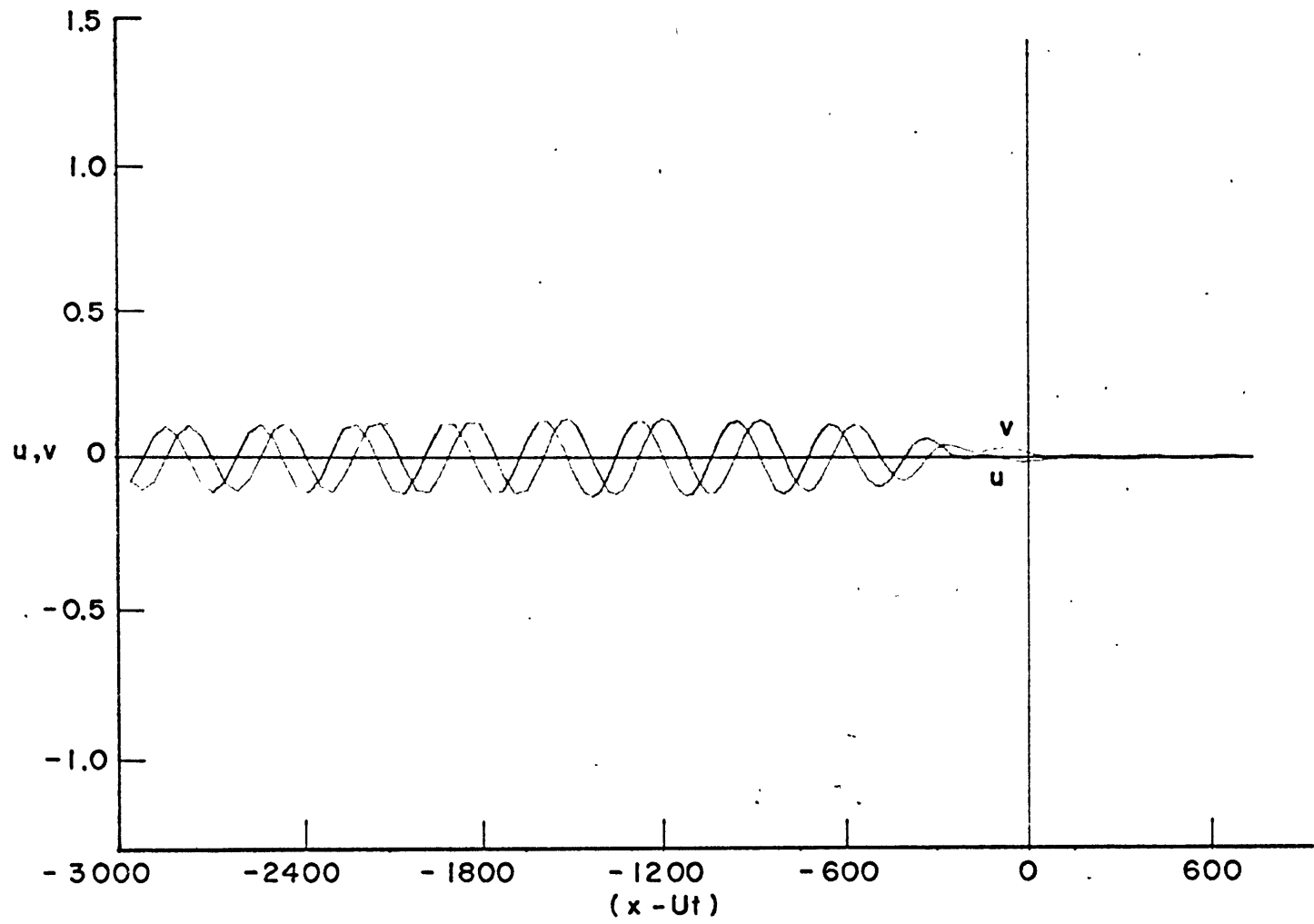


Figure 4.14 The same as 4.12 but $Z = 200$ m.

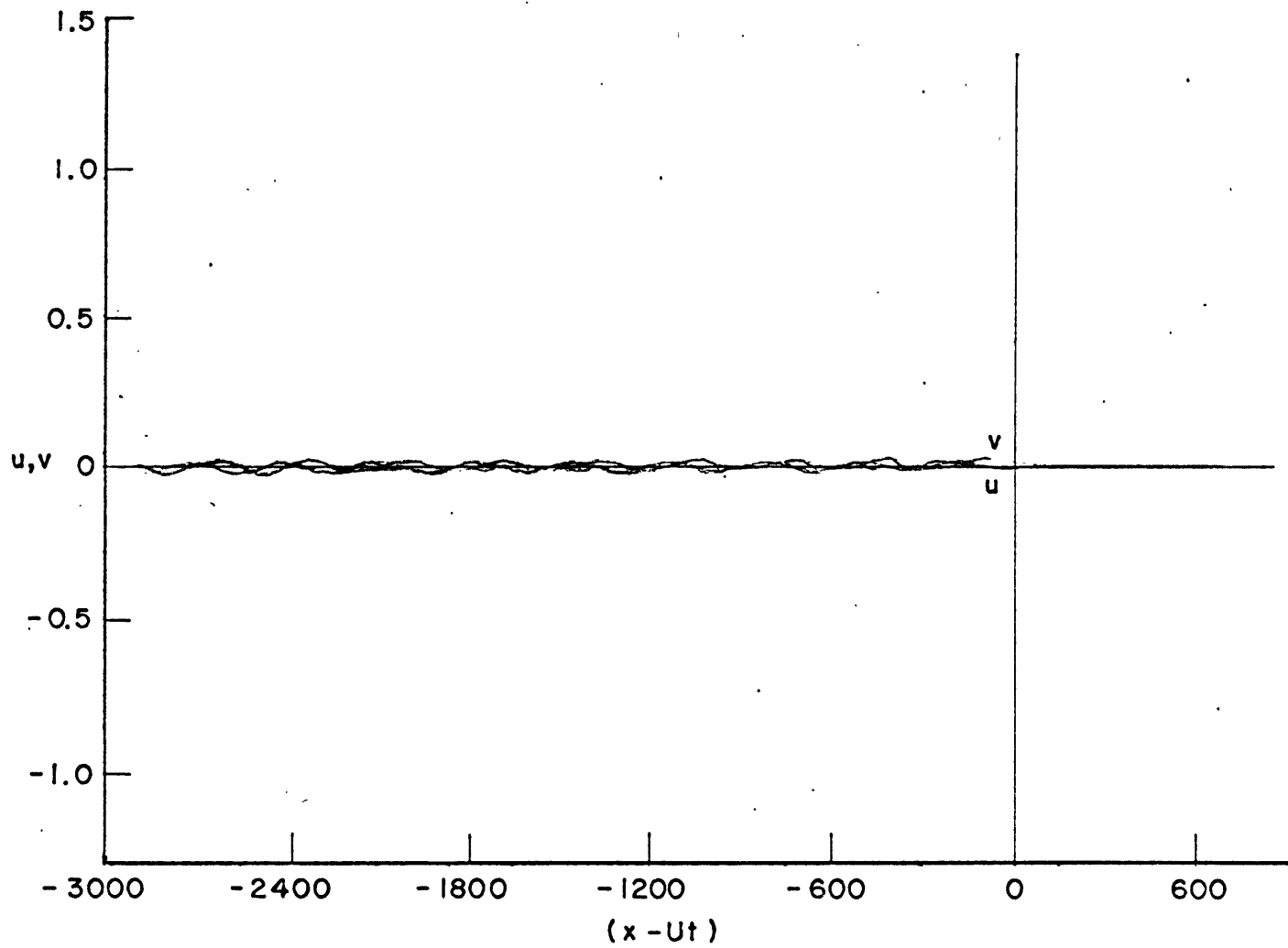


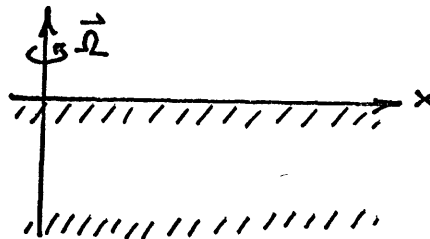
Figure 4.15 The same as 4.12 but $Z = 1000$ m.

5. The response to an idealized travelling wind distribution; the case of an infinitely deep ocean.

This chapter treats the response of an infinitely deep ocean to a travelling sinusoidal stress pattern as well as to the idealized front discussed in chapter 4. The infinite depth problem is far more tractable mathematically than the finite depth problem since, here, only three vertical wave numbers, rather than six, are needed to satisfy the boundary conditions. As a result, more analytical work can be done giving further insight into the nature of the solutions obtained in chapter 4.

The formulation of the problem has thus far utilized the depth H of the ocean as its length scale. This obviously loses its independent meaning in an infinitely deep ocean. H will continue to be used, however, and can be thought of in its relation to the thickness of the Ekman layer, δ . δ and H are related by $\delta = E^{1/2} H$.

The ocean is taken as occupying the lower half space ($0 \leq z < \infty$) as shown below



The equations of motion are (2.1) with $\sigma \rightarrow \infty$ and the boundary conditions are as follows:

$$z=0: \quad w=0, \quad \frac{\partial \bar{u}}{\partial z} = \bar{f}(x-ut)$$

$$z \rightarrow -\infty: \quad \bar{u}, p, \rho \rightarrow 0$$

\bar{f} will be either a sinusoid (section 5.1) or an idealized front (section 5.2).

5.1 The response to a travelling sinusoidal stress pattern

Suppose that \bar{f} is a one-dimensional sinusoid travelling with speed U in the positive x -direction:

$$\bar{f} = \bar{F} e^{ik(x-ut)}, \quad \bar{F} = (T_x, T_y), \text{ A CONSTANT} \quad (5.1)$$

Solutions will be of the form

$$(\bar{u}, p, \rho) = \sum_{j=1}^3 (\bar{u}_j, p_j, \rho_j) e^{im_j z} e^{ik(x-ut)}$$

where the m_j 's satisfy equation (3.1), $\chi_j^2 = k^2 + m_j^2$, $\omega = Uk$.

The m_j 's are such that $\text{Im } m_j < 0$ to satisfy conditions as $z \rightarrow -\infty$.

The north-south velocity v will be used as the working variable. Application of the boundary conditions at $z = 0$ yield the following set of equations for the v_j 's:

$$\begin{pmatrix} 1 & 1 & 1 \\ m_1^2 & m_2^2 & m_3^2 \\ \gamma_1 & \gamma_2 & \gamma_3 \end{pmatrix} \begin{pmatrix} i m_1 / \gamma_1 V_1 \\ i m_2 / \gamma_2 V_2 \\ i m_3 / \gamma_3 V_3 \end{pmatrix} = \begin{pmatrix} 0 \\ ik T_x \\ T_y \end{pmatrix}$$

$$\gamma_j = \frac{2i m_j^2}{k(-i\omega + E x_j^2)}$$

These are solved by

$$\begin{aligned} V_1 &= \frac{i \gamma_1}{m_1} \left[\frac{ik T_x (\gamma_3 - \gamma_2) - T_y (m_3^2 - m_2^2)}{D} \right] \\ V_2 &= \frac{i \gamma_2}{m_2} \left[\frac{-ik T_x (\gamma_3 - \gamma_1) + T_y (m_3^2 - m_1^2)}{D} \right] \\ V_3 &= \frac{i \gamma_3}{m_3} \left[\frac{ik T_x (\gamma_2 - \gamma_1) - T_y (m_2^2 - m_1^2)}{D} \right] \end{aligned} \quad (5.2)$$

where

$$D = \begin{vmatrix} 1 & 1 & 1 \\ m_1^2 & m_2^2 & m_3^2 \\ \gamma_1 & \gamma_2 & \gamma_3 \end{vmatrix}$$

The solution for the v velocity field may then be written as:

$$v = \sum_{j=1}^3 V_j e^{i m_j z} e^{ik(x-ut)}$$

or

$$v = \begin{vmatrix} 0 & i\frac{\gamma_1}{m_1} e^{im_1 z} & i\frac{\gamma_2}{m_2} e^{im_2 z} & i\frac{\gamma_3}{m_3} e^{im_3 z} \\ 0 & 1 & 1 & 1 \\ ikT_x & m_1^2 & m_2^2 & m_3^2 \\ T_y & \gamma_1 & \gamma_2 & \gamma_3 \end{vmatrix} e^{ik(x-ut)} \quad 60.$$

$$\begin{vmatrix} 1 & 1 & 1 \\ m_1^2 & m_2^2 & m_3^2 \\ \gamma_1 & \gamma_2 & \gamma_3 \end{vmatrix}$$

$$v \equiv V(k, z) e^{ik(x-ut)}, \text{ SAY.}$$

The behavior of $|V(k, z)|$ as a function of k and z is shown in figure 5.1 (with $T_x=0$ and $T_y=1$) and figure 5.2 (with $T_x=1$ and $T_y=0$). Note the strong peak just above the inertial frequency ($k = \frac{z}{U} = 0.037$). The ocean is thus most attuned to producing an inertial response when the wavelength of the stress pattern is in a range corresponding to the values of k discussed here.

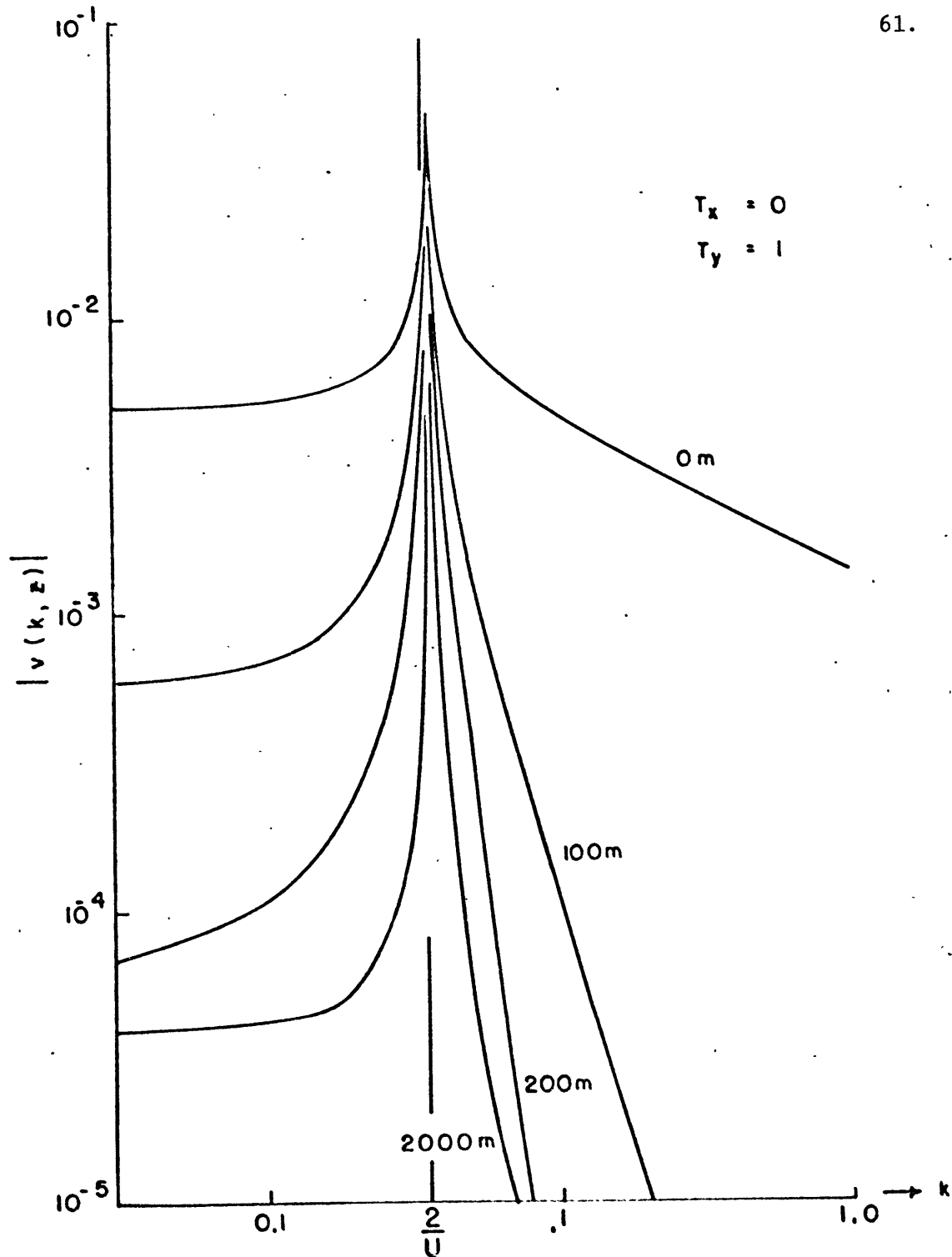


Figure 5.1 The response $|v(k, z)|$ to a travelling sinusoid $T_y e^{ik(x-ut)} \hat{j}$.
 $U = 54.083$.

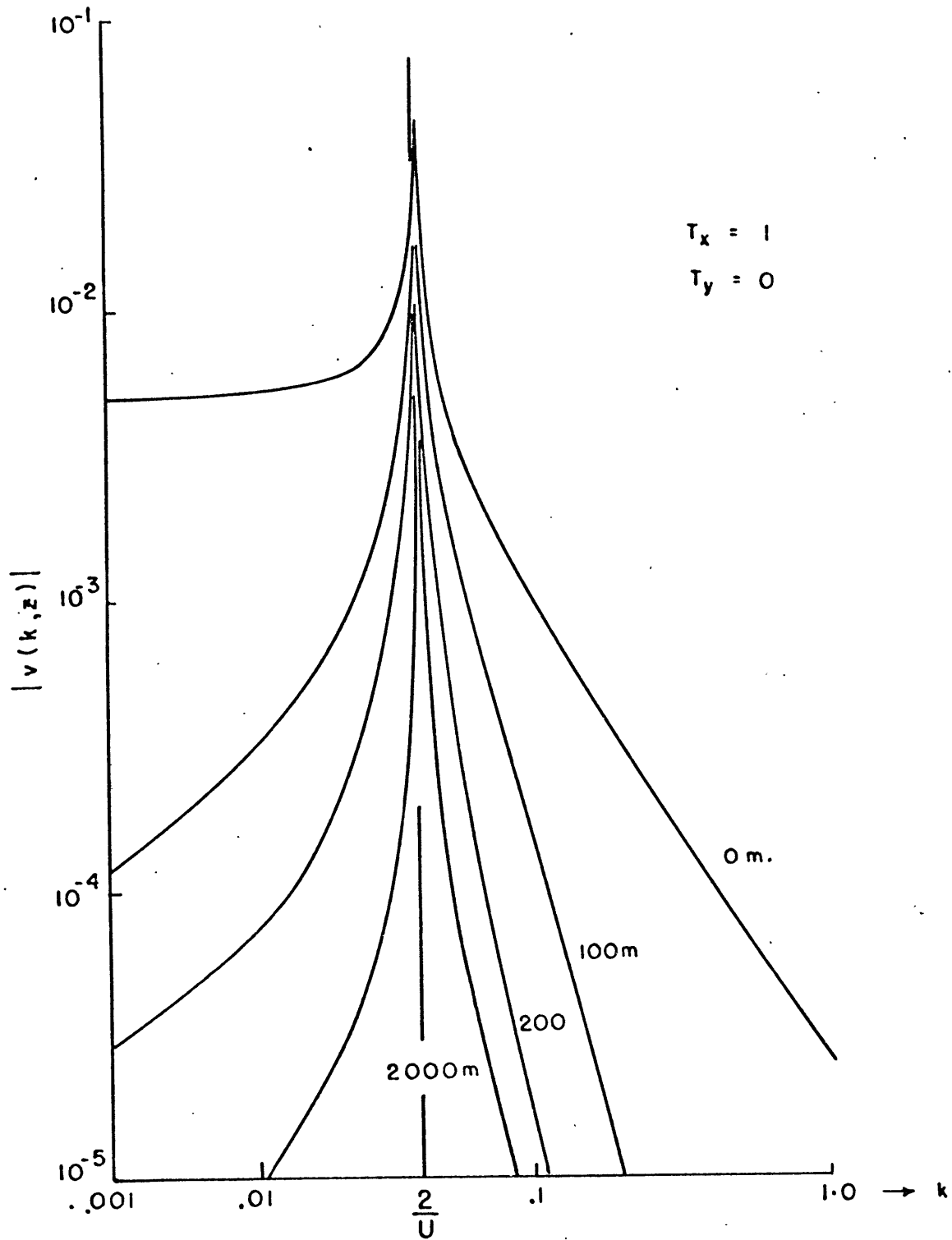


Figure 5.2 The response $|v(k, z)|$ to a travelling sinusoid $T_x e^{ik(x-ut)}$
 $U = 54.083$.

5.2 The response to the idealized travelling front

For a forcing function more complicated than a sinusoidal one, a Fourier synthesis must be used:

$$v = \frac{1}{2\pi} \int_{-\infty}^{\infty} V(k, z) e^{ik(x-ut)} dk \quad (5.4)$$

where $V(k, z)$ is the determinant quotient (5.3) in which T_x and T_y are no longer constants but Fourier transforms of the wind stress

$$\bar{T}(k) = \int_{-\infty}^{\infty} \bar{T}(\xi) e^{-ik\xi} d\xi \quad (5.5)$$

and are described in section 4.1.

The nature of the response to this pattern will depend on the location and type of singularities of $V(k, z)$ and these will be discussed now.

It is first necessary to study the behavior of the roots m_j for those values of k in the complex plane such that $|k| < O(\epsilon^{-1/2})$. It will be assumed that values of k beyond this region will not significantly affect the solution as they correspond to motions with extremely short horizontal length scales. If this assumption is made, then, the asymptotic expansions of Chapter 3 are valid away from the inertial frequency. Asymptotically, then, designate

$${}_1 M^2 = \frac{i(\omega+2)}{E} + O(1) \quad 64.$$

$${}_2 M^2 = \frac{i(\omega-2)}{E} + O(1) \quad (5.6)$$

$${}_3 M^2 = \frac{k^2(S-\omega^2)}{(\omega^2-4)} + O(E)$$

${}_1 M$ and ${}_2 M$ have no branch points away from the inertial frequency with this approximation while ${}_3 M$ has a square root type branch at $k = \sqrt{S}/U$. The above expressions suggest that all three vertical wave numbers might have branches near the inertial frequency and it is their behavior there that will be examined next.

Near the inertial frequency, it was shown that four of the six roots of (3.1) were of $O(E^{-1/4})$. A good approximation to these roots can thus be achieved by solving:

$$-2i\omega E m^4 - (\omega^2 - 4)m^2 + k^2(S - \omega^2) = 0 \quad (5.7)$$

which are the most important terms of (3.1) near $\omega = \pm 2$. This yields:

$$m^2 = \frac{(\omega^2 - 4) \pm \sqrt{(\omega^2 - 4)^2 + 8i\omega E k^2(S - \omega^2)}}{-4i\omega E} \quad (5.8)$$

This suggests that the m 's have branch points when

$$(\omega^2 - 4)^2 + 8i\omega E k^2(S - \omega^2) = 0, \quad \omega = Uk \quad (5.9)$$

Four of the five k -roots are found from the asymptotic expansion

$$k = k^{(0)} + E^{1/2} k^{(1)} + \dots \text{ and are:}$$

$$k_{1,2} = \frac{z}{U} \pm \frac{(1-i)}{\sqrt{2}} \frac{2\sqrt{S-4}}{U^2} E''^2 \quad 65.$$

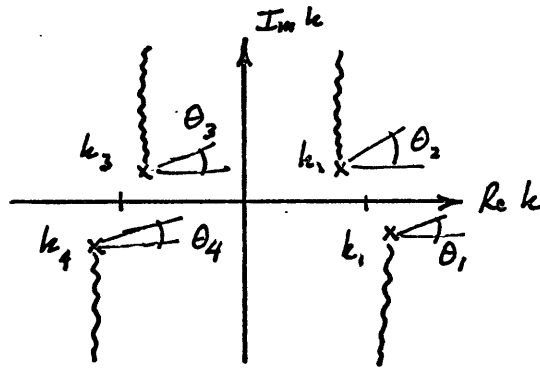
$$k_{3,4} = -\frac{z}{U} \pm \frac{(1+i)}{\sqrt{2}} \frac{2\sqrt{S-4}}{U^2} E''^2 \quad (5.10)$$

These are close to the inertial wave number. The fifth k-root is far away from $\pm \frac{z}{U}$:

$$k_5 = \frac{U}{8iE}$$

which is out of the range of validity of (5.7).

The branch points, (5.10), and branch cuts introduced to make the roots single valued are shown below



To examine the roots near these points define

$$\omega - \omega_j = \rho_j e^{i\theta_j}, \quad j=1,4, \quad \omega_j = Uk_j \quad (5.11)$$

where $\frac{3\pi}{2} > \theta_1, \theta_4 \geq -\frac{\pi}{2}$, $\frac{\pi}{2} > \theta_2, \theta_3 \geq -\frac{3\pi}{2}$

Substituting these into (5.8) yields the approximations:

$$M = \pm \frac{1}{2E^{1/2}} \left[\sqrt{\rho_1} e^{i(\frac{\theta_1 + \pi}{2} + \frac{\pi}{4})} \pm \sqrt{\rho_2} e^{i(\frac{\theta_2 + \pi}{2} + \frac{\pi}{4})} \right] \quad (5.12)$$

near $\omega = 2$ and

$$M = \pm \frac{1}{2E^{1/2}} \left[\sqrt{\rho_3} e^{i(\frac{\theta_3 + \pi}{2} + \frac{\pi}{4})} \pm \sqrt{\rho_4} e^{i(\frac{\theta_4 + \pi}{2} + \frac{\pi}{4})} \right] \quad (5.13)$$

near $\omega = -2$.

It is now necessary to identify these roots with their corresponding values away from the inertial frequencies. Refer to the rough figures in Chapter 3, page 12. Those branches of (5.12) and (5.13) that, on the real axis, have negative imaginary parts and behave like the above figures are:

$$\begin{aligned} M_3 &= -\frac{1}{2E^{1/2}} \left[\sqrt{\rho_1} e^{i(\frac{\theta_1 + \pi}{2} + \frac{\pi}{4})} + \sqrt{\rho_2} e^{i(\frac{\theta_2 + \pi}{2} + \frac{\pi}{4})} \right] \\ M_2 &= -\frac{1}{2E^{1/2}} \left[\sqrt{\rho_1} e^{i(\frac{\theta_1 + \pi}{2} + \frac{\pi}{4})} - \sqrt{\rho_2} e^{i(\frac{\theta_2 + \pi}{2} + \frac{\pi}{4})} \right] \end{aligned} \quad (5.14)$$

near $\omega = +2$ and

$$\begin{aligned} M_3 &= \frac{1}{2E^{1/2}} \left[\sqrt{\rho_3} e^{i(\frac{\theta_3 + \pi}{2} + \frac{\pi}{4})} - \sqrt{\rho_4} e^{i(\frac{\theta_4 + \pi}{2} + \frac{\pi}{4})} \right] \\ M_1 &= -\frac{1}{2E^{1/2}} \left[\sqrt{\rho_3} e^{i(\frac{\theta_3 + \pi}{2} + \frac{\pi}{4})} + \sqrt{\rho_4} e^{i(\frac{\theta_4 + \pi}{2} + \frac{\pi}{4})} \right] \end{aligned} \quad (5.15)$$

near $\omega = -2$. The above show that

$$\begin{aligned}
 \text{at } k = k_1 \quad \mu_3 &= -\mu_2, & \text{Im } \mu_3 < 0, & \text{Im } \mu_2 > 0; \\
 k = k_2 \quad \mu_3 &= \mu_2, & \text{Im } \mu_3 < 0, & \text{Im } \mu_2 < 0; \\
 k = k_3 \quad \mu_3 &= \mu_1, & \text{Im } \mu_3 < 0, & \text{Im } \mu_1 < 0; \\
 k = k_4 \quad \mu_3 &= -\mu_1, & \text{Im } \mu_3 < 0, & \text{Im } \mu_1 > 0.
 \end{aligned}$$

With this information, it is now possible to examine the singularities of the integrand (5.3). ν will again be used as the working dependent variable. The singularities of $V(k, z)$ are as follows:

1. The simple poles of the wind stress transforms T_x and T_y at $k = \pm id$.
2. The numerator and denominator of V both have zeroes when any row or column is a multiple of another. This occurs in the numerator when any of the roots μ_j become multiple roots and in the denominator when the roots μ_j become multiple or if their squares are equal. It also occurs when $(-i\omega + Ek^2) = 0$. This latter point reduces the ν_j 's to constants. It is, however, of $O(E^{-1})$ and, hence, will be ignored. Both numerator and denominator vanish when the roots become multiple, and it can be shown that these (k_2 and k_3) are not singular points of the integrand. The zeroes of the denominator, however, give a square root branch behavior to the integrand where the roots' squares are equal (k_1 and k_4). Singularities

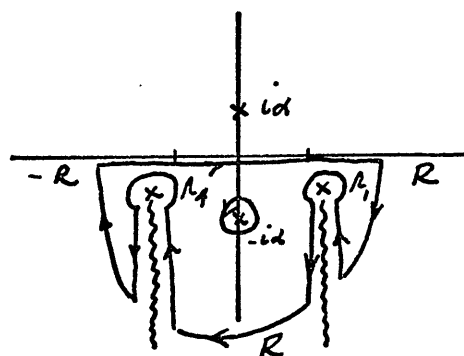
at the origin will be neglected; it is assumed that they will contribute only to the steady state response.

The author was unable to find a suitable contour of integration for all values of z . The function $e^{ik(x-ut)}$ decays rapidly in the upper half plane for $x-ut > 0$ and in the lower half plane for $x-ut < 0$. This damping, however, is not sufficient to overcome the behavior of e^{imz} for the roots which behave like

$$m^2 = \frac{k^2(5-U^2k^2)}{(U^2k^2-4)}$$

Some headway can still be made, however, for $z = 0$, as this eliminates any exponential behavior in k except for the highly damped $e^{ik(x-ut)}$ terms and, hence, allows the contours to be closed at infinity.

The contour taken for $(x-ut) < 0$ is as shown



The branch points at $k = \sqrt{5}/U$ will be neglected. This is equivalent to making the hydrostatic assumption in the original equations (2.1) and, for the scales of motion involved here, is

justifiable. By Cauchy's integral theorem then,

$$\int_{-R}^R + \int_{k_1-i\infty}^{k_1} + \int_{k_1}^{k_1-i\infty} + \oint_{\mathcal{R}_1} + \int_{k_4-i\infty}^{k_4} + \int_{k_4}^{k_4-i\infty} \\ + \oint_{\mathcal{R}_4} + \int_R = 2\pi i \text{ Residue } [V, -i\alpha]$$

Because of the factor $e^{ik(x-ut)}$, the integral along R (\int_R) vanishes. The integrals around \mathcal{R}_1 and \mathcal{R}_4 also vanish as $\mathcal{R}_{1,4} \rightarrow 0$.

The integral (5.4) then becomes

$$v = \frac{1}{2\pi} \int_{-\infty}^{\infty} V(k) e^{ik(x-ut)} dk \\ = i \text{ Residue } [V, -i\alpha] - \frac{1}{2\pi} \left[\int_{k_1-i\infty}^{k_1} + \int_{k_1}^{k_1-i\infty} + \int_{k_4-i\infty}^{k_4} + \int_{k_4}^{k_4-i\infty} \right] V e^{ikx} dk$$

where the integrand, $V(k)$, must be evaluated on the proper Riemann sheet for each integral. The integrals along the branch cuts were calculated asymptotically for large values of $x-ut$ (not a severe restriction considering the large horizontal scales of the problem). The behavior of these integrals, under this approximation, is such that the main contribution comes from that portion of the integral which is very close to the branch points. Accordingly, that portion of $V(k)$, say V_1 , which is singular at the branch point can be represented in an $\epsilon^{1/2}$ neighborhood of the inertial frequency by

$$V_1(k) = \frac{i}{2} (iT_x - T_y) \frac{(-m_2 e^{im_2 z} + m_3 e^{im_3 z})}{(m_3^2 - m_2^2)} + O(E^{3/4}) \quad (5.16)$$

near $\omega=2$, and

$$V_1(k) = \frac{-i}{2} (iT_x + T_y) \frac{(-m_1 e^{im_1 z} + m_3 e^{im_3 z})}{m_3^2 - m_1^2} \quad (5.17)$$

near $\omega=-2$. The remainder of the integrand, i.e., the functions involving $e^{im_1 z}$ at $\omega=2$ and $e^{im_2 z}$ at $\omega=-2$, can be shown to be regular at $\omega=2$ and $\omega=-2$ respectively.

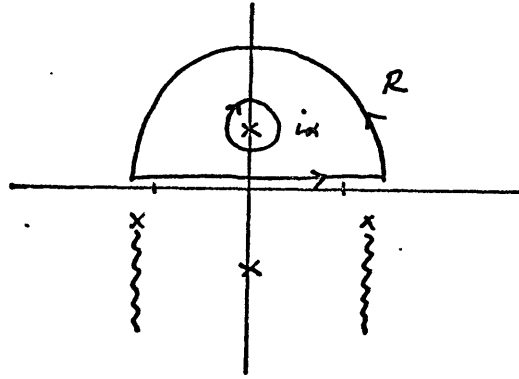
The details of the integrations around the branch cuts are relegated to Appendix 2. The solution for v is

$$v(x,t) = \text{Real} \left\{ \frac{-E^{1/2} e^{\alpha(x-ut)}}{2} \left[\frac{(c_{2x} - ic_{2y})}{\sqrt{\alpha U + 2i}} + \frac{(c_{2x} + ic_{2y})}{\sqrt{\alpha U - 2i}} \right] \right. \\ \left. - \frac{i e^{ik_1 \xi} E^{1/2}}{\sqrt{\pi U(x-ut)}} [iT_x(k_1) - T_y(k_1)] \right\} + O\left(\frac{1}{x-ut}, E^{3/4}\right) \quad (5.18)$$

The solution for $u(x,t)$ is obtained in a similar fashion and is

$$u(x,t) = \text{Real} \left\{ \frac{i E^{1/2} e^{\alpha(x-ut)}}{2} \left[\frac{(-c_{2x} + ic_{2y})}{\sqrt{\alpha U + 2i}} + \frac{(c_{2x} + ic_{2y})}{\sqrt{\alpha U - 2i}} \right] \right. \\ \left. + \frac{e^{ik_1 \xi} E^{1/2}}{\sqrt{\pi U(x-ut)}} [iT_x(k_1) - T_y(k_1)] \right\} + O\left(\frac{1}{x-ut}, E^{3/4}\right). \quad (5.19)$$

For $(x-ut) > 0$, the problem is much simpler; there is only a simple pole in the upper half plane:



Again because of $e^{ik(x-ut)}$, Imk70, the integral along R vanishes as $R \rightarrow \infty$ and the residue calculation yields

$$v(x,t) = \text{Real} \left\{ \frac{-E^{1/2} e^{-d(x-ut)}}{2} \left[\frac{(-C_{1x} + iC_{1y})}{\sqrt{-dU + 2i}} - \frac{(C_{1x} + iC_{1y})}{\sqrt{-dU - 2i}} \right] \right\} + O(E) \quad (5.20)$$

$$u(x,t) = \text{Real} \left\{ \frac{-iE^{1/2} e^{-d(x-ut)}}{2} \left[\frac{(-C_{1x} + iC_{1y})}{\sqrt{-dU + 2i}} + \frac{(C_{1x} + iC_{1y})}{\sqrt{-dU - 2i}} \right] \right\} + O(E) \quad (5.21)$$

These solutions are shown in figure 5.3 for $U = 54.083$. The first two terms in (5.18) and (5.19) represent the decaying exponential component and the second part, the decaying oscillatory component of the solution. Comparison of figure 4.7 with figure 5.3 shows that, away from the immediate vicinity of the frontal line, the asymptotic solution agrees well with the numerically integrated solution.

The exponential component decays as the stress does (e-folding distance of d^{-1}) while the oscillatory component decays to

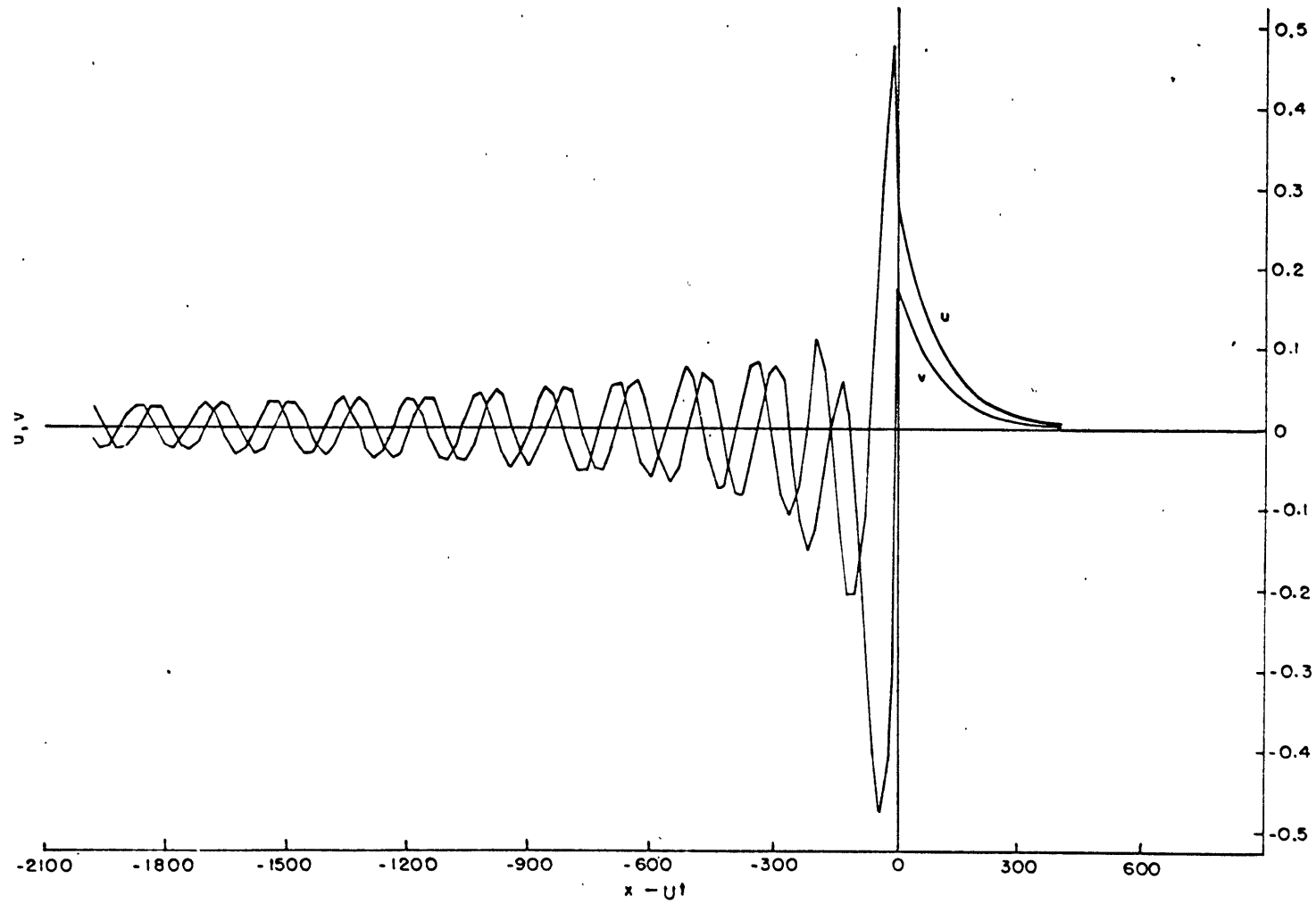


Figure 5.3 u and v given by 5.18, 5.19, 5.20, and 5.21 for $U = 54.083$ (10 m. sec.^{-1}).
 The scales of the axes are the same as in figure 4.7.

a first approximation as $\frac{1}{\sqrt{x-ut}}$.

The Doppler frequency of the wake may be computed from (5.10) as the solutions behave like $e^{ik_1 x}$:

$$\omega_1 = Uk_1 = 2 + \frac{(1-i)}{\sqrt{2}} \frac{2\sqrt{S-4}}{U} E^{1/2}$$

The wake frequency is above the inertial frequency by the amount

$$\Delta\omega = \frac{\sqrt{2(S-4)E}}{U} \quad (5.22)$$

For the three front speeds (13.411, 54.083, 100.0) this amounts to the following percentages above the inertial frequency:

U	$\frac{\Delta\omega}{\omega}$
13.411	2.28%
54.083	0.56%
100.0	0.31%

The dependence of $\Delta\omega$ on the square root of the eddy viscosity points clearly to a quite different mechanism than is given by inviscid theories for this phenomenon, e.g., the planetary dispersion mechanism described by Munk and Phillips (1968).

6. Comparison with a simple model and conclusions

6.1 Comparisons of solutions with the Pollard-Fofonoff model

This section compares the solutions obtained in Chapter 4 with those obtained with a more simple oceanic model proposed by Fofonoff (1968) and applied by Pollard and Millard (1970) to calculate the oceanic response to some actual wind systems at site D. The forcing used here will be the travelling front discussed in Chapter 4. Their model assumes that the ocean is characterized by a homogeneous surface layer, several tens of meters thick, in which the motion is uniform both horizontally and vertically.

Dimensional variables will be used throughout this section. The equations of motion averaged over the homogeneous layer are taken as

$$\frac{\partial \bar{u}}{\partial t} + f \hat{k} \times \bar{u} = \bar{F} - c\bar{u} \quad (6.1)$$

where f is the Coriolis parameter (equal to $0.92 \times 10^{-4} \text{sec}^{-1}$ at site D) and \bar{F} is the wind stress applied as a body force over the layer. $c\bar{u}$ is the frictional stress across the bottom of the homogeneous surface layer and is used to roughly model the dispersion which is formally prohibited by the requirement of horizontal and vertical homogeneity in the velocity fields.

It is now necessary to determine \bar{F} for the stress distribution discussed in Chapter 4.

$$\vec{F} = \frac{\rho_{air} C_D |\vec{V}| \vec{V}}{\rho_w z_0} \quad (6.2)$$

where

- ρ_{air} = density of air ($1.225 \times 10^{-6} \text{ gm cm}^{-3}$)
 C_D = drag coefficient
 ρ_w = density of water (1 gm cm^{-3})
 z_0 = thickness of the mixed layer (taken as 40 m)
 \vec{V} = wind velocity near the sea surface.

For the front, this becomes (in dimensional notation):

$$\vec{F} = \frac{2.44 \times 10^{-6} U^2}{z_0} \left[(0.276, 0.666) e^{\alpha U t} H(-t) + (0.666, -0.276) e^{-\alpha U t} H(t) \right]$$

where

$$\alpha = 0.25 \times 10^{-7} \text{ cm}^{-1}$$

$$U = 248, 10^3 \text{ OR } 1.845 \times 10^3 \text{ cm sec}^{-1}$$

The ocean surface sees the front passing and this appears locally as a time series of wind stress. The model assumes that this time series is without horizontal variation.

The solutions of (6.1) are easily obtained and take the general form

$$\vec{u}(t) = (\text{Real, Imag.}) \int_0^t e^{(if+c)(z-t)} [F_x(z) + iF_y(z)] dz$$

For the \vec{F} distribution above, this reduces to

$$t < 0: \vec{u}(t) = (\text{Real, Imag.}) \frac{A_1 e^{\alpha U t}}{i f + c + \alpha U} \quad 76.$$

$$t > 0: \vec{u}(t) = (\text{Real, Imag.}) \left\{ \left[\frac{A_1}{(i f + c + \alpha U)} - \frac{A_2}{(i f + c - \alpha U)} \right] \right\}. \quad (6.3)$$

$$\left. \begin{aligned} & e^{-(i f + c) t} \\ & + \frac{A_2 e^{-\alpha U t}}{(i f + c - \alpha U)} \end{aligned} \right\}$$

$t = 0$ corresponds to the frontal line "passing" the fixed observation station (site D, say). The numbers A_1 and A_2 are

$$A_1 = (0.276 + i 0.666) \frac{2.44 \times 10^{-6} U^2}{z_0}$$

$$A_2 = (0.666 - i 0.276) \frac{2.44 \times 10^{-6} U^2}{z_0}$$

$\vec{u}(t)$ was calculated for the three values of the frontal speed of translation U (2.48, 10, and 18.45 m sec⁻¹) and also for three values of the damping constant C (1, 4, and 8 days). The results appear in figures 6.1 through 6.9.

Comparison of these solutions with the results of Chapter 4 for $z=1$ shows similarity in the gross features of the motion but quite a few differences in detail. Perhaps the most significant difference in the solutions is the failure of the layer model to predict the spectral peak slightly above the inertial frequency; for all three frontal speeds, the wake frequency is exactly inertial. The Austausch model does predict a frequency slightly above inertial.

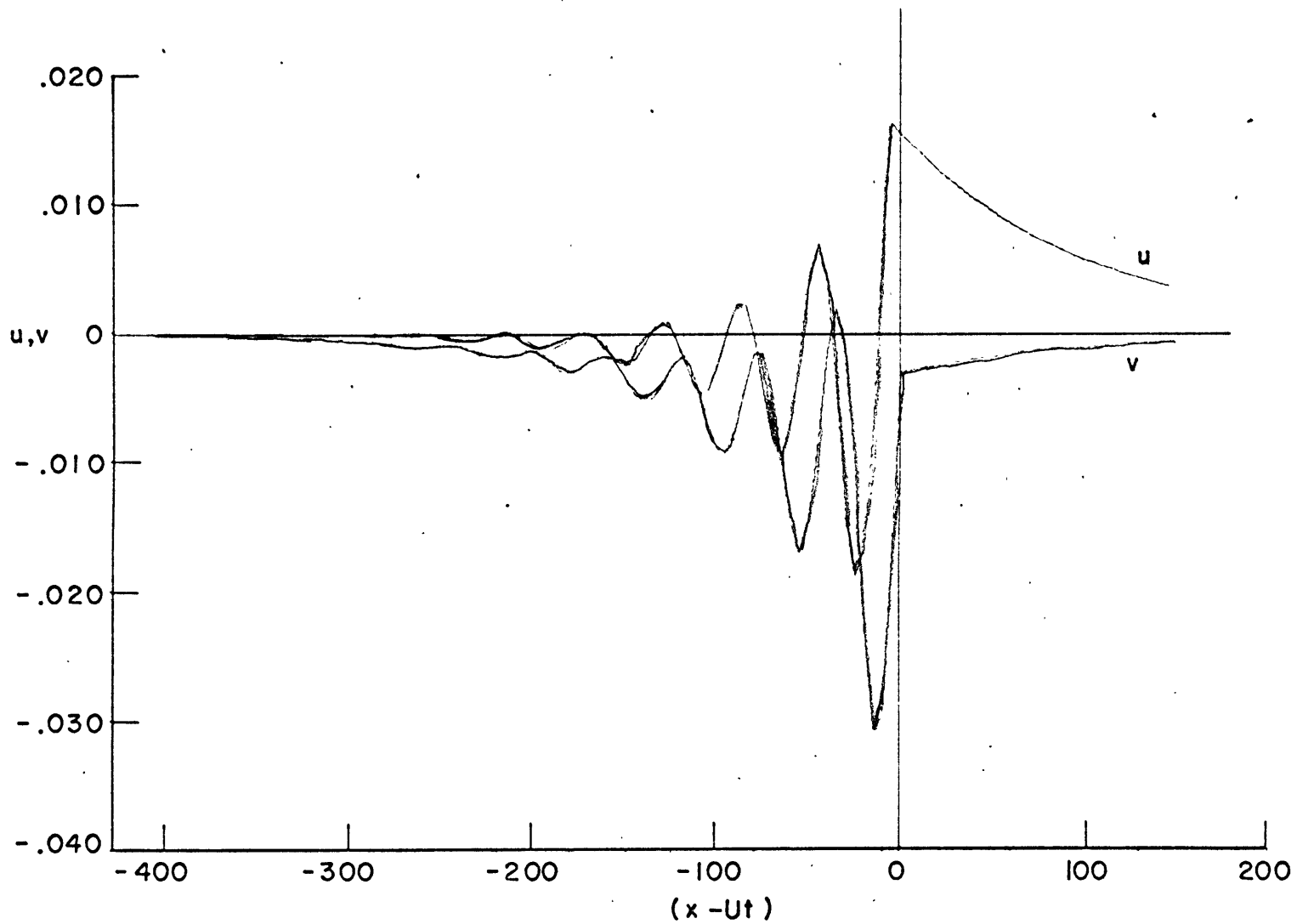


Figure 6.1 u and v for $U = 13.411$ (2.5 m. sec.^{-1}) and $c = 1$ day.
 The scales of the axes are the same as for figure 4.2.

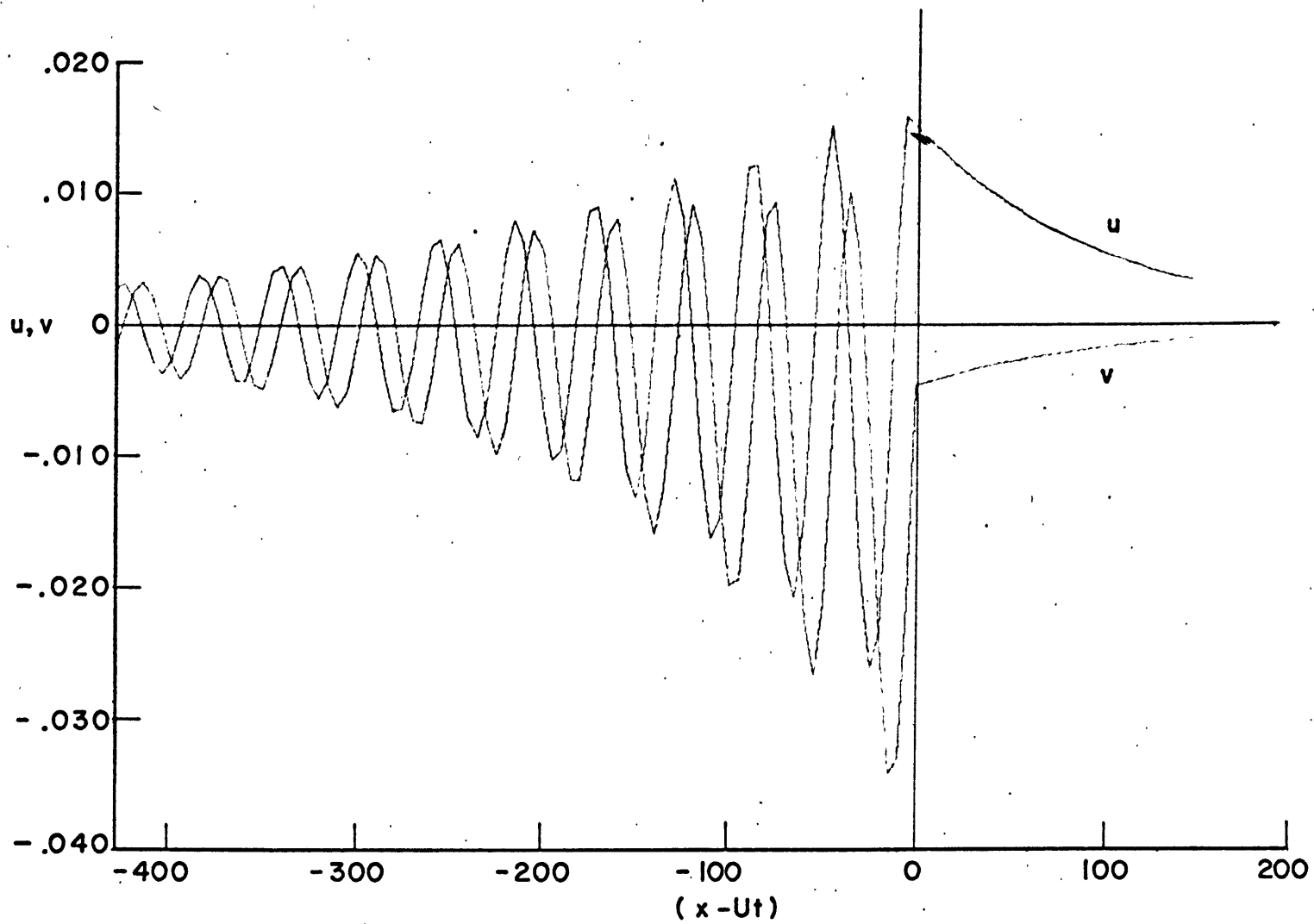


Figure 6.2 The same as 6.1 but $c = 4$ days.

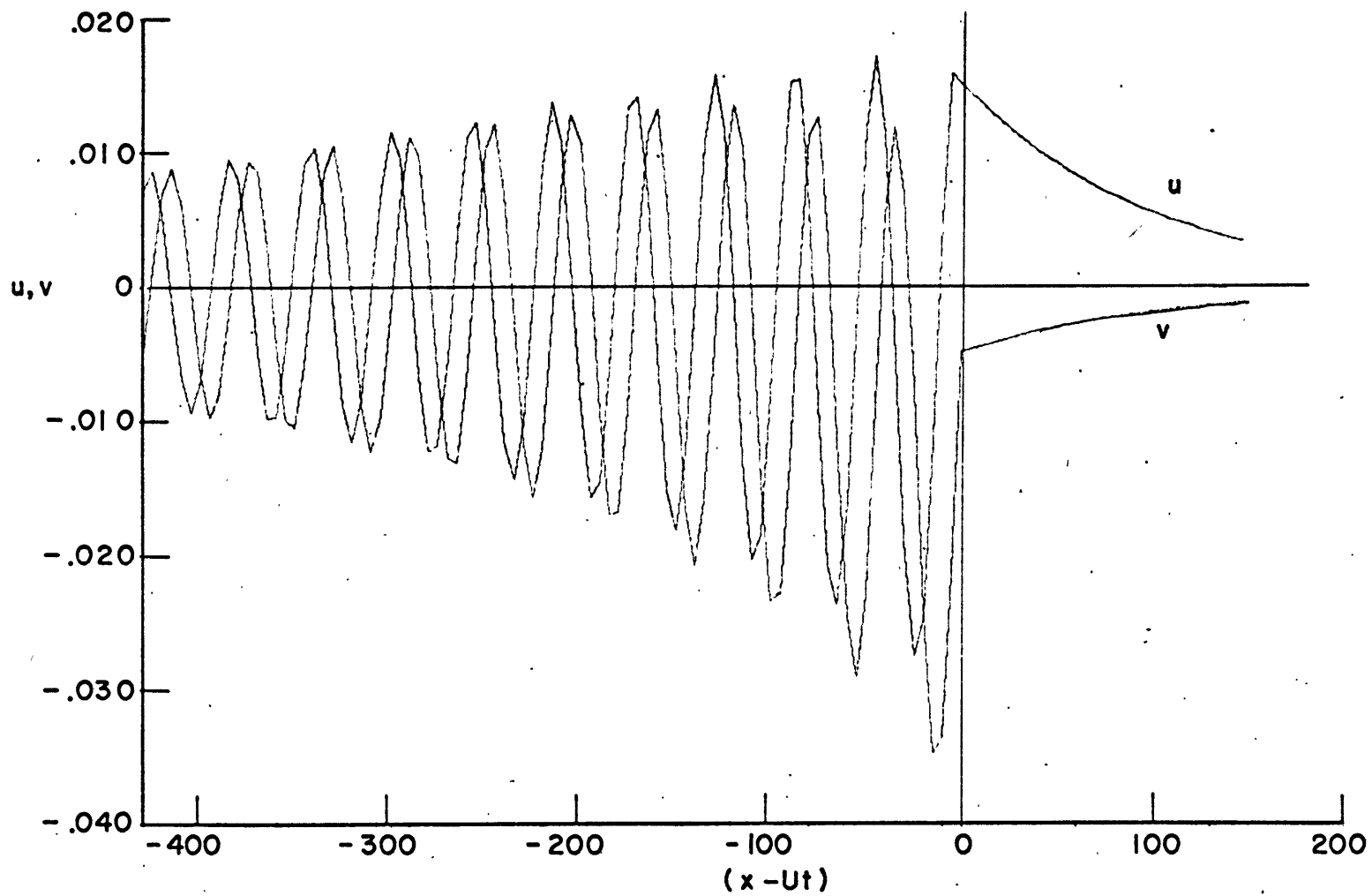


Figure 6.3 The same as 6.1 but $c = 8$ days.

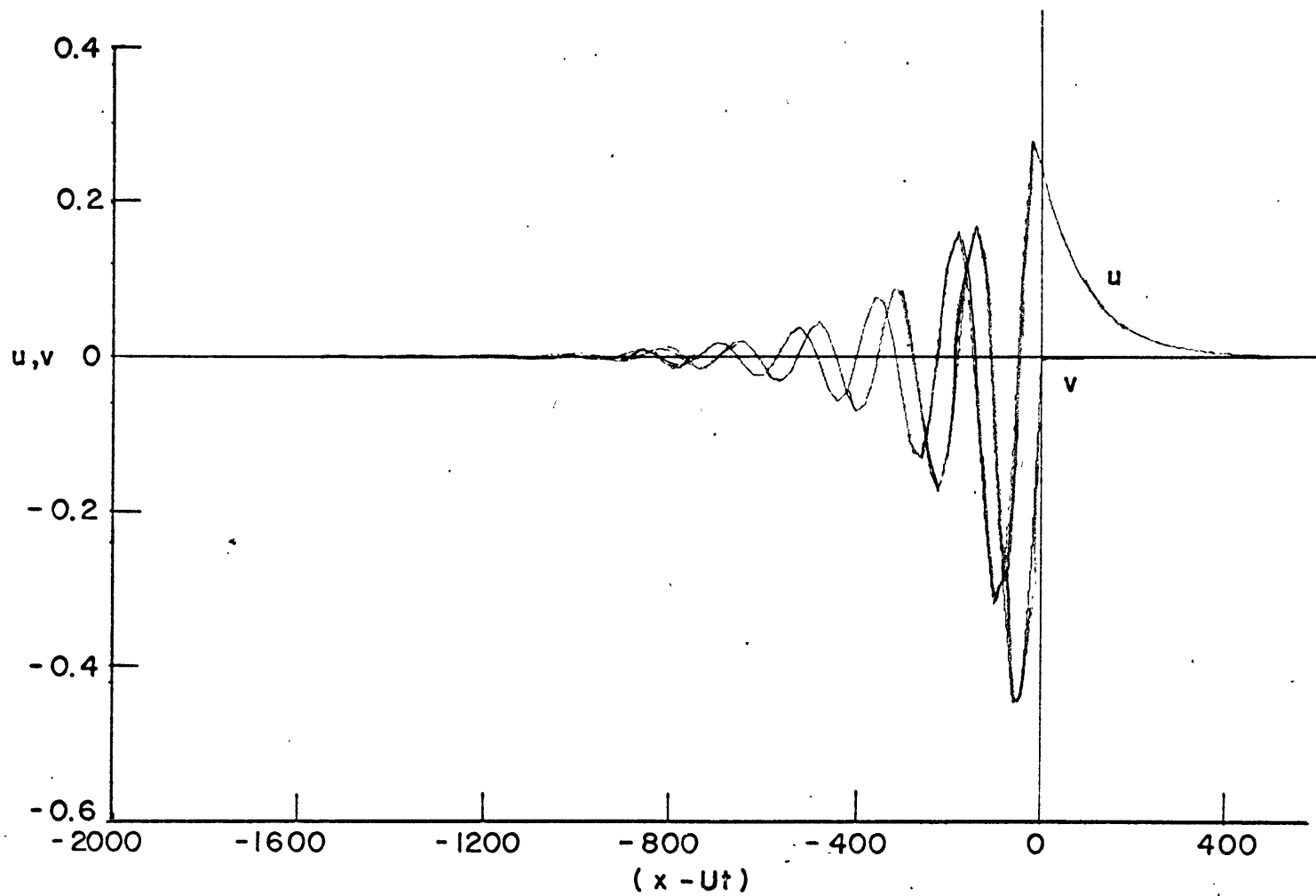


Figure 6.4 u and v for $U = 54.083$ (10 m. sec.^{-1}) and $c = 1$ day.

The scales of the axes are the same as for figure 4.7.

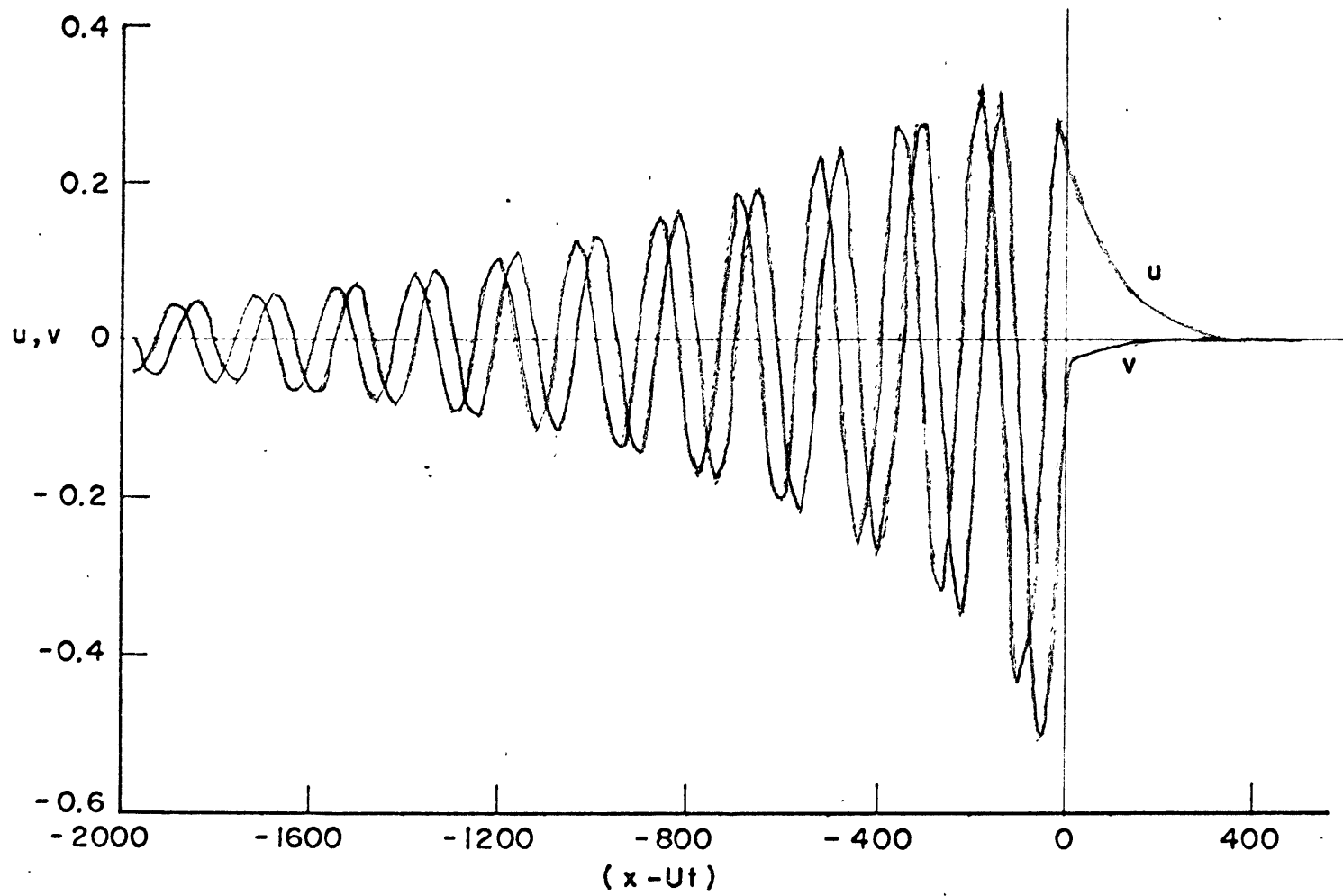


Figure 6.5 The same as 6.4 but $c = 4$ days.

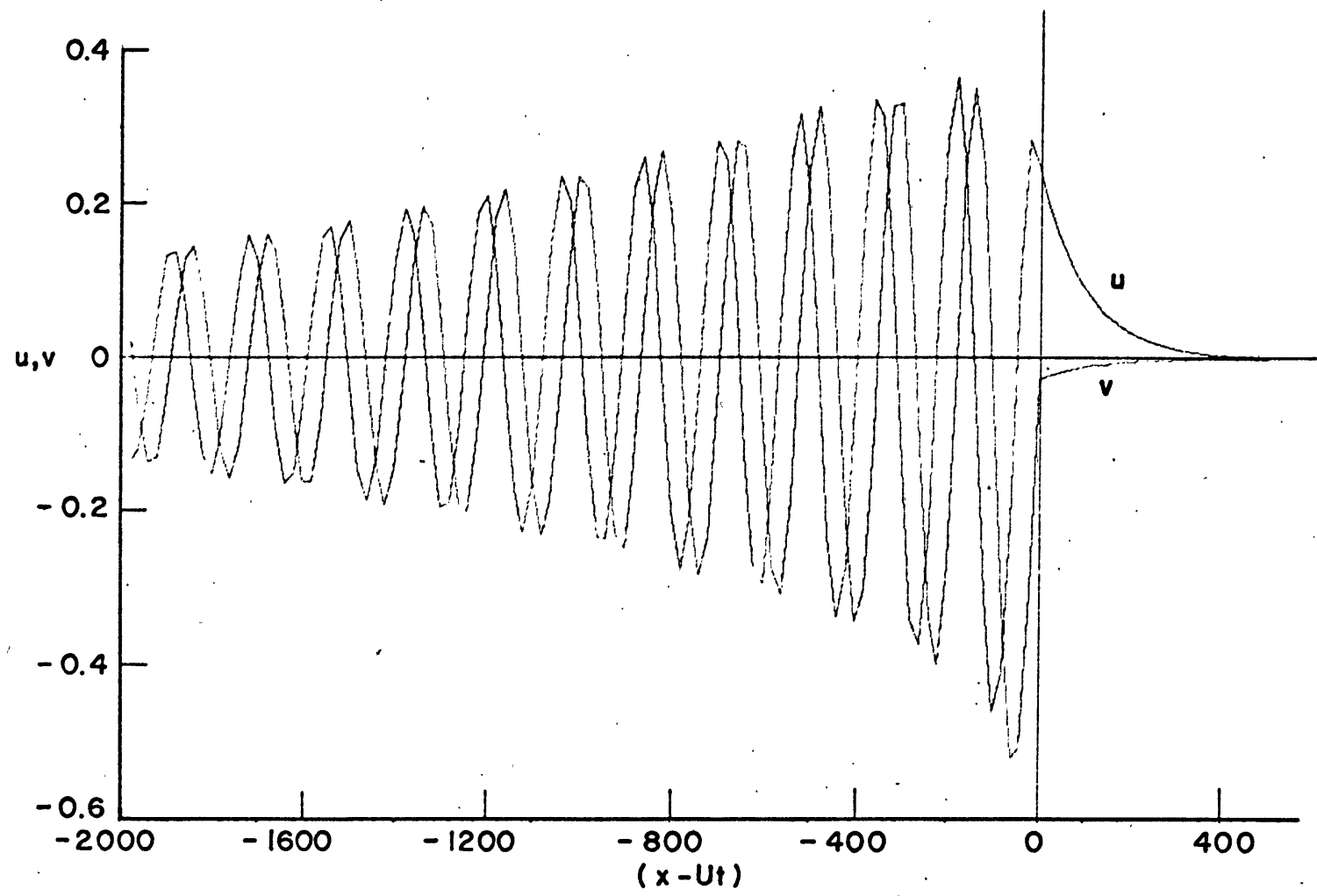


Figure 6.6 The same as 6.4 but $c = 8$ days.

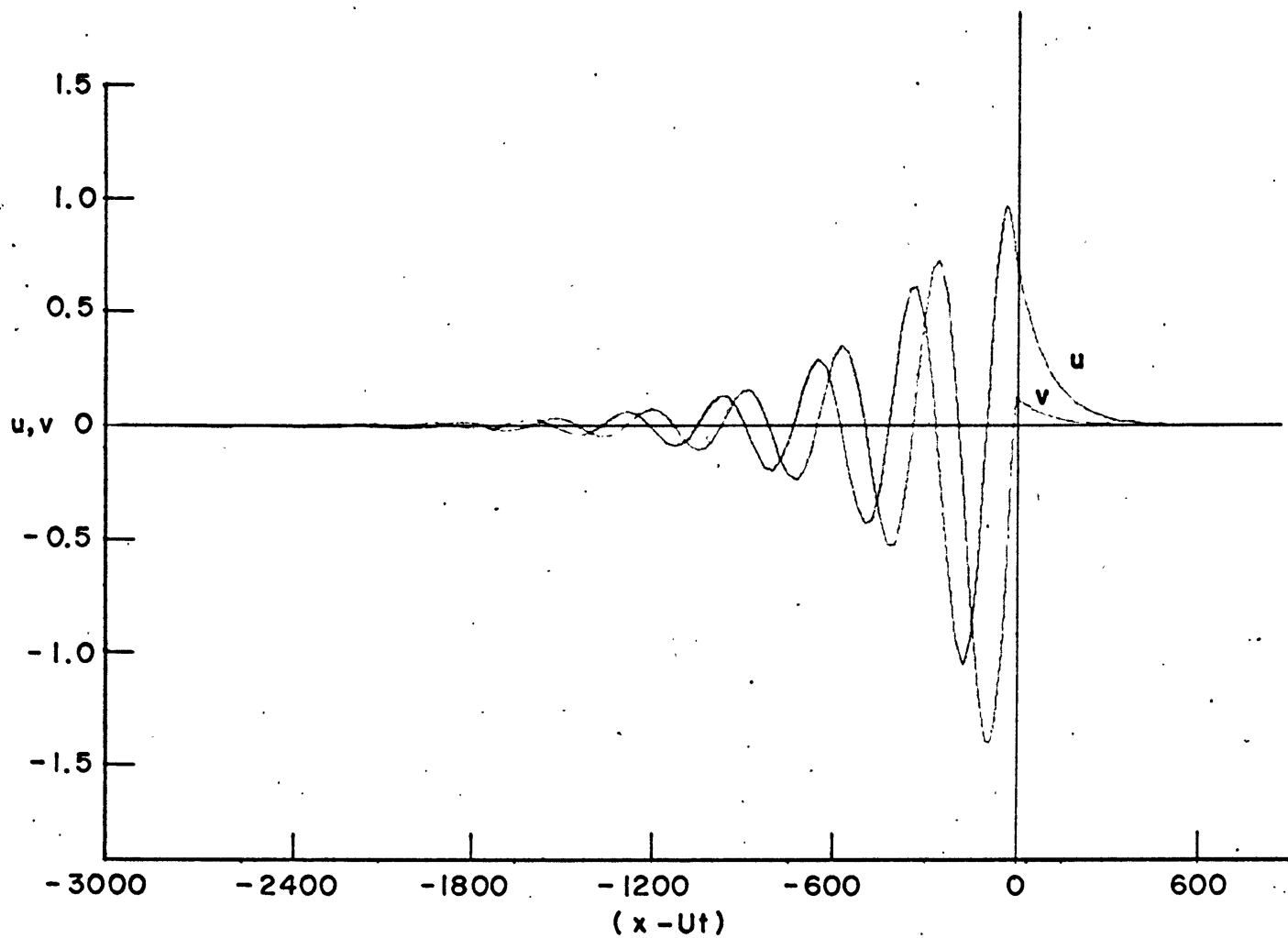


Figure 6.7 u and v for $U = 100.0$ ($18.45 \text{ m}\cdot\text{sec}^{-1}$) and $c = 1$ day.
 The scales of the axes are the same as for figure 4.12.

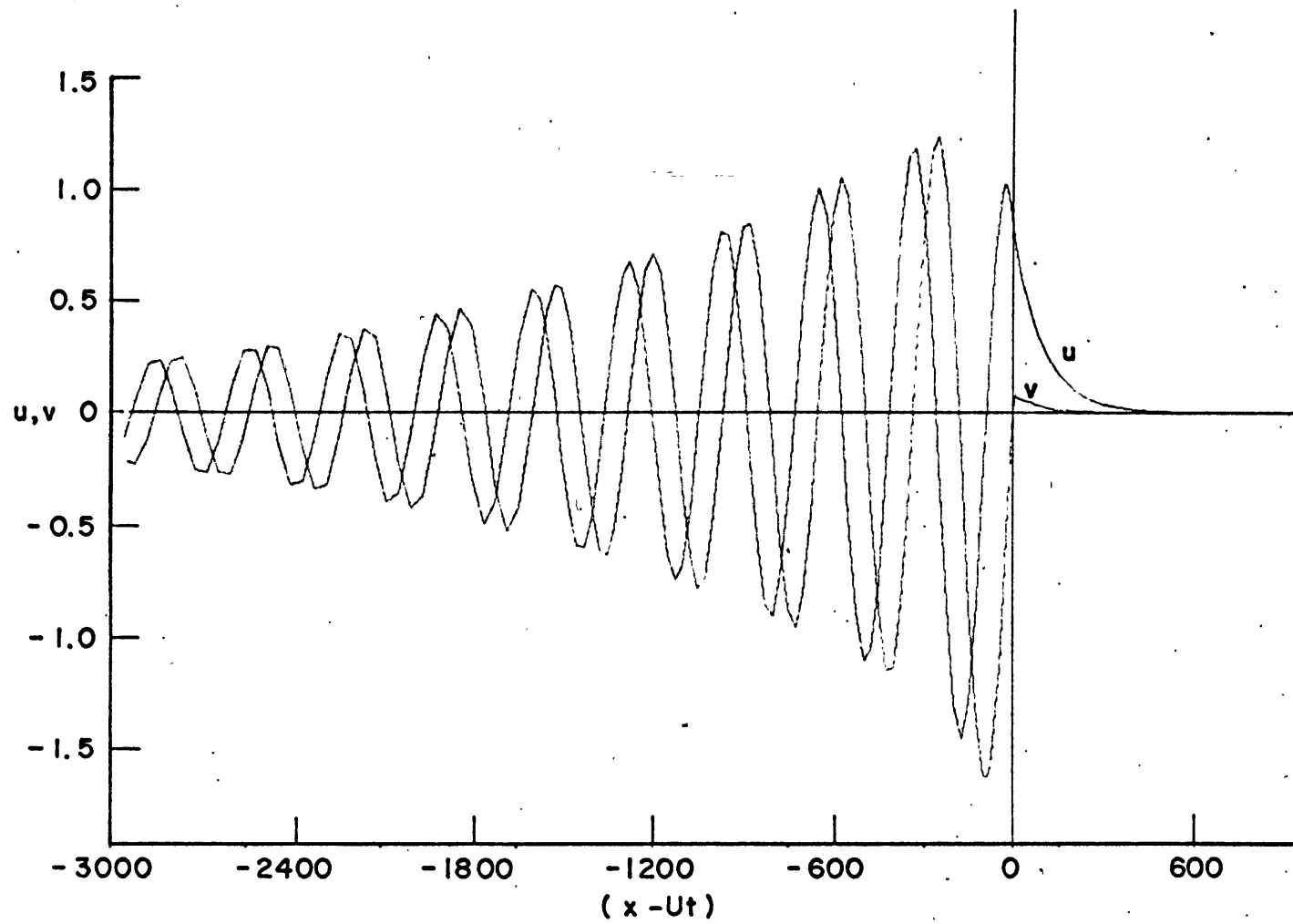


Figure 6.8 The same as 6.7 but $c = 4$ days.

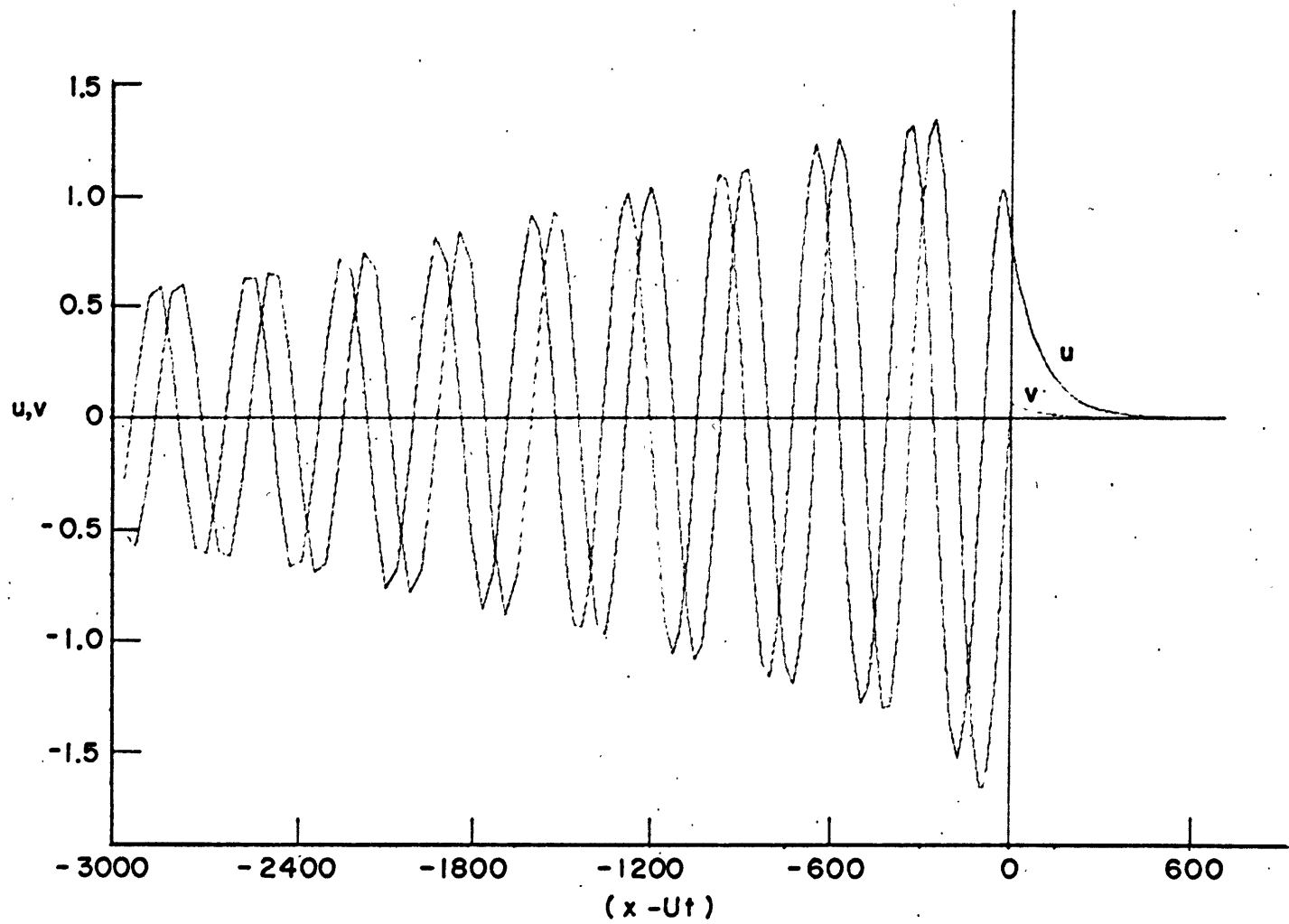


Figure 6.9 The same as 6.7 but $c = 8$ days.

Before the front ($t < 0$) the velocity field in the Pol-
lard-Fofonoff model is exponentially decaying but is directed much
more to the right of the stress vector than it is for the surface
velocity in the Austausch model. The angle between the stress vector
and velocity vector in front of the storm as given by equations
(6.3) as well as the approximate values in the Austausch model are
shown below:

	U (cm sec ⁻¹)	248	1000	1845
C				
(days)				
1		79.1°	68.2°	57.9°
4		85.2°	73.2°	62.0°
8		86.2°	74.0°	62.8°
Austausch		38°	35°	30°

This greater angle is at least partly due to the fact that
in the layer model the mass transport over the homogeneous layer
rather than only a surface velocity is being calculated. In the
Austausch model, the velocity field integrated over the depth of the
Ekman layer would be more to the right of the stress vector.

Another difference between the two models is the ratio
of magnitudes of the near front solution to that of the oscillatory
wake. In the Austausch model, the surface velocities near the front

are approximately twice as big as the wave amplitudes one or two cycles after the front. This is only true in the layer model for the highest value of the frictional coefficient ($C = 1$ day). The oscillatory field in the layer model generally has a larger amplitude than that of the Austausch model.

The similarity of the results from the two models can be interpreted as providing some theoretical justification for the simple layer model (at least if one believes in eddy viscosity!), and perhaps it is best to emphasize this aspect of the comparison.

6.2 Conclusions

It has become clear that atmospheric wind systems can be responsible for a large portion of the inertial motions observed near the ocean surface. The model presented in this paper, which includes both frictional and dispersive processes, gives wind generated inertial waves with velocities of the order of 10 cm sec^{-1} and with frequencies a few percent above inertial. The relatively realistic forcing function treated thus produces waves which resemble quite well those observed in nature.

Waves generated locally by an isolated wind field can decay horizontally in essentially two ways. The first is by dispersion of energy horizontally and vertically away from the forced area; the second is by forced destruction of the wave field by other wind fields. These mechanisms must be able to explain the observed persistence times which are of the order of one week. Figure 4.2 shows that the slowest moving front (2.5 m sec^{-1}) has a wake which decays in just about this time scale. Tomczak (1969) presents some data from the western Baltic (see figures 6.10 and 6.11) which shows horizontal decay rates (see records from 32 and 38 meters around July 1 and August 21, 1968) very similar to that of the near surface solutions for $U = 2.5 \text{ m sec}^{-1}$. Atmospheric fronts passed over the observation site on June 28 and again on August 20, 1968. It seems possible then, that under some circumstances, dispersion and viscous decay could

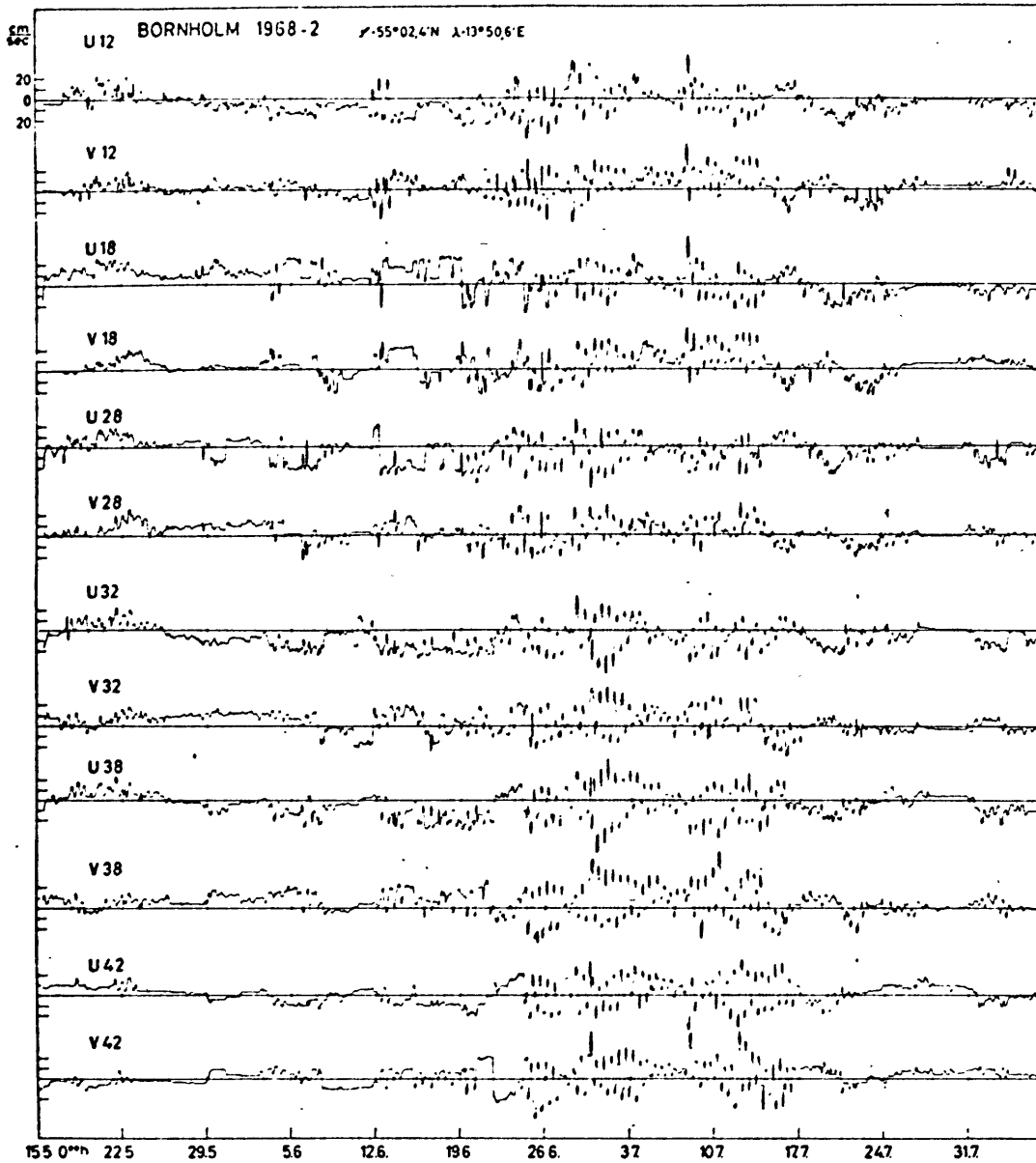


Figure 6.10 Observations of inertial motion in the western Baltic. (from Tomczak, 1969). The numbers following the horizontal velocity components U and V refer to the depth in meters. The horizontal axis covers the period May 15 to July 31, 1968.

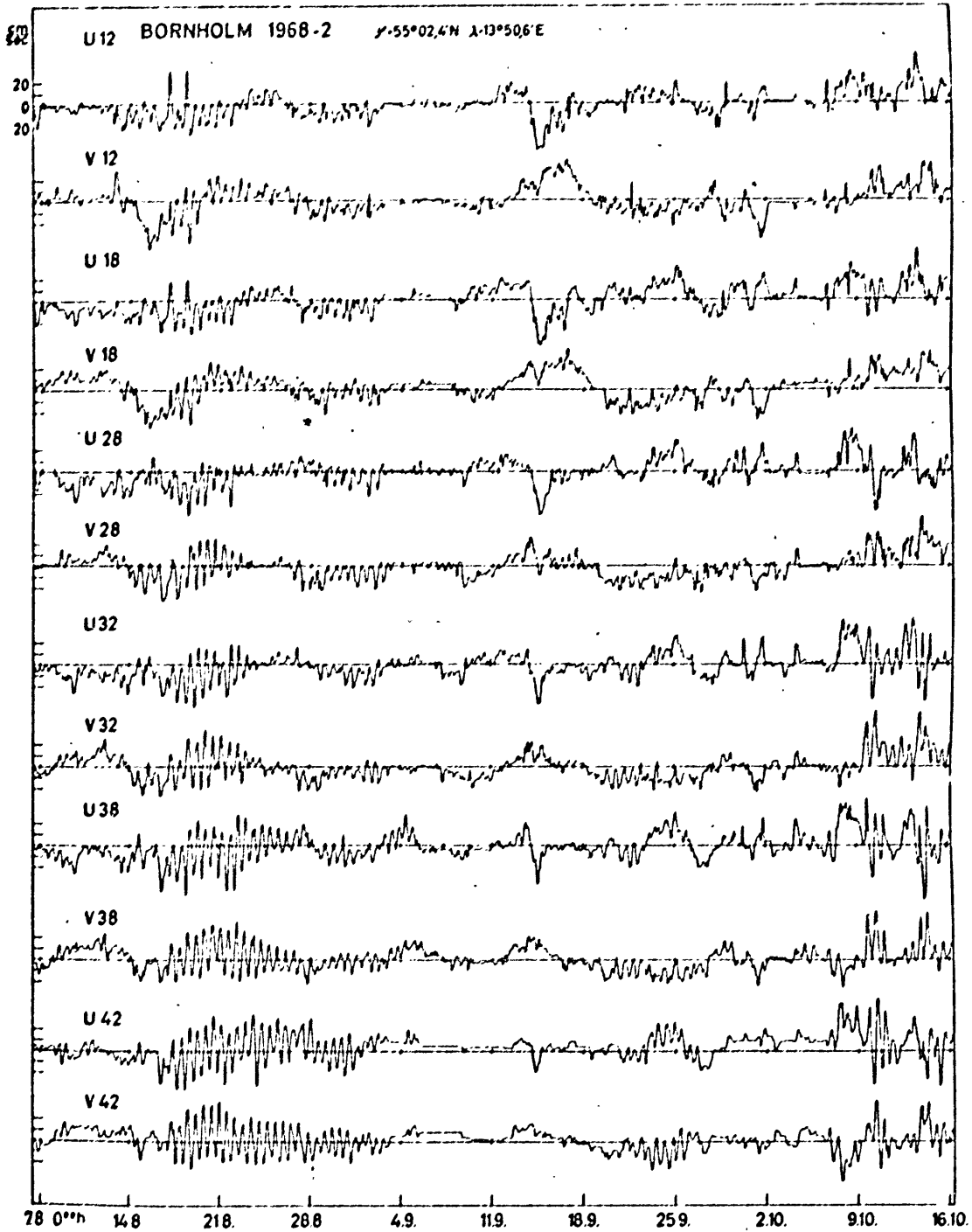


Figure 6.11 The same as 6.10 but for the period August 7 to October 16, 1968.

explain the reported persistence time. The reader should compare this result with Pollard (1970) who found slower dispersion rates but with a different forcing function. For the faster moving fronts, the horizontal decay is less rapid due to the lower group velocities associated with the waves' increased closeness to the inertial frequency. It is unlikely that these oscillations could decay by dispersion before other wind fields came along. This second mechanism, that of forced destruction by a new wind field would then be the main agent of decay.

The depth dependance of the waves produced with the model is such as to confine the motion to the upper several hundred meters of the ocean. The solutions of Chapter 4 show approximately a 90% decrease in wave amplitude between the surface and a depth of 1 km. Thus, very high surface velocities of 50 cm.sec.⁻¹ say, would correspond to motion at 1 km. of only 5 cm.sec.⁻¹ This depth, 1 km., seems to be the limit to which wind induced inertial motion could penetrate with a measureable amplitude. Motions below this depth must come from other sources. It can also be concluded that inertial motion produced at the ocean bottom would only penetrate upwards a distance of approximately 1 km. These statements are of course based on the model presented and would have to be modified by the inclusion of the β effect or a variable Austausch coefficient. It seems possible but improbable to the author that a variable f

would allow inertial waves to penetrate deep into the ocean. This opinion is based on the discussion in Chapter 3 of the effects of friction on waves with near inertial frequencies. A variable eddy coefficient could allow deeper penetration since the coefficient would be expected to diminish with depth away from the surface layers and, hence, decrease the frictional effects. The constant value assumed here ($\sim 10^3$) is appropriate to the surface layers. Aside from the problem of inertial motions at great depths, however, this Austausch model gives a realistic picture of the inertial motions in the upper layers of the ocean. For waves occurring at great depths, the hypothesis suggested by the above conclusions is that of wave generation within the body of the ocean, away from both the surface and the bottom. Possible mechanisms might be instabilities or adjustments associated with essentially geostrophic flows. An alternative to this mid-depth forcing is the global generation mechanism and this would require a generation mechanism for large scale internal waves (ω not close to f) which is, at present, not apparent.

Appendix 1. Discussion of the numerical procedure

All computations were done on an IBM 360 at the M.I.T.

Information Processing Center and consisted of the following steps:

1. The roots of equation (3.1) were solved iteratively as functions of k using Muller's method (the program is contained in the MIT subroutine library). The k -grid spacing was variable with k and was arranged to give minimum spacing near the inertial wave number $2/U$; it is given in table A.1:

U	k-range	number of grid points	grid spacing
13.411 ($\frac{2}{U}=0.149$)	0 - 0.144	25	0.576×10^{-2}
	0.144 - 0.167	175	0.131×10^{-3}
	0.167 - 0.227	75	0.214×10^{-3}
	0.227 - 0.700	50	0.946×10^{-2}
	0.700 - 1.10	125	0.32×10^{-2}
	1.10 - 9.9	50	0.178
54.083 ($\frac{2}{U}=0.0370$)	0 - 0.031	10	0.31×10^{-2}
	0.031 - 0.055	390	0.616×10^{-4}
	0.055 - 1.055	50	0.2×10^{-1}
	1.055 - 10.055	50	0.2
100.0 ($\frac{2}{U} = 0.02$)	0 - 0.019	50	0.38×10^{-3}
	0.019 - 0.023	200	0.2×10^{-4}

0.023 - 1.023	200	0.5×10^{-2}
1.023 - 11.023	50	0.2

For all three cases, 1000 k points were used, 500 for $k > 0$ and 500 for $k < 0$. In the above table only $k > 0$ is presented; the points were symmetric about $k = 0$.

2. The roots obtained above were then substituted into equations (4.8), the transform variable \overline{T} calculated using (4.5) and the resulting sixth order system of equations inverted for each value of k . The coefficient matrix is rather ill-conditioned due to the different orders of magnitude of the vertical wave numbers, m_j . To avoid computational problems, the wave numbers were identified with the top or bottom boundary ($\text{Imag } m < 0$ on top and $\text{Imag } m > 0$ on bottom) and the exponentials in (4.8) were then written as $e^{im_j(z-1)}$ (upper boundary term) and $e^{im_j z}$ (lower boundary term). Terms like $e^{im_j z}$ become very small as z approaches 1 and are neglected in the calculations. Physically, this procedure amounts to neglecting the influence of the top boundary layer near the bottom of the fluid and that of the bottom boundary layers near the top of the fluid, when $|\text{Im } m|$ is large.

3. The solutions, w_j , of (4.8) were converted into U_j , V_j and R_j by (4.7) and these were then placed into (4.6) and

integrated over a finite range in k . The cut-off value of k was determined by comparing the integrand, for the case $U = 100$, to a test function of k which was always bigger than the integrand and which was known analytically and, hence, could be integrated. The error in this comparison, using $k_{\text{cut-off}} = 10$, was much less than 1%. The value $k = 10$ corresponds to a wavelength of 2.51 km. and, judging from the scale of motion in the solutions, seems to have been large enough.

Difficulty was encountered in integrating by Simpson's rule the function $(u, v, r) e^{ik(x-ut)}$ for large values of $x-Ut$ due to the high frequency of its oscillations; with such a high frequency the integrand is aliased by a fixed grid space. The difficulty appeared as a failure of the solution to satisfy the finite-difference test described below. To correct this the integrand was approximated by a linear function between grid points and the integral for u , say, calculated as follows:

$$u = \frac{1}{2\pi} \int_{-\infty}^{\infty} U e^{ik\xi} dk \approx \frac{1}{2\pi} \sum_{j=-499}^{500} \int_{k_{j-1}}^{k_j} (a_j k + b_j) e^{ik\xi} dk$$

$$= \frac{1}{2\pi} \sum_{j=-499}^{500} \left[a_j e^{ik\xi} \left(\frac{k}{i\xi} + \frac{1}{i\xi^2} \right) + b_j \left(\frac{e^{ik\xi}}{i\xi} \right) \right]_{k_{j-1}}^{k_j}$$

$$\xi = x - Ut, \quad a_j = \frac{U_j - U_{j-1}}{k_j - k_{j-1}}, \quad b_j = \frac{k_j U_{j-1} - k_{j-1} U_j}{k_j - k_{j-1}}$$

The integration for u , v , and ρ was carried through for the various values of $x-Ut$ and z shown in the solution curves of Chapter 4.

In the case $U = 100$, a finite difference scheme was used to test the accuracy of the numerical solutions in satisfying the equations of motion and the boundary conditions. A horizontal grid interval of 100 m. and a vertical grid interval of 1 cm. was used with points at and near the surface. The errors in the various equations, defined as the ratio of the residue of the equation to the largest term were as follows:

u-momentum eq'n.	2%
v-momentum eq'n.	3%
w-momentum eq'n.	0.6%
continuity eq'n.	0.2%
density eq'n.	0.1%

The boundary conditions were satisfied to within 1%. The boundary conditions were tested in the other two cases and similar accuracy was found.

Appendix 2 Calculation of the branch cut integrals of Chapter 5A-2.1 Evaluation of an integral used on the branch cuts.

It will be necessary to evaluate the integral

$$I(\nu) = \int_0^{\infty} \frac{\varphi(\mu) e^{-\mu\nu}}{\sqrt{\mu}} d\mu \quad \text{A-2.1}$$

where $\nu > 0$ and $\varphi(\mu)$ is regular and bounded for $0 \leq \mu < \infty$.

$I(\nu)$ will be evaluated asymptotically for large ν using integration by parts following Copson (1965), p. 21 ff. For any function $f(\mu)$:

$$\int_a^b \varphi(\mu) f(\mu) d\mu = \left[\sum_{n=0}^{N-1} (-1)^n \varphi^{(n)} I^{n+1} f(\mu) \right]_a^b + (-1)^N \int_a^b \varphi^{(N)} I^N f(\mu) d\mu$$

where $\varphi^{(n)}$ denotes $\frac{\partial^n \varphi}{\partial \mu^n}$ and $I f(\mu) = \int_a^{\mu} f(t) dt$

Copson shows that
$$I^n f(\mu) = \frac{1}{(n-1)!} \int_a^{\mu} (\mu-t)^{n-1} f(t) dt$$

where a is arbitrary. Here,

$$f(\mu) = \frac{e^{-\nu\mu}}{\sqrt{\mu}}$$

so that

$$I^n f(0) = \frac{(-1)^n}{(n-1)!} \int_0^{\infty} t^{n-\frac{1}{2}-1} e^{-\nu t} dt$$

$$= \frac{(-1)^n}{(n-1)!} \frac{\Gamma(n-1/2)}{\nu^{n+1/2}}$$

Since $\lim_{\mu \rightarrow \infty} \varphi^{(n)}(\mu) f(\mu) = 0$:

$$I(\nu) = \int_0^{\infty} \frac{\varphi(\mu) e^{-\nu\mu}}{\sqrt{\mu}} d\mu = \sum_{n=0}^{N-1} \frac{\varphi^{(n)}(0) \Gamma(n+1/2)}{n! \nu^{n+1/2}} + R_N \quad \text{A-2.2}$$

$$R_N = (-1)^N \int_0^{\infty} \varphi^{(N)}(\mu) \frac{I^N f}{\nu^N} d\mu = O\left(\frac{1}{\nu^N}\right)$$

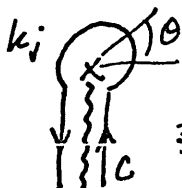
(SEE COPSON)

If the approximation is carried only to the first term:

$$I(\nu) = \frac{\varphi(0)\sqrt{\pi}}{\sqrt{\nu}} + O\left(\frac{1}{\nu}\right) \quad \text{A-2.3}$$

A-2.2 Evaluation of the branch cut integrals.

5.16 and 5.17 show that the integrals to be evaluated on the branch cuts are of the general form:



$$\frac{3\pi}{2} > \theta \geq -\frac{\pi}{2}$$

$$I = \frac{1}{2\pi} \int_C \frac{F(k) m e^{ik\xi}}{m^2 - n^2} dk$$

A-2.4

where $F(k)$ involves the stress transforms and m and n are two of the roots of (3.1). 5.14 and 5.15 allow m and n to be written

$$\text{on } \theta = -\frac{\pi}{2} \quad m = \alpha a + \beta b \\ n = \gamma a + \delta b$$

$$\text{on } \theta = \frac{\pi}{2} \quad m = -\alpha a + \beta b \\ n = \gamma a + \delta b$$

where a vanishes at the branch point (e.g., $a = \frac{\sqrt{\rho_j}}{2E\eta}$ for m_3 on $\theta = -\frac{\pi}{2}$) and $\alpha, \beta, \gamma, \text{ and } \delta$ are either $+1$ or -1 .

A-2.4 becomes

$$I = \frac{1}{2\pi} \left[\int_{k_j - i\omega}^{k_j} \frac{F(\alpha a + \beta b) e^{ik\xi} dk}{2(\alpha\beta - \gamma\delta)ab} + \int_{k_j}^{k_j - i\omega} \frac{F(-\alpha a + \beta b) e^{ik\xi} dk}{-2(\alpha\beta + \gamma\delta)ab} \right]$$

since the integral around the small circle vanishes in the limit of zero radius.

$$I = \frac{1}{2\pi} \int_{k_j}^{k_j - i\omega} -\frac{\beta F}{a} \frac{e^{ik\xi} dk}{(\alpha\beta - \gamma\delta)}$$

Now, $\omega - \omega_j = U_k - U_{k_j} = -i\rho_j$ on $\theta = -\frac{\pi}{2}$

$$\therefore k = k_j - \frac{i\rho_j}{U} = k_j - \frac{i4Ea^2}{U}$$

from 5.14 and 5.15. Define $a^2 = \mu$ and $-\frac{4E\xi}{U} = \nu > 0$.

Then,

$$I = \frac{i\beta}{(\alpha\beta - \gamma\delta)} \frac{4E e^{ik_j \xi}}{2\pi U} \int_0^\infty \frac{F e^{-\nu\mu} d\mu}{\sqrt{\mu}}$$

Using A-2.3

$$I = \frac{\beta}{(\alpha\beta - \gamma\delta)} \frac{E^{1/2} e^{ik_j \xi} F(k_j)}{\sqrt{\pi U \xi}} \quad \text{A-2.5}$$

A-2.5 may be used as a formula to compute the contributions from the integrands 5.16 and 5.17 along the various branch cuts.

These contributions sum to ψ :

$$\psi = \int_{C_1} + \int_{C_2} = \frac{E^{1/2}}{\sqrt{\pi U(x-ut)}} \left[\frac{i}{2} (iT_x - T_y) e^{ik_1 \xi} - \frac{i}{2} (iT_x + T_y) e^{ik_2 \xi} \right]$$

From 5.10, $k_1 = -\bar{k}_2$ and from 4.5 $\bar{T}(k) = \bar{T}(-k)$; $\bar{\quad} = \text{CONJUGATE}$.

Using the fact that $\bar{T}(k_2) = \bar{T}(-k_1) + O(E^{1/2})$, ψ becomes

$$\psi = R \frac{i e^{ik_1 \xi} E^{1/2} [iT_x(k_1) - T_y(k_1)]}{\sqrt{\pi U(x-ut)}}$$

References

- Copson, E.T. (1965) Asymptotic Expansions. Cambridge Univ. Press, 120 pp.
- Day, C., and Webster, F. (1965) Some current measurements in the Sargasso Sea. Deep-Sea Res., 12, 805-814.
- Deacon, E.L., Sheppard, P.A., and Webb, E.K. (1956) Wind profiles over the sea and the drag at sea surface. Australian Jour. Physics, 9, 511-541.
- Fofonoff, N.P. (1966) Spectral characteristics of a simple Ekman wind drift model. Unpublished manuscript.
- Hasselmann, K. (1970) Wave driven inertial oscillations. Preprint.
- Hunkins, K. (1967) Inertial oscillations of Fletcher's ice island. (T-3) , Jour. Geophys Res., 72, 1165-1174.
- Munk, W., and Phillips, N. (1968) Coherence and band structure of inertial motion in the sea. Rev. Geophys., 6, 447-472.
- Phillips, O.M. (1966) The Dynamics of the Upper Ocean. Cambridge Univ. Press, 261 pp.
- Pollard, R. (1970) On the generation by winds of inertial waves in the ocean. To appear in Deep-Sea Res.
- Pollard, R., and Millard, R. (1970) Comparison between observed and simulated wind-generated inertial oscillations. To appear in Deep-Sea Res.
- Saelen, O.H. (1963) Studies in the Norwegian Atlantic current. Geofysiske Publikasjoner, 23, 1-82.
- Taylor, G.I. (1915) Eddy motion in the atmosphere. Phil. Trans. Roy. Soc. London, (A), 215, 1-26.
- Tomczak, M. (1967) Uber den Einfluss fluktuierender Windfelder auf ein stetig geschichtetes Meer. Deutsche Hydr. Zeitschr., 20, 101-129.

Tomczak, M. (1969) Über interne Tragheitsbewegungen in der westlichen Ostsee. Deutsche Hydr. Zeitschr., 22, 158-162.

Webster, F. (1968) Observations of inertial -period motions in the deep sea. Rev. Geophys., 6, 473-490

Acknowledgements

The author is very grateful to Prof. Norman Phillips for his continued patience and his example of sound reasoning. He is also grateful to Dr. Peter Baines, Mr. Anthony Hollingsworth, and Mr. Robert Knox for helpful discussions and to Mrs. Karen McQueen for cheerfully typing the manuscript.

This research was supported under National Science Foundation Grant GA402X.

Biographical note

The author was born on January 13, 1942 in Staten Island, New York. He studied Civil Engineering at Manhattan College from September 1959 to June 1963. After working for a master's degree in oceanography for the next two years at New York University, he entered MIT in September, 1965. While at NYU and MIT he was employed as a research assistant in physical oceanography.